UiT
THE ARCTIC UNIVERSITY OF NORWAY

Faculty of Science and Technology

Department of Geosciences

# Scales of tectonic processes controlling fluid flow systems

*On the Svyatogor Ridge, Fram Strait*

—

**Kate Alyse Waghorn**

*A dissertation for the degree of Philosophiae Doctor – April 2019*

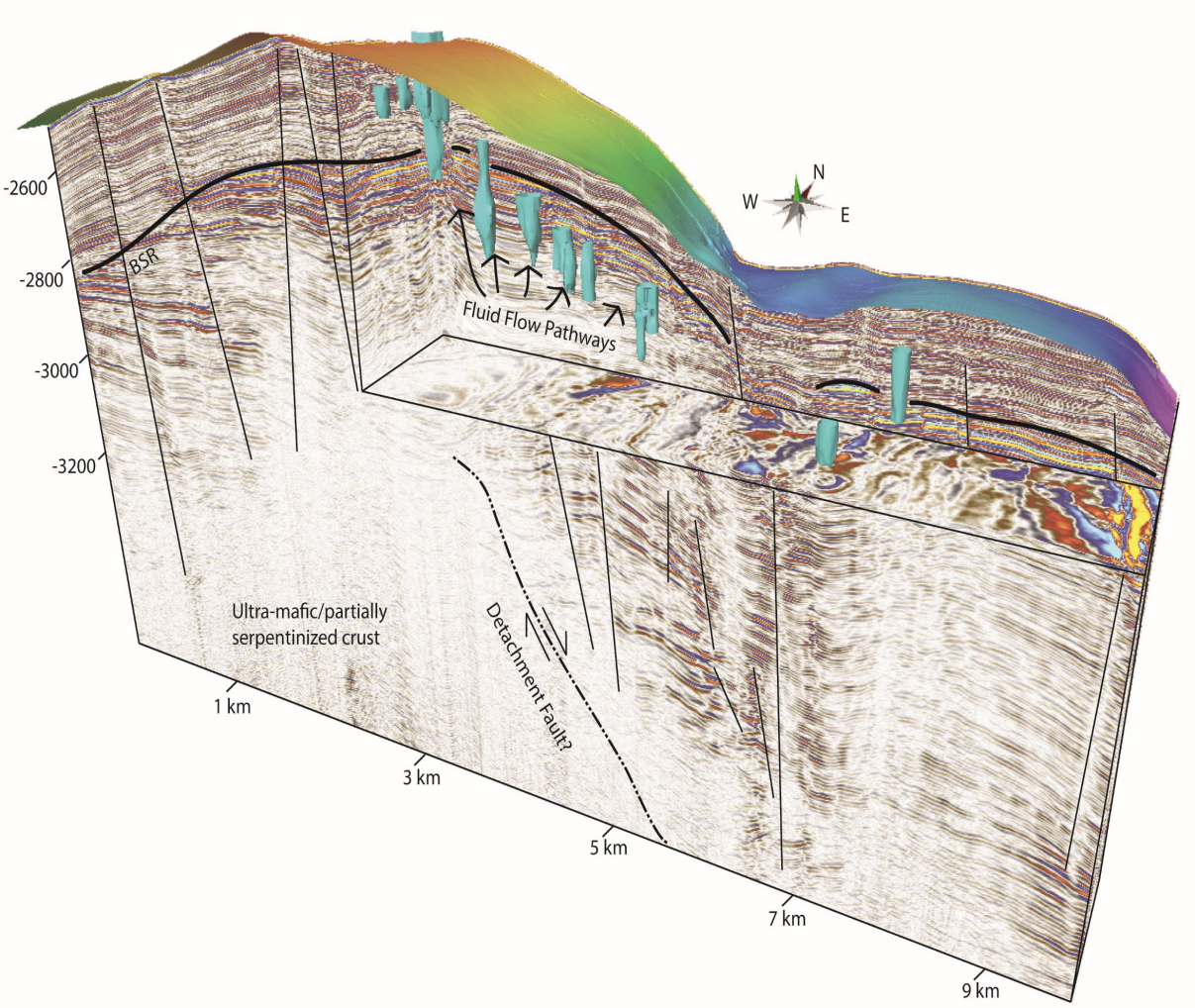


UNIVERSITY OF TROMSØ

# Scales of tectonic processes controlling fluid flow systems

## On the Svyatogor Ridge, Fram Strait

*Kate Alyse Waghorn*

*April 2019*

A dissertation for the degree of Philosophiae Doctor

Tromsø 2019

CAGE – Centre for Arctic Gas Hydrate, Environment and Climate

Department of Geosciences

UiT

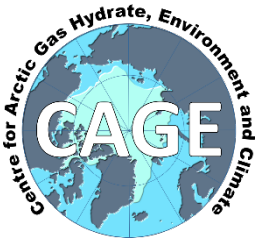


Cover Image: Svyatogor Ridge Northern 3D dataset – acquired in 2016 aboard *R.V. Helmer Hanssen* – processed courtesy of Rowan Romeyn. Structural elements and fluid flow system highlighted.

# Preface

This doctoral thesis was undertaken at the Department of Geosciences (formerly Geology) at UiT-Norges Arktisk Universitetet, Tromsø, between October 2014 and April 2019. This research integrates with CAGE - the Centre for Arctic Gas Hydrate, Environment and Climate – an NSF Centre of Excellence funded by the Norwegian Research Council (grant 223259). The main supervisor was Professor Stefan Bünz (CAGE-UiT) and co-supervisor Dr. Andreia Plaza-Faverola (CAGE-UiT) with significant input from Professor Joel E. Johnson (University of New Hampshire, New Hampshire, USA). Additional support for this PhD came from AMGG – the trainee school for arctic marine geology and geophysics, ResClim – Research school in climate dynamics, CHESS – Research School on changing climates in the coupled earth system and DEEP – Norwegian Research school for dynamics and evolution of Earth and Planets. Support from research and trainee schools came in form of travel grants, funded workshops and seminars to improve presentation and dissemination skills, and conferences.

All seismic data presented in this thesis was acquired in collaboration with CAGE, aboard the *R.V. Helmer Hanssen.* I took part in data collection cruises not only for my PhD but also participated in other CAGE research expeditions, which broadened the scope for collaborations with other researchers within CAGE. Results from this research were disseminated at four international scientific conferences and workshops, and seven national or institutional conferences and workshops. Publically available results in the form of online media resources, open access (green) publications are available on ScienceOpen and ResearchGate profiles, along with dissemination on my open social media profiles. Datasets are available on UiT Open Research Data, a subset of DataverseNO.

The four-year PhD programme at UiT requires that 25% (1-year equivalent) consist of work pertaining to improving the quality of education and research at the Institute. This entailed involvement with AMGG – Arctic Marine Geology and Geophysics – PhD trainee school as the secretary. This work enabled me to organise conferences, workshops and ultimately the BUBBLES 2017 Trainee School, with students and speakers participating from all over the world. Additionally, as part of duty work requirements I have prepared, taught and assessed a practical seismic data processing course, organised lunch seminars within the institute and assisted other PhD students collecting data aboard the *R.V. Helmer Hanssen.*

# Acknowledgments

Firstly, thanks must go to my supervisor Stefan Bünz for initiating the project and always telling me results have been worthwhile despite ever-looming imposter syndrome. My co-supervisor Andreia Plaza-Faverola gave an incredible amount of time to this thesis and for that, I am grateful. All data for this thesis was collected aboard the *R.V Helmer Hanssen* so a huge thanks to the crew and scientists aboard all the research expeditions. Special thanks must go to Steinar Iversen, without whom the P-Cable system would not function. I would also like to thank Joel Johnson, Sunil Vadakkepuliyambatta and Rowan Romeyn for collaborations and contributions over the course of this PhD.

Giuliana, you are owed a very deep thank you for all that you have done, the experiences I have had during my time as AMGG secretary are some of the most personally meaningful during the last four years. Rick Coffin, Lorna Strachan and Ingo Pecher, even though my Master thesis ended a long time ago, encouraged me to start a PhD and have provided support, guidance and encouragement extending far beyond the time frame of our collaboration.

Friede, you have been the best flattie – I cannot imagine not having shared this experience with you. Everyone at IG, of whom there are too many to name, have enhanced the PhD experience. Giacomo and Îla, thanks for just being awesome. Magnus – why do I always break things when I ski with you? Lene, our wine nights, shopping trips and general troublemaking were a blast and I wish you would move back.

Mum and Dad, you guys know it would have been impossible without you. I do not expect you to read further but know that all your sacrifices for me over the years have led to something, I hope. Frans and Kassie – you came at the end, but you have kept me grounded when I needed it, you have given me so much love and support and I owe you more than you can imagine.

Kaua e mate wheke mate ururoa

# Abstract

The Svyatogor Ridge, located in the Fram Strait, is a site hosting a fluid flow system. The Svyatogor Ridge is part of the inside corner high at the Knipovich Ridge-Molloy Transform Fault intersection. The Knipovich Ridge is an ultra-slow, melt-poor spreading ridge with ~8 mm/yr spreading rate. At this northernmost segment of the Knipovich Ridge, spreading is predominantly accommodated by crustal-scale detachment faults. While fluid flow systems are not atypical on mid-ocean ridge flanks, the geothermal gradients are generally too warm and sediment cover too underdeveloped for generation of gas hydrates, despite methane release from hydrothermal vent systems being well documented. In this study area, the convergence of a well-developed sedimentary cover atop partially serpentinized ultra-mafic mantle material and a comparatively cool geothermal gradient entails a gas hydrate system in an 'unusual' location.

Carbon pool and gas hydrate estimates worldwide have not considered abiotic methane, produced inorganically through gas-water-rock interactions, in their inventories as natural accumulations of abiotic methane in sediments or gas hydrates have remained a hypothesis. This thesis characterises a potential marine abiotic methane hydrate accumulation site in terms of structure, sedimentology, evolution and fluid flow systems. We find a link between crustal faulting in serpentinized mantle material and gas hydrate/free gas accumulations leading to the conclusion that abiotic methane is likely contributing to the gas hydrate system here. The stress regime has been an important factor on the Svyatogor Ridge for controlling fluid flow through geological time and into the future. High-resolution 3D P-Cable seismic data was integral for identifying fault and fracture networks, which drive fluid migration as normal extensional faulting becomes sub-optimally oriented for fluid migration.

# Table of Contents

# 1. Introduction

## Motivation

This work has concentrated on one study area, a section of the sub-seafloor to the west of the Knipovich Ridge in the Fram Strait. 2D seismic data collected over a small part of the study area in 2013, showed a gas hydrate Bottom Simulating Reflection (BSR). This prompted a discussion relating to how and why gas hydrates should form on an actively spreading, albeit ultra-slow, mid-ocean ridge. The hypothesis of an abiotic methane source was of interest to the Centre for Arctic Gas Hydrate, Environment and Climate (CAGE). Several studies have crossed the Svyatogor Ridge with conventional 2D seismic, however the majority of prior studies featuring the Svyatogor Ridge relate to either deep crustal structure or characterisation of spreading environment on the Knipovich Ridge using bathymetry and side-scan sonar data. Therefore, a significant contribution of this thesis has been to establish a framework for future studies on the Svyatogor Ridge. This framework needed to include 1) seismic stratigraphy, including depositional environment 2) tectonic setting and stress environment 3) an integrated sedimentary and tectonic history of the study area and 4) the fluid-flow system evolution and dynamics. Work produced from this thesis covers three scientific articles. Article 1 focuses on creating a geologic and tectonic framework for the area as well as detailing the fluid flow regime over the Svyatogor Ridge. Manuscript 2 extends the framework to the surrounding areas and develops the linkage between fluid flow regimes and tectonic setting while manuscript 3 focuses on the tectonic/structural development of the Svyatogor Ridge and the implications of stress style for fluid flow processes here.

## Objectives

The overall objective of this thesis was to determine the origins of, and mechanisms controlling, the gas hydrate and related fluid flow system on the Svyatogor Ridge. To meet this objective, I investigated the following:

- Sedimentary history and depositional processes over the study area
- Tectonic evolution, stress regime characterisation and classifying the role of tectonism in fluid migration
- Mapping and characterising major areas of fluid accumulations, determining their likely migration pathways and seepage history

## 1.1 Geologic and Tectonic Background

### Tectonic Deformation

Deformation is the process whereby rock material alters from an initial state due to stress, synonymous with strain (Scholz, 2002). Scales of deformation range from grain boundary (µm scale) to plate tectonics (>km scales). Stress is the force that is applied to an object, measured in force per area, where the four types of stresses applied to rocks are confining stress (burial for example), compressive stress, tensional stress and shear stress (Scholz, 2002). These stresses translate into three modes of faulting, assuming all rock has a confining stress – compressional faulting, extensional faulting and strike-slip faulting. Any change in shape of the material due to an applied stress is strain, or deformation (Scholz, 2002). Elastic deformation occurs when a stress is applied and the material deforms but reverts to the original state upon removal of stress, while plastic deformation occurs when the material remains deformed when a stress is removed (Scholz, 2002). Faults, or brittle deformation, occur when the stress overcomes the strength of the rock (Scholz, 2002). In an extensional faulting regime, the Andersonian fault style is a fault dipping approximately 60°, perpendicular to the direction of maximum horizontal stress, $SH_{max}$ (Zoback and Zoback, 2002). $S_v$, the vertical stress tensor, is the greatest stress (Fig. 1).

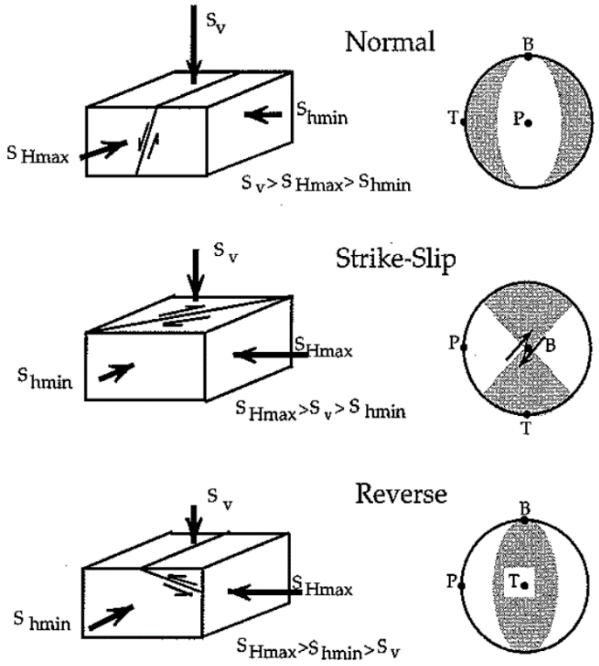


**Figure 1. Andersonian Faulting regimes (Anderson, 1905), and focal mechanisms. Figure from Zoback and Zoback (2002). $S_v$ – vertical stress, $SH_{max}$ – Maximum horizontal stress, $SH_{min}$ – Minimum horizontal stress, P – Compression, B – Intermediate, T – Tension.**

If there are changes in the regional stress regime over time, or the typical stress field for creating normal faults changes, faults may re-activate causing apparently oblique components (Reeve et al., 2015). When faults with very acute or very obtuse dip angles occur, fluid movement through the subsurface is often the cause of the deviation from 60° dip predicted by Andersonian faulting (Axen, 1992; McCaig, 1988; Scholz, 2002). Water permeation and metamorphosis may cause low-angle dips in faults through exhumed mantle rock, for example. Water contact with rock may change the physical properties of the rock, in some cases locally weakening the rock and allowing rock to fault at lower angles than normal, whereas high-angle dips in sedimentary environments are often attributed to compaction de-watering or overpressures generated by hydrocarbon accumulations (Cartwright et al., 2003; Sibson, 2000). Faulting in sediments vs. lithified material may present differently despite the same tectonic stress regime, as the material strength contrast is stark (Fig. 2). If faulting occurs in a mechanically strong material underlying mechanically weak material the fault may occur as one large offset plane in the mechanically strong material whereas it may be expressed as a number of smaller offset faults 'radiating' around the propagation tip beneath (Hardy and McClay, 1999).

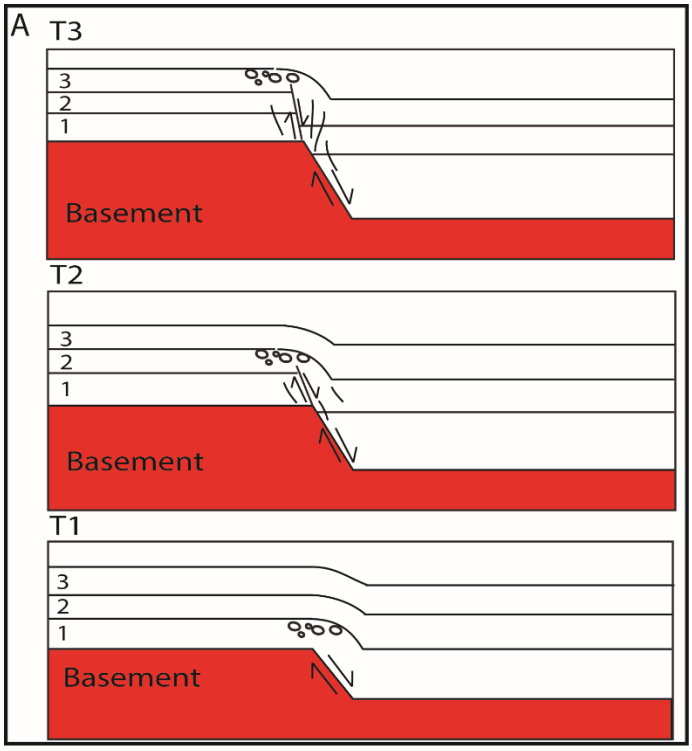


**Figure 2. Example of growth faulting in an extensional regime, where sediment overlays mechanically stronger basement. Figure from Waghorn et al. (2018a). As basement offsets, sediment is forced to fold to accommodate the fault beneath. Brittle deformation then follows as faults grow upwards.**

Given fluid pressures (the amount of pressure imposed by fluid on the rock) in pore space of rocks, the regional tectonic stress regime can be overridden (Sibson, 2000). The most common example of this are compaction dewatering faults or polygonal fault systems, where the faults form at a random array of strikes and typically dip very steeply (Cartwright et al., 2003). In environments where there is extensive subsurface fluid circulation, typically much of the fluid movement occurs through small-offset (cm-m scale) faults and fracture networks despite the presence of large-offset faults available for water circulation (Sibson, 1990). The presence of faults in the subsurface alter pressure gradients

and can drive fluid circulation, via the process of seismic pumping, which occurs when the release of seismic energy at the moment of a fault rupture agitates and drives fluid circulation through faults (Sibson et al., 1975). In areas with high fluid pressure after a fault rupture, seismic pumping and the consequent movement of fluid through the subsurface can force new faults to form or faults to reactivate (Sibson et al., 1975; Sibson, 1996). In settings where reactivations are more common than new fault formation due to fluid pressure, the faults may develop wide core zones, branches and complex linkages (Fossen and Rotevatn, 2016; Sibson, 1994). Where fluid movement through the subsurface is the predominant forcing mechanism of fault development, areas of linkages or fault intersections have been shown to be the loci of fluid migration (Hansen et al., 2005; Sibson, 1996).

## Plate Tectonics

Movement style at plate boundaries govern the regional tectonic setting in the surrounding lithosphere (Zoback et al., 1989). The three types of plate-plate motions occur; divergence, convergence and transformation (Kearey et al., 2009). Of interest in this study are transform and divergent margins.

Transform faults generally occur as intermediary faults between segments of mid-ocean ridges, for example, the Molloy Transform fault acts as an intermediary fault between the Knipovich Ridge and the Molloy Ridge. A small number of transform faults form between convergent margins, for example the Alpine Fault, New Zealand, connects Puysegur subduction system in the south and the Hikurangi subduction system in the north (Lamarche and Lebrun, 2000; Lebrun et al., 2000).

Divergent plate boundaries on earth today are predominately in oceanic settings because newly created crustal material in divergent boundaries is generally denser than continental crust, creating basin structures, which eventually fill with water. This type of plate boundary can be categorised several ways, for example by speed of spreading, spreading mechanism, or length between transform faults (Searle, 2013). Ultra-slow to fast are the common classes of spreading speeds, where ultra-slow is generally classed as ridges creating crustal material at less than 20 mm/yr (Dick et al., 2003; Grindlay et al., 1996), while slow spreading ridges have a rate less than 50 mm/yr (Lonsdale, 1977). Intermediate settings spread between 50-90 mm/yr and fast spreading ridges greater than 90 mm/yr (Lonsdale, 1977). The mechanism of the spreading environment often is dependent on the speed of the spreading. Magmatic spreading occurs where crustal thinning is extensive and through submarine volcanism new basaltic (Mid-Ocean Ridge Basalt, or MORB) oceanic crust forms (Searle, 2013). On melt-poor spreading ridges, new crust is exhumed as mantle material along crustal scale detachment faults (Cannat et al., 2006). Mantle material is ultra-mafic,

implying a lowered silica content compared to that in the crust. Mid-Ocean Ridges are often delineated along their lengths into segments (Searle, 2013). Individual segments along a mid-ocean ridge can have a slightly different orientation, mode of spreading (magmatic, melt-poor or some temporal combination) or speed of spreading. The Low Seismic Velocity Zone (LVS) is the approximate transition between lithosphere and asthenosphere, and underneath ultra-slow spreading ridges, the LVS is up to 4 km deeper than fast spreading ridges (Purdy et al., 1992), implying they are cooler than their faster counterparts. This is likely due to detachment faults, as well as exhuming mantle material, circulating cool seawater deep into the lithosphere, hindering asthenosphere upwelling and therefore hindering speed increases (Purdy et al., 1992).

Ridge-Transform Intersections (RTI's) tend to be tectonically complex, as they represent the area where two stress regimes interact (Fig. 3). Seamounts of a hotspot nature have been found at RTI's, in the inside corner, which contrasts to the understanding of magmatic induced spreading compared to hotspot seamounts (Beutel, 2005; Delaney et al., 1981; Fujita and Sleep, 1978) where the spreading ridge is a site of crustal weakening, with a strong thermal and pressure gradient which funnels magma towards the seafloor. However, these conditions do not necessarily exist at RTI's – if slip along the transform fault is impeded, immense extensional stresses concentrate at the RTI that can give rise to localised pressure and thermal gradients or, upon faulting, allow decompression melting to occur giving rise to hotspot signature volcanism (Beutel, 2005). The same factors can also cause upwelling of other fluids such as deep circulating water and provide some additional thermal buoyancy of the crust making RTI's and especially the inside corner high topographically higher (Fig. 3) than other ridge segments with subsidence occurring as the area moves off-axis (Blackman and Forsyth, 1989; Buck et al., 2005). As a mid-ocean ridge or transform faults propagate, RTI's can become 'extinct' however crustal fluid circulation and processes triggered by the former RTI setting might remain active after the locus of activity has migrated away, such as where serpentinization has occurred (Charlou et al., 1998; Kelley et al., 2001; Schroeder et al., 2002).

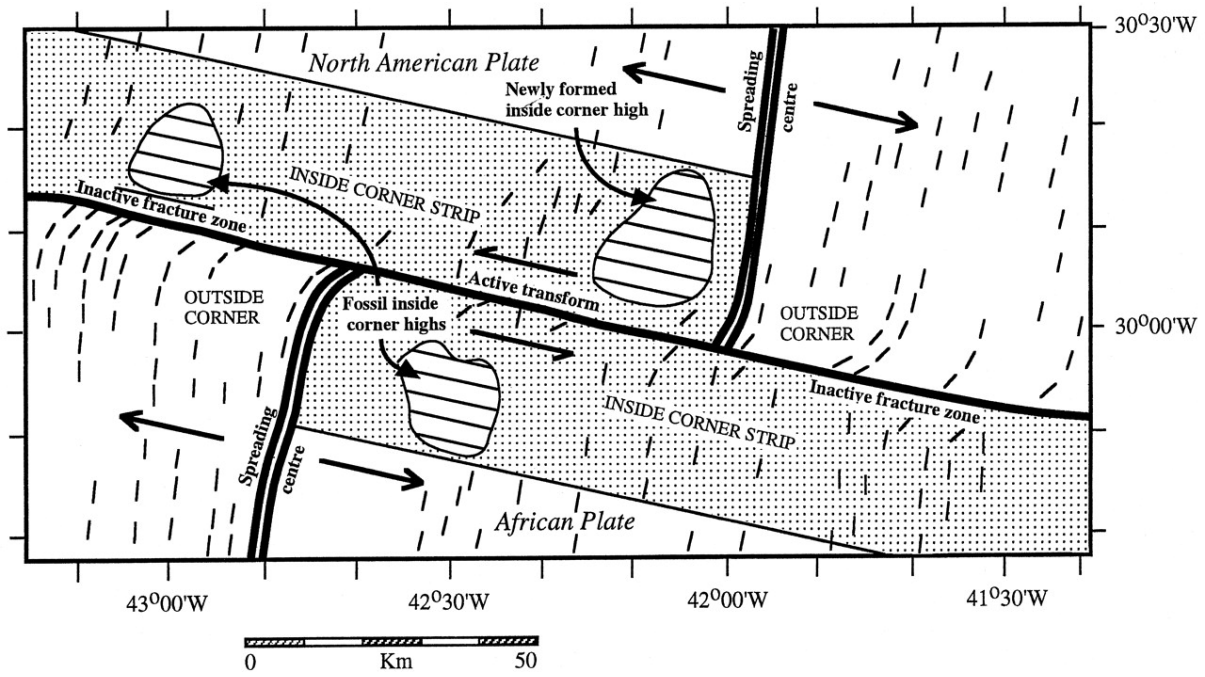


**Figure 3. An example of a Ridge Transform Intersection and the inside corner high at 30° N on the Mid-Atlantic Ridge. Figure from Cann et al. (2001)**

## Sedimentary Depositional Environment and Contourites

The sedimentary environment of deposition as suggested by the name pertains to the biological, chemical and physical processes occurring during sedimentation (Pettijohn, 1957). Locality is a typical initial classification of such environments, for example alluvial or fluvial on land, deltaic or tidal at the seashore and shallow or deep marine environments. In general, inferences can be made about the environment at which sediments deposit based on characteristics such as grain size, mineral abundances, presence or absence of biological markers (Pettijohn, 1957). In deep marine environments, common sediment deposition mechanisms are 1) down slope processes, where sediment is transported from the continental shelf, fluvial systems or land, to depth via turbidity currents, slope failures, gravity currents (Dott Jr, 1963; Visher, 1969). 2) along slope processes, where sediment is transported by geostrophic oceanic currents (Visher, 1969) and 3) hemipelagic settling, where particles fall out due to gravity (Visher, 1969).

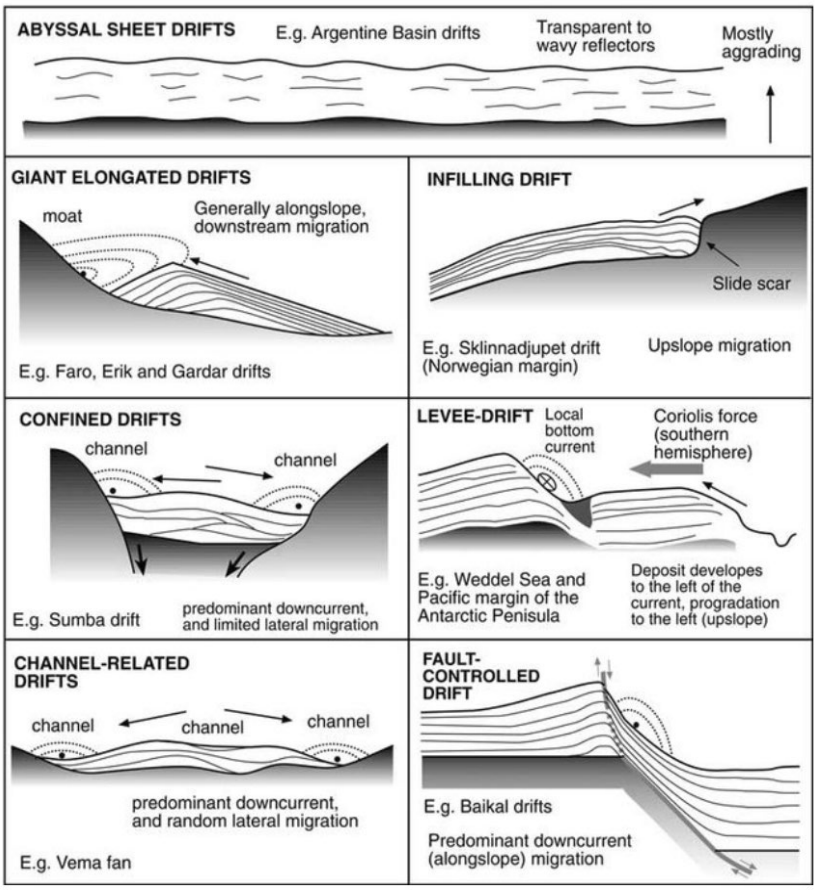


**Figure 4. Styles of contourite development, figure from Rebesco and Stow (2001)**

Contouritic deposition is a type of depositional/erosional process controlled by large-scale geostrophic oceanic currents (Stow and Lovell, 1979). The current velocity is important in determining the style of contourite development at any given location (Stow et al., 2002). In general, oceanic bottom currents have velocity variations in four dimensions, and material on the seafloor and already entrained in a current have a critical velocity, below which grains will fall out and above which grains will entrain or stay entrained (Sutherland, 1967). Depending on the material and current velocity along the seafloor, currents preferentially entrain or deposit material, with the centres of the current (laterally) generally moving faster than the edges. Confinements, such as slopes, creates asymmetrical velocity variations, which in turn preferentially erodes or deposits material asymmetrically (Fig. 4), resulting in mounded or mound-moat style contourites (Faugères et al., 1999). Eddying has a similar effect, where material is preferentially deposited as the current slows to below a critical, grain-size dependant, entrainment velocity (Eiken and Hinz, 1993; Faugères et al., 1999). Sheet contourites form on abyssal plains (Fig. 3), for example, where there is no confinement or obstacle and current velocity, therefore deposition or erosion, is relatively symmetrical (Faugères et al., 1999). Seafloor roughness can also promote preferential contourite development, whereby localised roughness such as pockmarks have been linked to the localised velocity variations and development of mounded contourite development (Waghorn et al., 2018b). Given the proximity of the West Svalbard Margin as a confinement of the West Spitsbergen Current, mounded style contourites are typical (Eiken and Hinz, 1993; Rebesco et al., 2013).

## 1.2 Fluid Systems

### Subsurface Fluid Flow

Fluid flow through the subsurface is a widespread, persistent phenomenon that occurs in any given environment given fluid availability, a function of the geologic processes occurring in the area of interest (Collins, 1976). Types of fluid flow through the subsurface includes hydrothermal systems, magmatic processes, hydrocarbon migration, or simply circulation of water (Fig. 5). In hydrothermal systems, some processes (often related to magmatism or serpentinization reactions) heat or create water, which must then rise to the surface. Magmatism is also fluid flow when ductile deformation occurs, and the molten rock acts as a fluid. In hydrocarbon fluid flow systems, flow or migration occurs when the buoyancy of the hydrocarbon forces the fluid to migrate towards lowered pressure environments (Collins, 1976). Remobilized sediment may also constitute fluid flow, although requires that a fluid has flowed with a velocity higher than the fluidization velocity of the material, prior to entrainment, so might be considered a secondary process (Huuse et al., 2010a). Faulting is an important factor in fluid migration, as faults or structural fabric (pre-existing weaknesses) either act as convenient migration pathways, or trap fluids given certain trapping conditions (Sibson, 1981). Migration of fluid through the subsurface requires some permeability within the host material. Fault damage zones are often higher permeability than the surrounding, however this is dependent on rheology or secondary processes such as mineral precipitation (Sibson, 1981).

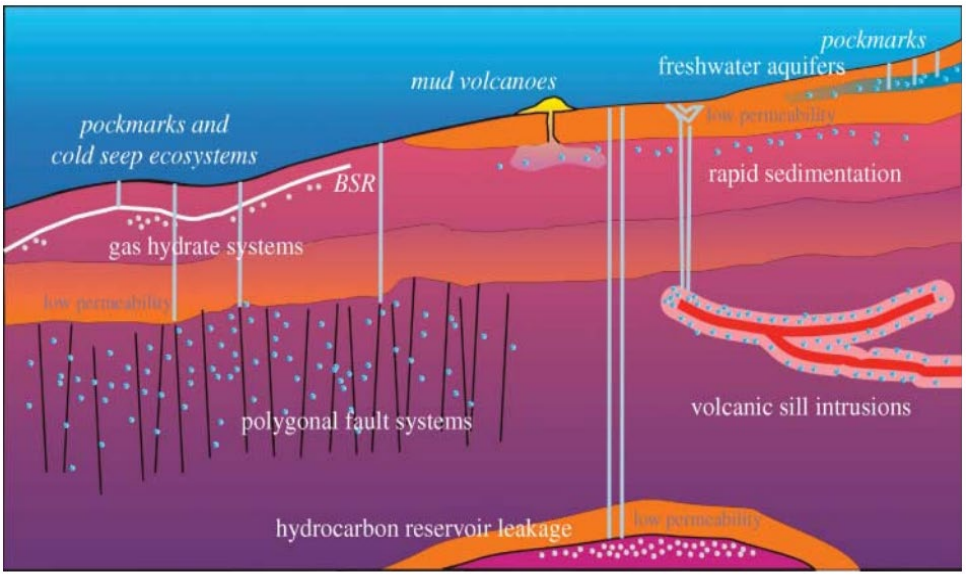


**Figure 5. Illustration of fluid flow systems on continental (passive) margins. Figure from Berndt (2005).**

Fluid flow or fluid accumulation in the subsurface can have a variety of expressions in geophysical data. Pockmarks are seafloor depressions that are generally circular to elliptical and form in response to fluid migrating across the seafloor-water interface (Judd and Hovland, 2009). Pingo-like structures (Serié et al., 2012), pagodas or gas hydrate mounds form where localized accumulations of gas and/or gas hydrate near the seafloor increase pressure in the pore-space, pushing overlying sediment up or increasing volume of the area (Judd and Hovland, 2009). Chimneys and pipes are expressions in seismic data that are generally vertical or near-vertical zones of lowered amplitude (Cartwright and Santamarina, 2015). Pipes are usually smaller and offset of surrounding sedimentary strata is small, while the zone of influence – disruption of pre-existing strata – is limited. Chimney zones tend to be wider, often with zones of apparently undisturbed strata configuration, faults and paleo-pockmarks interpretable within the chimney structure (Cathles et al., 2010; Petersen et al., 2010; Waghorn et al., 2018a). Chimneys, pockmarks and pipes are often related to gas hydrate formation and migration of free gas through the subsurface (Berndt, 2005), and the internal architecture of chimney structures gives insight into evolution of the fluid flow system. Long-term episodic fluid flow indicators are often recorded in chimney structures (Hustoft et al., 2009), while Riboulot et al. (2014) correlate paleo-pockmarks in chimney structures with sea-level changes in the Mediterranean Sea over the Quaternary. Paleo-pockmark distribution and infill rate in the subsurface has also been used to determine longevity and spatial variations of fluid flow systems (Judd and Hovland, 2007; Moss and Cartwright, 2010). The size of pockmarks and paleo-pockmarks indicates the nature of gas release, for example massive blow out or sustained seeping (Andreassen et al., 2017; Davy et al., 2010; Judd and Hovland, 2007). Due to the density of hydrocarbon compared to sediment/water in pore space, accumulations of hydrocarbons express in seismic data as high amplitude bright or flat spots which may cross-cut strata (Brown, 2004). Vents, mounds and crater-eye structures are generally related to hydrothermal fluid flow (Planke et al., 2005).

Sediment remobilization features include diapirs, mud volcanoes or intrusions, sand injectites for example (Huuse et al., 2010b). Often, hydrocarbon fluid flow is involved in these processes, acting as secondary buoyancy to move the material even closer to the subsurface, or to breach the seafloor (Huuse et al., 2010a).

The source of fluid flowing in the subsurface may vary; however, sedimentary pore-space contains water buried along with the sediment, fluid may form at depth through igneous processes or clay remineralisation reactions, or meteoric fluid can reach depth via permeation through faults or permeable strata (Judd and Hovland, 2009). Hydrocarbons generally form at depth and migrate

upwards, the extent to which is dependent on the buoyancy of the specific hydrocarbon. Of particular interest to this study is methane gas, which forms in a variety of ways. As with other hydrocarbons, thermogenic methane forms at depth under appropriate temperature and pressure conditions, given the availability of sufficient organic material (Etiope and Klusman, 2002; Schoell, 1988; Stolper et al., 2014). Biogenic methane is formed through degradation of organic matter by a methanogenic microbial community, generally in shallower subsurface environments compared to thermogenic methane (Claypool and Kvenvolden, 1983). Abiotic methane forms generally through magmatic processes or gas-water-rock interactions and is discussed in detail later in this chapter (Etiope and Sherwood Lollar, 2013).

## Hydrothermal Systems

Hydrothermal systems on mid-ocean ridge settings can be categorised as peridotite-hosted (Kelley et al., 2005) or magmatic hydrothermal systems (Cathles, 1990). In mid-ocean ridge settings, peridotite hosted systems occur atop crustal scale fault and/or detachment faults (Fig. 6), where the mode of mid-ocean ridge spreading is predominantly exhumation, while magmatic hosted hydrothermal systems predominantly occur where the mode of mid-ocean ridge spreading is magmatically driven crustal thinning and creating of MORBs (Cathles, 1990; Kelley et al., 2005). Commonly mid-ocean ridge, peridotite hosted hydrothermal systems are heated by mantle material being near the surface (Charlou et al., 1998; Etiope and Sherwood Lollar, 2013) although crustal melts on axis may also play a role in heating and driving crustal fluid flow. Fluids in hydrothermal

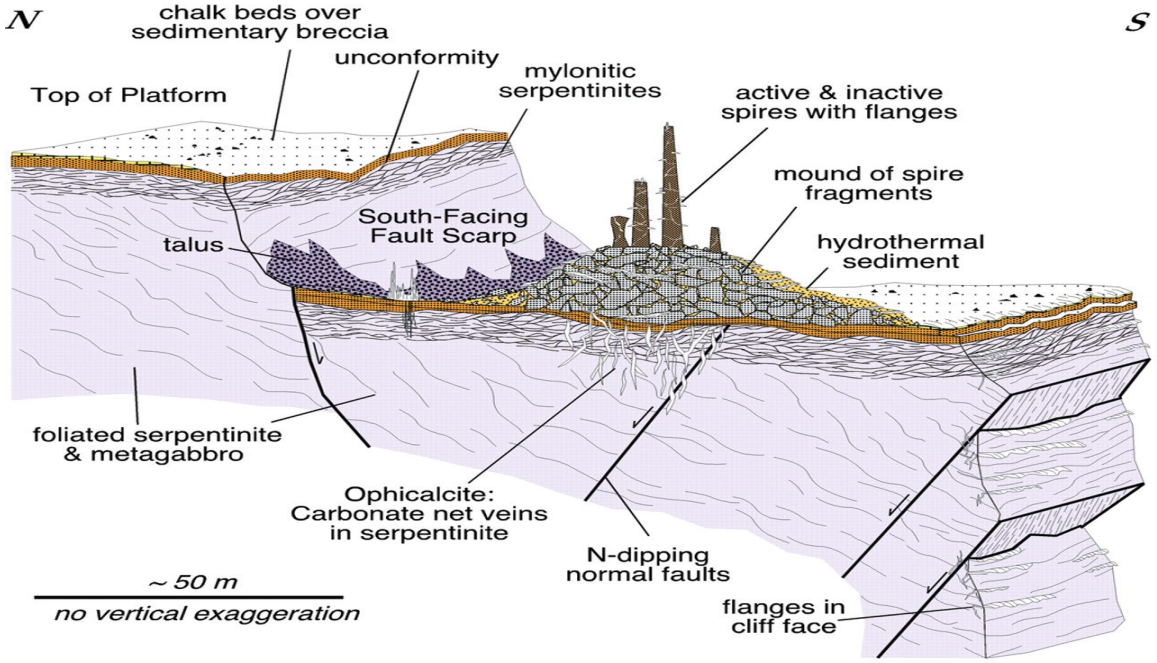


**Figure 6. Schematic sketch of the tectonic and geologic relationships at the peridotite hosted Lost City hydrothermal field. Figure from Kelley et al., 2005**

systems can have a variety of origins, from fluids derived from the magma itself to seawater buried with sediments, or seawater that percolates down through faults and/or porous media (Cathles, 1990). Fluid heated at depth will then begin to migrate back towards the surface. Peridotite hosted system fluids commonly contain by-products of interactions between seawater and the peridotite, including $H_2$ and $CH_4$ (Charlou et al., 1998; Kelley et al., 2005; Proskurowski et al., 2008).

## Abiotic Methane on Earth

There are a variety of methods for producing methane inorganically, including high-temperature reactions in the mantle (Fig. 7), hydrogenation of metal carbides ($Fe_3C + 4H^+ = 3Fe + CH_4$), $CO_2$ evolving into $CH_4$ during magma cooling ($CO_2 + 2H_2O = CH_4 + 2O_2$) and gas-water-rock reactions, such as the Sabatier reaction, Fischer-Tropsch reactions and decomposition of iron carbonate or thermal decomposition of carbonate. Serpentinization is the metamorphic process that occurs when olivine-rich rock is exhumed (lowering pressure and temperature) and the olivine becomes hydrated, producing $H_2$ (Sherwood Lollar et al., 1993). $H_2$ may then react with $CO_2$ or CO to form $CH_4$. The Fischer-Tropsch reaction refers to reactions involving catalytic hydrogenation of CO, producing hydrocarbons. This can occur in one-step, the Sabatier reaction ($CO_2 + 4H_2 = CH_4 + 2H_2O$) or in two steps ($CO_2 + H_2 = CO + H_2O$, $CO + 3H_2 = CH_4 + H_2O$). These reactions require a catalyst, and the metals or metal oxides which provide the surface for converting to gas molecules are commonly found in ultra-mafic rocks, such as peridotite (Etiope and Sherwood Lollar, 2013; Sherwood Lollar et al., 1993). Theoretically, the speed at which these reactions may occur is a function of the temperature, whereby higher temperatures produce methane faster while lower temperatures produce methane slower. However, the initial olivine reaction occurs at temperatures less than 400°C (Foustoukos and Seyfried, 2004).

The heat generated during serpentinization reactions is proportional to the amount of water that reacts to form serpentinite (Früh-Green et al., 2004). Rock expansion under heat creates additional faults and fractures allowing water to come into contact with a larger surface of the ultra-mafic rock, producing more $H_2$ (Früh-Green et al., 2004). In this way, heat from serpentinization is hypothesized to sustain hydrothermal vent systems (Proskurowski et al., 2008) in lower temperature hydrothermal systems although debate still surrounds the role of serpentinization producing heat and sustaining hydrothermal systems, where proximal magmatic heat sources may still have a larger influence (Allen and Seyfried Jr, 2004).

Although abiotic methane production has been shown to occur in laboratories, in mid-ocean ridge hydrothermal systems of peridotite-hosted type (Proskurowski et al., 2008) as well as in some

ophiolite belts (Abrajano et al., 1990; Etiope et al., 2013), the implications of abiotic methane to the global carbon inventory are unknown. As the processes associated with serpentinization and abiotic methane production generally occur at or close to the seafloor in locations where significant sedimentary sequences are unlikely to occur (i.e. abyssal settings), or in settings where the temperature is high enough to drive hydrothermal seeps (Fig. 7), the potential for hydrocarbon storage in sediment is low. Additionally, sediment often does not accumulate fast enough on mid-ocean ridges in abyssal settings, before the processes forming methane are extinct, to provide a suitable reservoir. Ultra-slow spreading ridges, however, move at such slow speeds that they can become sedimented while still active (Johnson et al., 2015; Waghorn et al., 2018a). The major

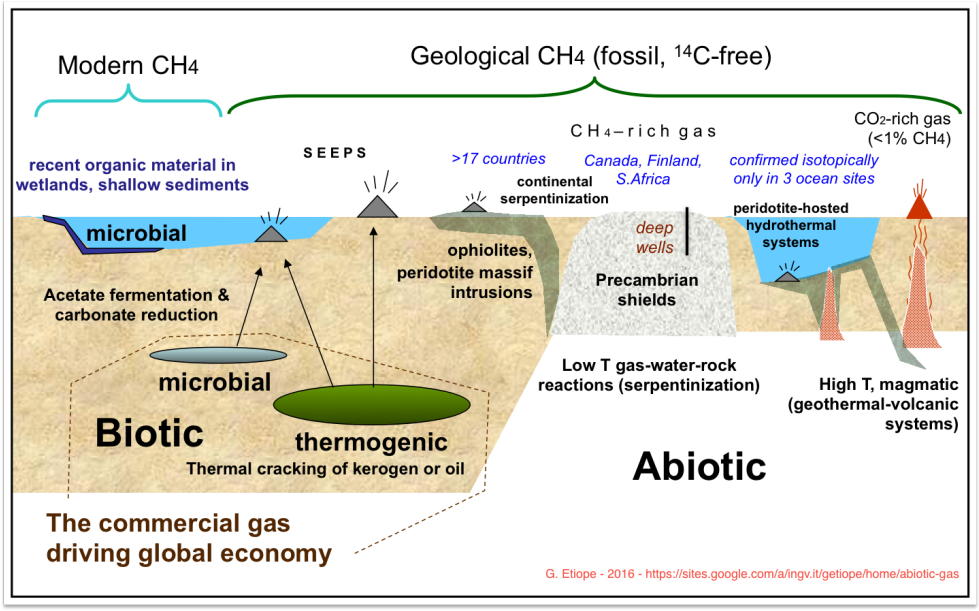


**Figure 7. Diagram indicating methane origins (Biotic vs. abiotic) and environments (terrestrial or marine). Peridotite hosted hydrothermal system fluids may contain abiotic $CH_4$ from low temperature gas-water-rock interactions or high temperature magmatic systems. Figure from Giuseppe Etiope (2016; https://sites.google.com/a/ingv.it/getiope/home/abiotic-gas)**

limiting factors for methane sequestration into the sediment often are 1) the scarcity of sediment fall-out at the depths of mid-ocean ridges and 2) the sediment that is deposited is often fine silt, clay and ooze material (Pettijohn, 1957). Therefore, abiotic methane sequestered into gas hydrates in natural settings is not a common phenomenon.

Detachment faults are usually invoked as the main mechanism for bringing mantle material towards the surface and acting as migration pathways for water to circulate across mantle material (Fig. 6), and therefore the main mechanism in formation of abiotic methane through Fischer-Tropsch reactions (Escartin et al., 2008). However, transform faults offsetting spreading centres may also have the ability to act in a similar role, whereby given oblique movements (some component of extension or compression) on the transform (Rüpke and Hasenclever, 2017), mantle material exhumed on-axis may be brought closer to the seafloor and undergo serpentinization. Transform

faults may also bring seawater into contact with deeper, but previously unaltered mantle material (Rüpke and Hasenclever, 2017). Rüpke and Hasenclever (2017) show that the amount of abiotic methane produced at transform faults rivals the amounts produced at detachment faults, although the speed of offset is an important factor.

## Gas hydrate in marine sediments

Gas hydrates form as crystalline compounds in the shallow subsurface and are found in continental margins and permafrost areas worldwide (Sloan, 1998). Methane is the most common constituent of naturally occurring gas hydrates, although ethane, butane, propane and potentially $CO_2$ can be constituents in hydrate structures (Mohammadi et al., 2008). Gas Hydrate stability is dependent on the pressure and geothermal gradient in the subsurface and/or water column temperature, however, for gas hydrate to form, salinity conditions, methane availability and pore-space are also important factors (Sloan, 1998). Generally, the zone of potential gas hydrate stability covers much of the oceans floor (Kvenvolden et al., 1993), except in abyssal plain settings or mid-ocean ridge settings, where temperatures are too high and/or methane production is low (Kvenvolden et al., 1993). Typically, large sedimentary sequences found on continental margins or contourite deposits are ideal locations for gas hydrate accumulations as the organic matter input is sufficient for the formation of methane either thermogenically or microbially. In addition, the material deposited tends to be coarser-grained than in abyssal plains providing ample pore-space and pressure-temperature regimes are appropriate for gas hydrate stability (Kvenvolden, 1998; Mienert et al., 2005). In contrast, areas of the seafloor where active crust-creation is occurring tend to have limited organic matter, limited sediment deposition and limited biological activity (Calvert, 1987; Canfield, 1993), excepting chemosynthetic communities at hydrothermal vents.

The gas hydrate stability zone, and base thereof, can be predicted using numerical models. The geothermal gradient, bottom water temperature, water depth (pressure), gas composition and salinity are all variables in modelling the base of the gas hydrate stability zone (BGHSZ) and local variations as well as regional variations (spatially and temporally) in these parameters are often attributed to differences in observed and modelled BGHSZ (Vadakkepuliyambatta et al., 2015). Discrepancies between the base of hydrate accumulation and the modelled BGHSZ, or lack thereof, give insight into the gas flux from below the hydrate accumulation, whereby gas flux must exceed a critical value for the base of actual hydrate accumulation and modelled BGHSZ to coincide (Xu and Ruppel, 1999). Inconsistencies in the gas hydrate system, such as cooler temperatures than the regional geothermal gradient would dictate (Ruppel, 1997), have been used to explore the role of pore water composition, pore size and the effect of capillary forces (Ruppel, 1997) in hydrate

stability. The composition of porewater affects the formation and stability of hydrate by certain ions such as NaCl acting to decrease the activity of water (Dickens and Quinby-Hunt, 1997; Ruppel et al., 2005). Capillary forces between sediment grains in very fine-grained sediment (i.e. clay) are high because the meniscus of the water in pore space is small. Strong capillary forces in fine grained clays have been cited as an inhibitor to hydrate formation in such sediments (Ruppel, 1997). Salinity as an inhibitor to hydrate formation is also thought to have an influence on how free gas might migrate through the hydrate stability zone without being sequestered into hydrate. The formation of hydrate increases salinity in porewater (as $H_2O$ is used in the hydrate forming process), which thus inhibits further formation of hydrate for subsequent migrating methane (Liu and Flemings, 2006, 2007).

Inconsistencies in the depth of the BGHSZ compared to the observed bottom simulating reflection have been used to explore the role of faults as conduits of local warm fluid (Fig. 8; Pecher et al., 2010), as well as the local effect of increased salinity due to salt diapirsm (Ruppel et al., 2005), while modelling the gas hydrate stability zone under past conditions has attempted to explain large scale submarine landslides such as the Storegga Slide on the mid-Norwegian margin (Mienert et al., 2005) and assessing how gas hydrate stability might be affected by future oceanic warming (Biastoch et al., 2011).

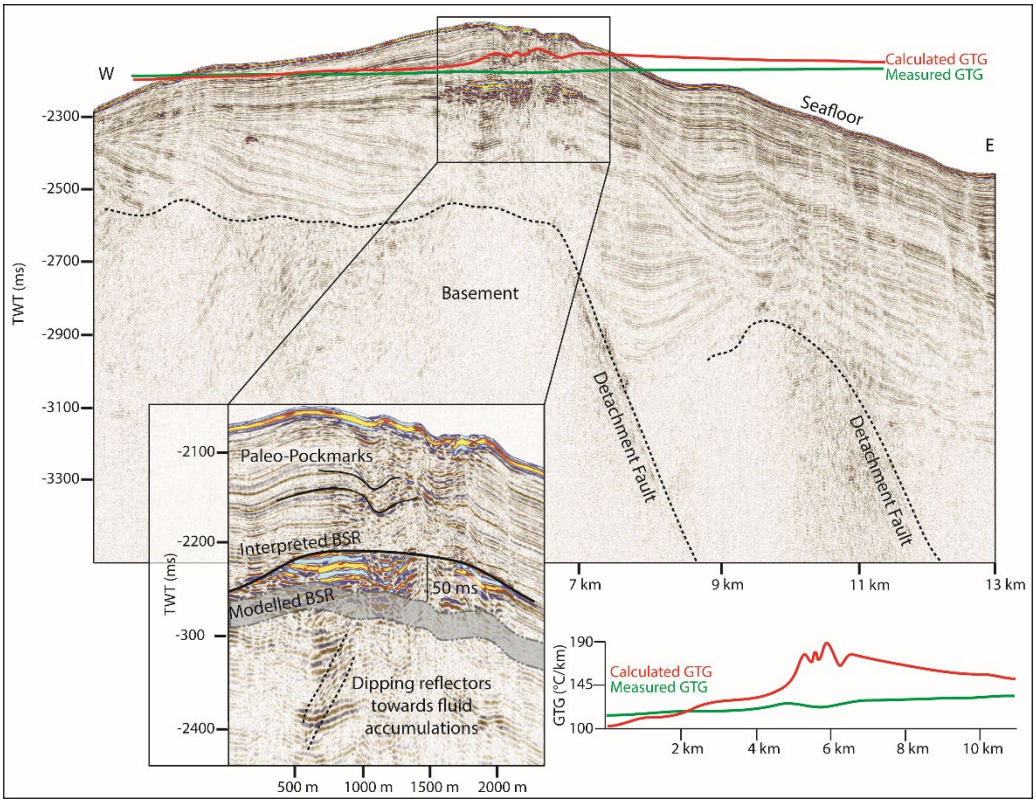


**Figure 8. Example of a discrepancy between the modelled and observed BSR being used to infer subsurface conditions, in this case that there are local areas of higher geothermal gradient due to focussed fluid flow along detachment faults. Figure from (Waghorn et al., Submitted).**

## 1.3 Study Area

The area of interest for this thesis is located in the central Fram Strait on the western flank of the Northern Knipovich Ridge (Fig. 9). The Svyatogor Ridge, the main location discussed in this thesis, is the inside corner high of the Ridge-Transform Intersection (RTI) between the extensional Knipovich Ridge and the strike-slip Molloy Transform Fault (Johnson et al., 2015; Waghorn et al., 2018a). The crust underlying the extended study area is dated with magnetic anomaly data from Chron 6 (19.6 Ma) to Chron 2A (2.8 Ma) while the Svyatogor Ridge is between Chron 5 (9.8 Ma) to Chron 2A (2.8 Ma) (Engen et al., 2008). Fluid flow indicators, including BSR reflections, occur predominantly over the crest of the Svyatogor Ridge (Fig. 9); however, occur elsewhere in the study area where basement outcrops and/or basement faults occur.

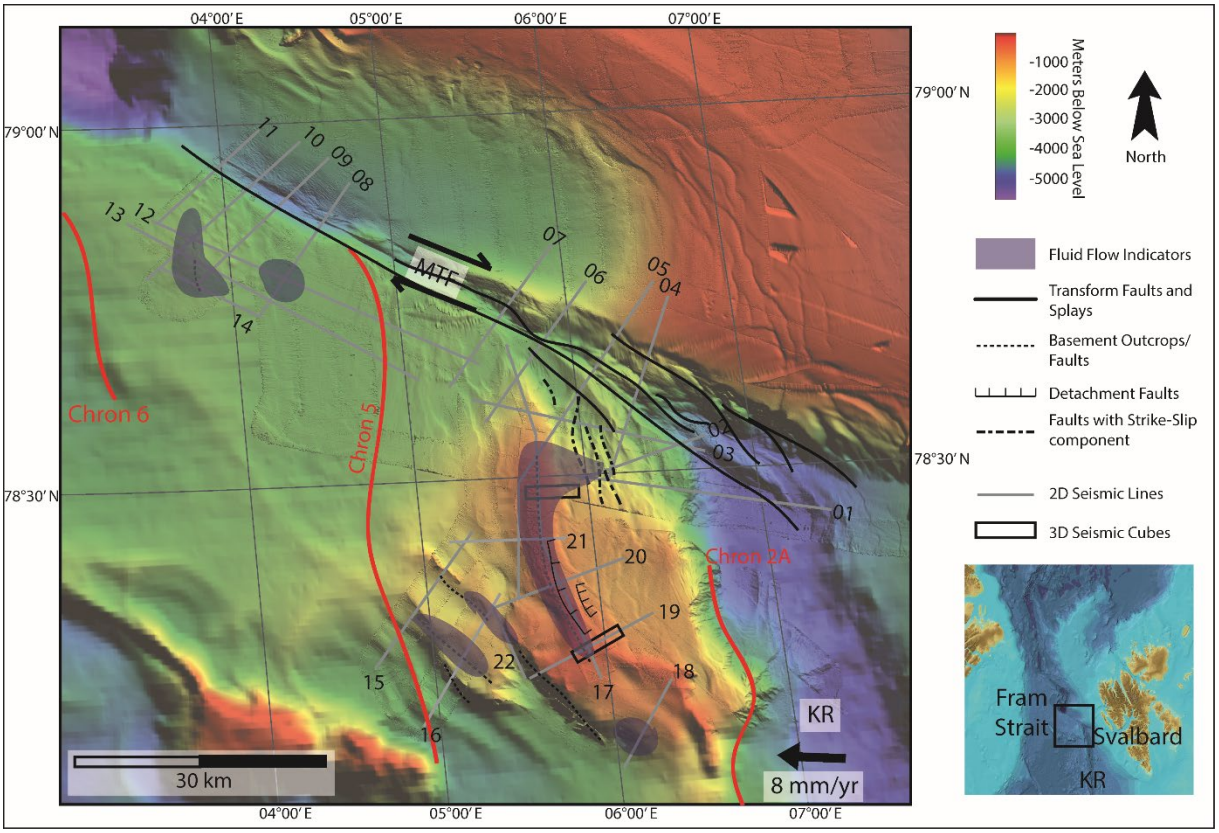


**Figure 9. The study area presented in this thesis. The Svyatogor Ridge lies at the intersection between the Knipovich Ridge (KR) and Molloy Transform Fault (MTF). Seismic lines are numbered as per Waghorn et al. (submitted). The Knipovich Ridge is melt poor, and ultra-slow (~8 mm/yr). The crust underlying Svyatogor Ridge is between 9.8 and 2.8 Ma (Engen et al., 2008), indicated by magnetic Chrons 5 and 2A. Fluid flow indicators documented in Waghorn et al. (2018a) and Waghorn et al. (submitted) are indicated by blue areas. Detachment faults as interpreted in Waghorn et al. (2018a) are marked on the map by ticked lines. Dot-dash lines indicated faults with a strike-slip component as interpreted by Waghorn et al. (submitted), while dotted lines indicate the authors' crustal outcrop or fault interpretations.**

## Tectonic Setting

The Knipovich Ridge orients at approximately 308° and is spreading asymmetrically, at ~8 mm/yr on the western flank (Engen et al., 2008; Okino et al., 2002). The segment of the Knipovich Ridge pertaining to this study area is ultra-slow and melt-poor at present, however some studies suggest that there are igneous intrusions underlying the eastern flank of the Knipovich Ridge (Ritzmann et al., 2002), indicating that magmatic spreading may have occurred in the past. As the Knipovich Ridge is sedimented at this northern segment, it is difficult to determine what the underlying crustal material is, however on the western flank of the Knipovich Ridge, Ritzmann et al. (2002) suggest that the seismic velocities (from OBS data) are concurrent with partially serpentinized material which is consistent with melt-poor spreading. It is worth noting that the distance between Chrons indicate that the Knipovich Ridge spreading rate has changed between 19.6 Ma and recent, which perhaps correlates to changes in spreading mechanism. Chron 6 (19.6 Ma) and Chron 5 (9.8 Ma) conjugate anomalies on the eastern flank of the Knipovich Ridge are not present, indicating that the junction between transform and spreading ridge has migrated northwards (Engen et al., 2008). The Molloy Transform Fault (MTF) delineates the northern extent of the Knipovich Ridge and is oriented non-orthogonally to the spreading axis of the Knipovich Ridge, implying a non-negligible secondary stress orientation. Bathymetry data indicates that the overall MTF is composed of 6-12 individual strike-slip faults with two major branches at the eastern end (Fig. 9). Splay faults off major branches extend into the study area at the Svyatogor Ridge (Fig. 9).

## Oceanographic and Sedimentary Setting

The West Spitsbergen Current (WSC; Fig. 10) is a northward flowing oceanic current that transports warm North Atlantic water into the Arctic Ocean (Beszczynska-Möller et al., 2012). The WSC is an important sediment transportation and deposition current for the entire West Svalbard Margin and slope. The WSC, and eddying therefrom (Fig. 10), are responsible for the formation of contouritic drifts further north (Eiken and Hinz, 1993). Although the WSC has migrated upslope, eastwards, as the West Svalbard Margin has built out, it has likely been an important transport mechanism to the study area (Eiken and Hinz, 1993; Waghorn et al., 2018a). Downslope sedimentation processes such as turbidity currents or slope failures are, at present, an unlikely sediment supply source as the Knipovich Ridge acts as a basin to catch sediment before reaching the Svyatogor Ridge in its present uplifted position. As the method for crustal creation here is exhumation, it follows that exhumation and creation of oceanic crust began before sedimentation (Amundsen et al., 2011; Johnson et al., 2015). In the manner of confined contourites, an uplifted

footwall would likely create the velocity variation required for onset of contourite deposition (Faugères et al., 1999; Rebesco and Stow, 2001).


**Figure 10. The major oceanic circulation in the Fram Strait. Eddying of the West Spitsbergen Current at approximately 78° N is responsible for the sediment deposition and formation of Vestnesa Ridge. Figure from Beszczynska-Möller et al. (2012)**

A stratigraphic framework with confirmed dating for the Svyatogor Ridge is not available in prior literature as of yet, however the YP stratigraphy constrains sediment age on the West Svalbard Margin. YP-1 to YP-3 are the regional framework correlated to ODP leg 151 sites 908-912 (Thiede et al., 1995). YP-1 is the oldest unit with a variable basal age, composed of syn-rift and post-rift sedimentation, deposited atop oceanic crust (Eiken and Hinz, 1993). YP-2 sequence comprises the onset of contouritic deposition with a basal age between 11 Ma and 14.6 Ma (Eiken and Hinz, 1993). YP-3 corresponds to the beginning of glacially transported sediment approximately 2.7 Ma (Eiken and Hinz, 1993). These three seismostratigraphic units correlate to ODP 908 and 909 boreholes using 2D regional seismic data (Knies et al., 2009; Mattingsdal et al., 2014).

# 2. Materials and Methods

This thesis utilized seismic and bathymetry data in order to achieve the objectives outlined in Chapter 1. Acquisition of 18 2D seismic lines, two 3D seismic cubes and bathymetry data (Fig. 9) occurred in conjunction with CAGE cruises aboard the *R.V. Helmer Hanssen* between 2014 and 2018. Seismic data sets, both 2D and 3D are the foundation of articles and manuscripts in this thesis, so seismic data acquisition, processing and interpretation detail follows in subsequent subchapters 2.1 and 2.2. Manuscript III details the process for stress regime analysis, while Manuscript II covers the methods for bathymetric data interpretation and gas hydrate stability zone modelling.

## Overview of seismic reflection for subsurface exploration

Seismic waves are elastic waves that travel through the solid earth, produced by natural phenomena, such as strain release (earthquakes) or artificial sources. Seismometers record these waves, which are visualised as amplitude vs time graphs, or seismograms. As the earth is a heterogeneous medium, it is extremely complex and therefore the propagation of seismic waves through the earth is equally complex (Lowrie, 2007). A number of different types of waves can travel through the earth – body waves (compression and shear waves) and surface waves (Love and Rayleigh waves) – categorized predominately by particle motion along the wave path (Lowrie, 2007). Compression (P) waves can travel through both fluid and solid while shear (S) waves cannot travel through liquids as liquid cannot be undergo shear. Using active source seismology to target specific locations in the subsurface is an important exploration tool. The basic principle for using seismic energy as a subsurface imaging tool is that elastic waves follow some fundamental rules as they propagate through the subsurface. Firstly, given a medium with homogeneous, isotropic properties, a wave will travel with a velocity defined by the bulk modulus (incompressibility), the shear modulus (rigidity) and the density of the material (Lowrie, 2007). Secondly, at an interface between two media with differing impedance properties, some energy will transmit while some energy will reflect. The amplitude of reflected waves will be dependent on the impedance contrast between the two materials (Lowrie, 2007). Reflected waves then travel back towards the surface, where hydrophones or seismometers record the incoming signal. The resolution of seismic data is typically ¼ of the wavelength, which is a function of the frequency and velocity. Therefore, high-resolution seismic data by nature will have lesser penetration that lower resolution data sets. It has been a goal of seismic data acquisition and processing to increase the resolution while attaining sufficient penetration. Broadband seismic, where the frequency band of the data covers a larger range (ex 'conventional' data usually has a frequency band of 8-80 Hz, while broadband can range from 2-200

Hz) is the state-of-the-art for optimising both resolution and penetration, however in marine settings the low frequency end of the spectrum is still limited by low frequency noise. Using only near-offset data is another solution, where the far offset hydrophones record data with greater penetration while the near-offset hydrophones can be isolated for resolution purposes however the P-Cable 3D seismic acquisition system (see Chapter 2.1) combines a relatively broadband frequency range with near-offset data to increase the resolution in the shallow subsurface.

Ideally, the seismic record should only contain signal reflected back from interfaces between materials of differing properties. However, noise is an inevitability; therefore, processing steps improve the signal-noise ratio by removing external sources or unwanted signal in the data (Yilmaz, 2001). Generally, processing workflows follow the same basic steps of improving the signal to noise ratio by attenuating random and coherent noise, reducing artefacts such as multiples and improving the resolution of the data while retaining a wavelet representative of the interface that reflected the signal (Brown, 2004; Yilmaz, 2001). The goal of seismic processing workflows are to provide the best possible image of the subsurface and allow the end-user to interpret features present with confidence (Yilmaz, 2001).

## 2.1 Seismic data acquisition and processing

The P-Cable seismic acquisition system is a high-resolution acquisition set-up, which enables users to acquire 3D data sets with relative ease and low cost, and it can also be re-configured into 2D mode to acquire 2D seismic data. The data collected for this study utilized the P-Cable system. For 2D acquisition, 4 x 25 m streamers are connected resulting in a 100 m streamer with receiver intervals of 3.125 m. Typically, the source was 15/30 $in^3$ mini-GI airguns firing at 160-170 bar, while the firing rate depended on the depth of the water column. Recording parameters of 2D seismic data also was a function of the water depth however typically with a sampling rate of 0.25-0.5 ms and recording length of up to 5 s. 3D data acquisition involves a cross-cable with 14 streamers spaced ~12.5 m apart (Fig. 11). All streamers have a receiver interval of 3.125 m, 8 channels per streamer. The cross-cable is towed perpendicular to the sailing direction approximately 150 m behind the ship, held taut by two paravanes. Both 3D surveys utilized airguns set up in harmonic GI mode, where the generator chamber produces the primary pulse and the secondary injector chamber injects a second pulse at or near the maximum expansion of the primary pulse. Air gun setup for the southern 3D dataset was 15/15 $in^3$ in while the northern 3D dataset was 45/45 $in^3$,

both at 150-160 bar of pressure and a shooting interval of 6 s. Recording parameters included a sampling rate of 0.25 ms and recording length of 2 s.

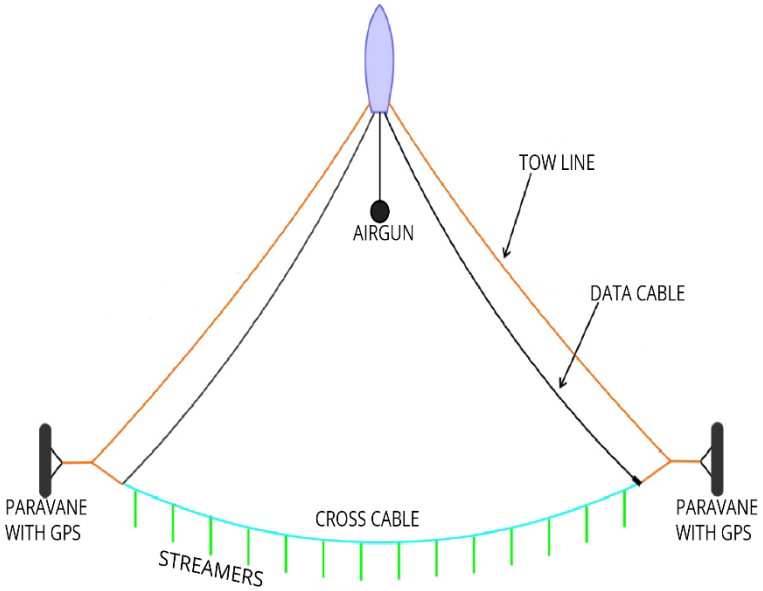


**Figure 11. Simple schematic of the 3D P-cable systems. Modified from www.geometricspcable.com, accessed 27.03.2019**

Processing of both 2D and 3D data sets followed standard processing workflows using RadEx Pro seismic data processing software, described in detail in paper I and III for the 3D data sets and paper II for the 2D data sets. The processing workflow for 3D data sets followed the same basic procedure and differed where case-specific steps were necessary.

**Processing workflow**

1. SEG-D Input
2. Geometry assignment in RadEx Pro
3. Bandpass Filtering using a simple filter where frequencies outside the range of 15-300 Hz were completely removed and frequencies between 15-30 Hz and 250-300 Hz were ramped
4. Burst noise removal (only necessary for northern 3D data set)
5. Adjustment of geometry* (post publication for southern 3D data set)
6. Tidal correction*[1]
7. Wavelet based processing *[2]
8. CDP Binning to 6.25 m

9. NMO and Stack
10. Interpolation
11. Static corrections *[1]
12. Migration *[3]
13. SEGY-Output

*The geometry adjustment was implemented during the shipboard processing of the 2016 data set because the software supposed some form of symmetry when calculating a catenary for the crosscable (Romeyn, 2017). However, when current influences the crosscable orthogonally, symmetry in the streamer is lost and the geometry assignment in RadExPro was misfitting significantly for one half of the streamers, alternating with sailing direction.

*[1]Tidal correction for the southern data set was ~0.02 m extrapolating between sites near Longyearbyen and offshore Greenland. As this assumption could not account for the funnelling effect of tides into fjords, it was deemed inadequate. A predictive static correction later in the processing workflow, along with migration, served to reduce static artefacts in the data to a sufficient level

*[2]Wavelet based processing included debubbling, deghosting and denoising as well as deconvolution. For the southern 3D dataset, the data was published prior to implementing these steps so the version presented is the non-wavelet based processing version.

*[3]We migrated the southern 3D data set in SeisSpace using a velocity model that combined assumptions of velocities based on predicted material present (for example assuming similar deposition as that found in the closest drill site, IODP 910 (Thiede et al., 1995)), published velocity information (Ritzmann et al., 2002) and calculating diffraction hyperbola velocities. The northern 3D dataset was migrated in RadEx using a pre-stack Kirchhoff Time migration, and a velocity model created using diffraction hyperbola.

Although there were differences in the processing workflows between the two 3D dataset as the base processing workflow improved, the interpretability of the southern data set was not significantly affected after implementing additional steps. This is likely in part due to the water depth (travel time differences between the source and receiver ghosts and reflected signal are less significant in greater water depths and bubble pulses are attenuated more).

All 2D data was re-processed in conjunction with paper II so that lines were consistent, with the exception of 2018 data. The 2D data processing method was very simple, and consisted the following

1. SEG-D Input
2. Geometry assignment in RadEx Pro
3. Bandpass Filtering using a simple filter where frequencies outside the range of 15-300 Hz were completely removed and frequencies between 15-30 Hz and 250-300 Hz were ramped
4. Burst noise removal
5. CDP Binning to 3.125 m
6. NMO and Stack
7. Migration using Kirchhoff Time Migration (aperture dependent on water depth and reflector depth, velocity from Ritzmann et al. (2002))
8. SEGY-Output

## 2.2 Interpretation of seismic data

Interpretation of all seismic data occurred in Petrel Software. The three focuses for interpretation were 1) stratigraphy 2) structure and 3) fluid indicators. Interpretation procedure generally first mapped reflectors and determined a base depositional environment and history, followed by structure mapping, structural analysis and finally fluid-flow indicator mapping and analysis.

### Stratigraphy

Chapter 1.3 summarizes the regional stratigraphy, where the YP sequences are the regional seismostratigraphic framework used in the region of this study (Eiken and Hinz, 1993; Mattingsdal et al., 2014). The YP framework was initially the basis for interpretation here. However, it became clear that the correlation of the YP units across the Molloy Transform Fault was too uncertain especially given a large difference in resolution between correlation lines (Mattingsdal et al., 2014) and the data sets used here. The method for determining stratigraphy for all the seismic data

became to develop a seismic stratigraphy/facies model independent of the YP stratigraphy. Changes in depositional dynamics can often create unconformable features such as erosional truncations, onlaps, downlaps or changes in internal reflection character (Mitchum Jr et al., 1977). In this data set, two unconformable horizons and changes in thickness (indicating a change in depocentre) delineate the stratigraphy (Waghorn et al., 2018a). Significant changes in reflection characteristics, such as a change from conformable, continuous horizontal reflections to chaotic, incoherent reflections determined changes between sedimentary material and igneous/metamorphic material.

## Structure

Fault mapping is the first step for determining a structural framework and tectonic history of the study area. Faults in the data from this study area are identified as either 1) low amplitude discontinuities through the data set, generally sub-vertical, whereby reflections on either side of the discontinuity are offset (Brown, 2004) or 2) Areas of reflection orthogonal to the main sedimentary reflection orientation, where sedimentary material is adjacent to interpreted basement material. As faults with very small offsets (i.e. reaching the limit of resolution) may be difficult to interpret with vertical seismic sections, variance/coherence attributes have been used in conjunction with fault mapping and structural interpretation (Brown, 2004; Chopra and Marfurt, 2007). Variance computes the continuity between traces in a specified window, preferably a horizon, and outputs the variance on a scale of 0 (no discontinuity, grey) to 1 (complete discontinuity, red). Any discontinuity is highlighted with this attribute, however for the data sets used here faults were the discontinuity of interest. Fault picks can be input into a structural model, where reference horizons act as checks that the fault planes are geologically feasible. Creating a geologically sound structural model allows dip and dip direction information to be extracted from the fault plane, or from discreet segments along the plane. From this, the azimuth, dip and dip direction of fault planes interpreted in 3D seismic data can be plotted on a stereonet (van Gent et al., 2009). This method of using 3D seismic data for stress analysis is useful in determining the stress regime that formed faults.

Win_Tensor software (Delvaux and Sperner, 2003) uses Schmidt Lower Hemisphere stereonets to extract orientations of faults' kinematic axes. Each fault plane has a P (compression) B (neutral) and T (tensional) axis that approximate the directions of principle stress (Célérier, 2010) where the P axis represents the maximum compressive stress direction and T the minimum compressive stress direction. For this analysis, the Right Dihedra method divides the hemisphere into four quadrants, where two are compressional and two extensional (Delvaux and Sperner, 2003). As multiple fault planes are plotted, the possible locations of the kinematic axes are narrowed until an approximation can be made.

## Fluid Indicators

Again, seismic sections are the predominant means of interpreting fluid features in these data sets. BSR reflections were interpreted based on their high amplitude, cross cutting, sea floor simulating, and reverse polarity nature. Other direct hydrocarbon indicators were otherwise lacking. Pockmarks were interpreted when a clear u-shaped surface existed that acted as an erosional surface, and generally had a higher amplitude than the on-lapping infill (Judd and Hovland, 2007). Other indirect fluid flow indicators such as pipes were largely absent in these data sets although one chimney structure was interpreted in article I (Waghorn et al., 2018a), it was based on the interpretation of paleo-pockmarks rather than interpreted as a discreet feature. Other fluid indicators, such as mounds (manuscript II), were interpreted based on anomalies in reflector configuration and/or amplitude, coupled with for example, the presence of clustered small offset faults in otherwise continuous reflections. In general, disruptions in normal reflection configuration and continuity were investigated for potential links to fluid migration and accumulation.

# 3. Summary of Articles and Manuscripts

## Article I

**Kate A. Waghorn**, Stefan Bünz, Andreia Plaza-Faverola, Joel E. Johnson. 3D Seismic investigation of a gas hydrate and fluid flow system on an active mid-ocean ridge; Svyatogor Ridge, Fram Strait. *Geochemistry, Geophysics, Geosystems. 19*(8), 2325-2341, DOI: 10.1029/2018GC007482

**Article I** focused on creating a framework for the sedimentary and tectonic setting of the Svyatogor Ridge, on the western Knipovich Ridge flank. Using a high-resolution, 3D P-Cable seismic data and supplementary bathymetry data, we created a seismic stratigraphy based on strata configuration and character, determined the sedimentary deposition history to the extent possible with remote methods. Article I established a basis for future studies on tectonic activity and stress environments on the Svyatogor Ridge by characterising patterns in faulting and asserting a tectonic history of the region. Lastly, this article gives insight into the fluid flow system present on the Svyatogor Ridge and draws some conclusions based on the sedimentary depositional environment and tectonic environment as to the longevity of fluid seepage here.

Key findings with regard to the sedimentary depositional environment on the Svyatogor Ridge are that the depocentre of stratigraphies has migrated east with time, in agreeance with the presumption that as the West Spitsbergen Current has migrated upslope in the east, the Svyatogor Ridge has migrated west. Four types of faults were identified – basement detachment faults, sedimentary growth faults, radial faults and small-offset fault/fracture networks. The environment and spreading regime of the Knipovich Ridge, and the Svyatogor Ridge being an inside corner high, supported the interpretation of detachment faults in the data set. Sedimentary fault terminations focus around the downthrown hanging wall of detachment faults and based on their offsets have grown in stages upwards (increasing throw with depth), indicating they are growth faults which form as a mechanically stronger basal material faults underneath a sedimentary sequence. In some cases, growth faults reach the seafloor indicating that seismicity on the detachment faults has occurred syn or even post sedimentation, however it was not possible to determine whether these faults have reactivated post detachment fault activity, in response to fluid migration.

The extent and distribution of the gas hydrate system is limited to the apex of the ridge structure, centred about the detachment fault. This article asserts that this is a function of the detachment fault focussing fluid migration, however the antiformal shape of the ridge structure may play a role. The dataset provides evidence of 4 distinct time periods of paleo-fluid seepage, as

evidenced by paleo-pockmarks occurring only on four horizons. This article hypothesizes that seismicity, a seismic pumping system, may be playing a role in determining when gas migrates into the sedimentary column, and further to the seafloor.

## Manuscript II

**Kate Alyse Waghorn**, Sunil Vadakkepuliyambatta, Andreia Plaza-Faverola, Joel E. Johnson, Stefan Bünz, Malin Waage. Crustal processes sustain arctic abiotic gas hydrate and fluid flow systems. Submitted to *Scientific Reports* for consideration 26/02/2019.

**Manuscript II** investigates the linkage between large-scale tectonic features and fluid flow/gas hydrate systems considering a larger region than investigated in Article I. While article I established a framework for further studies, this manuscript gives further insight into the tectonic environment, large-scale tectonic features captured in our seismic data sets and the influence the regional tectonism has on methane migration. For this study 22 2D seismic lines were used, covering the entire inside corner high of the Knipovich Ridge-MTF intersection.

A significant observation presented in this paper is the strong correlation between fluid accumulations, interpreted as free gas trapped underneath gas hydrate, and crustal faults or tectonic lineaments related to spreading or transform fault dynamics. Underneath the majority of free gas accumulations, we identify uplifted crust, and often can identify fault planes within the interpreted crust. We therefore modelled the expected Base of Gas Hydrate Stability (i.e., where the BSR should form) with geothermal gradient data from previous studies. The result of this modelling is that where we identify crustal structure beneath a free gas accumulation, the location of the BSR in the sedimentary sequences correlates with a higher geothermal gradient value than published data suggests. However, in areas of free gas with no observable basement structure beneath, BSR depths fit within a margin of error to the depth expected based on published geothermal gradient values. We attribute this to crustal structure locally increasing the geothermal gradient through circulation of warmer fluids from depth.

This manuscript also asserts that these accumulations above crustal structure where there are likely increased temperatures, support initial hypotheses of abiotic methane contributing to the gas hydrate system here. Although we cannot support this hypothesis with geochemical evidence at this point, we assert that the geophysical evidence favours an abiotic methane source.

## Manuscript III

**Kate A. Waghorn**, Rowan Romeyn, Andreia Plaza-Faverola, Stefan Bünz. Shallow gas redistribution coupled to Arctic Mid-Ocean Ridge tectonics. Manuscript in preparation.

Manuscript III details the stress environment on the Svyatogor Ridge based on mapping sedimentary growth fault planes in 3D, across two 3D seismic data sets. One data set is located at the Northern end of the ridge, with another in the south. As the Knipovich Ridge has propagated northwards into its present-day position, and is likely propagating further northwards, the orientation of minimum horizontal stress acting on the Svyatogor Ridge and environs has likely rotated with regards to the sediment accumulated on the Svyatogor Ridge to account for this propagation. The aim of Manuscript III was to determine if some record of changing stress regimes existed in the orientation (dip, dip direction and azimuth) of the fault planes in the sedimentary sequences. As the sedimentary faults on the Svyatogor Ridge have grown because of crustal detachment fault propagation, the orientation of slip should reflect a combination of the orientation of the master (crustal) fault and the orientation of minimum horizontal stress. This manuscript finds that the orientation of stress axes differs across groups of faults (with converging principle stress axes) indicating that faults in both data sets have developed under two phases of extensional motion, and along fault planes we find that the oblique slip nature indicates a reactivation under different stress orientations. It was not possible to determine what role reactivation due to fluid migration may have played in these faults. Typically, fluid migration forcing reactivation of faults results in fault planes with steep dips, and azimuths which are not necessarily consistent with the regional stress regime, as fluid overpressure can override the regional stress. Although the role fluid overpressure may play in reactivation here could not be determined, there is no additional evidence of fluid migration, such as pockmarks or bright spots, associated with most of the sedimentary fault planes. The only fault which exhibits fluid-related features is a single sedimentary fault piercing the BSR and culminating in seafloor pockmarks.

Small faults interpreted in Article I as fault and fracture networks are only identified within a small area encompassing the free gas zone and into the gas hydrate stability zone. None of these faults had appropriate stress axes to form a general stress orientation and so could not be grouped as per the sedimentary faults. However, following the interpretation from Article I that these faults are fluid migration-forced faults, this is unsurprising. That we do not identify similar faults in the northern dataset hints to timing of fluid migration and stress regime orientation changes – we do however note that all pockmarks and paleo-pockmarks in the northern dataset are along growth faults and chains of pockmarks strike at an orientation predictable given the present day tectonic

regime. We assert that stress orientation rotation over time has limited fluid migration through growth faults in the southern dataset, forcing fluid redistribution through networks of small faults and fractures – a phenomenon often observed in compressional stress environment hydrothermal systems. We conclude that changing stress regimes through time have controlled faulting, fault reactivation and determined the mechanics of fluid migration through the subsurface.

# 4. Synthesis

## 4.1 Summary

The overall aim of this thesis was to determine the origins of the fluid flow and gas hydrate systems on the Svyatogor Ridge and in the surrounding inside corner of the Knipovich Ridge-MTF intersection, and the mechanisms controlling fluid migration and accumulation.

Although the Svyatogor Ridge hosts a gas hydrate system, a major conclusion from the work presented here is that cold-seep systems are not the ideal analogue for the Svyatogor Ridge, and that many of the processes interpreted here have fitting analogies in hydrothermal seep systems. Such interpretations include seismic pumping causing episodic intervals of fluid seepage followed by prolonged inactivity (Sibson, 1990), and the potential contribution of abiotic methane – documented extensively in peridotite hydrothermal systems (Charlou et al., 1998; Etiope and Sherwood Lollar, 2013; Proskurowski et al., 2008). Although only spatially linked, the discovery that gas hydrates/free gas occurs coincident with basement outcrops, basement faults and major tectonic lineaments in the area is perhaps the most conclusive evidence this study has found to support the hypothesis of an abiotic methane contribution here (Johnson et al., 2015). It certainly indicates that basement faults are central in the distribution of gas hydrate and fluid flow systems in the study area. This finding also supports Rüpke and Hasenclever (2017) findings that transform faults are overlooked sources of serpentinization reactions and abiotic methane generation.

Fluid migration through small-offset faults despite the presence of optimally oriented larger faults is typically observed in hydrothermal systems but undocumented in gas hydrate fluid systems (Sibson, 1996). RTI's are areas of high stress, which can lead to hotspot-type seamount formation when faulting through the crust create pressure gradients to funnel fluid upwards. This study has found that on the Svyatogor Ridge, especially in the southern data set (Waghorn et al., 2018a) fluid is predominately migrating through small offset faults on the footwall of larger sedimentary growth faults. This phenomenon typically manifests where compression stresses are predominant rather than in extensional regimes, however Manuscript III asserts that the high stress nature of the RTI setting, coupled with a stress rotation as the Knipovich Ridge migrates, is creating an environment where fluid overpressure is the driver of faulting, and reactivations of sedimentary growth faults are temporally constrained.

Globally, settings where gas hydrate accumulations can occur at spreading margins are rare. This thesis has documented a landmark case of potential abiotic methane hydrate reservoirs, which are currently unaccounted for in the global carbon inventory, and opens up sedimented, melt-poor

spreading ridges and their paleo-counterparts as potential carbon reservoirs in the deep oceans. Although likely these settings do not pose significant risks for release of methane into the atmosphere presently, the long-term stability and future consequences for carbon cycles are not yet known.

## A note on methane origins

It is likely the most scientifically controversial conclusion drawn here; this thesis supports abiotic methane contributions to the gas hydrate system. Although determining the origin of methane was not a predominant objective as stated in chapter 1, the abiotic hypothesis was a driver for this project beginning. Without geochemical data to support hypotheses, any assertions are still highly speculative; however, the following observations and factors were important in drawing the conclusion that abiotic methane is being produced and contributing to the hydrate system:

- A significant correlation between basement faults and free gas accumulations. While correlation and causation are not intrinsic, areas of uplifted basement and/or crustal faulting are the only places where we observe BSR.

- Timing of contourite development vs. rifting and separation from the West Svalbard Margin. Article I posits that detachment fault uplift occurred prior to the bulk of sedimentation on the Svyatogor Ridge, implying that spreading was developed and underway during gas charge into the sediment. This indicates that, with continued mid-ocean ridge spreading, fluid migration from a West Svalbard Margin gas source must traverse an increasingly defined tectonic boundary to accumulate on Svyatogor Ridge

- After rifting began, the likelihood of thermogenic methane charge from the north (Vestnesa Ridge area) is low. Major tectonic features, the Knipovich Ridge and MTF, separating this study area from the West Svalbard Margin act as impediments for migrating methane rather than conduits. In addition, the paleo-detachment fault (Crane et al., 2001; Peive and Chamov, 2008) acts as a major tectonic barrier to fluid migration from the Hovgård Ridge area where thermogenic methane also forms (Knies and Mann, 2002). Lastly, from any of the known sites of thermogenic methane formation, stratigraphy based on our seismic data indicates significant down-dip migration to reach the study area, which is also unlikely.

- In-situ thermogenic methane formation at this study site is improbable. Thermogenic methane formation occurs at significant pressure and temperature. Although the thermal regime is conducive to thermogenic methane generation, the crust is too young to have accumulated the

Miocene source rock that generates thermogenic methane found at other study sites in the area, and the basement outcrops to less than 500 m below the seafloor in much of this study area implying pressure conditions less than ideal. Although there are likely localized basins surrounding the study area that have a thicker sediment column, it is unknown whether the sediment contains enough organic matter for thermogenic methane generation.

- Many of the locations on the eastern flanks of the Svyatogor Ridge (manuscript II) with fault-trapped free gas accumulations imply some down-dip fluid migration, unless sourced from underlying crustal faults.

While there is no evidence that thermogenic methane is not migrating into the study area (i.e. crustal faults as conduits), nor that microbial methane is not being produced in-situ, there is a strong likelihood that abiotic methane is contributing to the hydrate system here.

## 4.2 Outlook

The Svyatogor Ridge and the Knipovich-MTF intersection in general has shown that Arctic mid-ocean ridges, sedimented mid ocean ridge flanks and melt-poor, exhumation dominated mid-ocean ridges have potential to store methane in the form of gas hydrate regardless of gas source. As the history of fluid processes from the mantle into the ocean have been capped by sediment for a significant portion of the history of Svyatogor Ridge, changes in the fluid flow system may be recorded in terms of pore-water geochemistry, remineralisation processes etc. Hints towards spreading processes in the past may also be recorded in the sedimentary sequences in this study location. If this is the case, sites similar to the Svyatogor Ridge have potential to provide insight into not only gas hydrate systems, but also interactions and processes that occur and change through time at mid-ocean ridge settings. Understanding such processes through geological time, as well as linking deep processes to shallow subsurface processes in the present and past, gives an important insight into how systems might react to oceanic, climatic and tectonic changes in the future.

The potential for this site to host abiotic methane is also exciting for future studies. Due to the lack of natural abiotic methane hydrates, there are several unknowns. For example, do other fluid constituents produced in the gas-water-rock interactions that form abiotic methane affect the formation and stability of the hydrate in these settings? Debate still surrounds the exact formation mechanisms for abiotic methane (Etiope and Whiticar, 2019) and also the amount of methane that can be produced by gas-water-rock interactions. A site such as Svyatogor Ridge, which is storing methane within the sedimentary column, could help to answer how much abiotic methane is produced and over what time scales these processes occur.

Etiope and Whiticar (2019) assert that the amount of methane emissions from continental abiotic methane sites could be of a similar amount to emissions from natural gas seeps in petroleum basins. If this is indeed an accurate representation of the amount of $CH_4$ produced in abiotic methane environments, it is not insignificant and should be accounted for in global carbon inventories. Not all sites shown in this thesis have evidence of fluid seepage in the past (see manuscript II), which may be due to lack of forcing (not enough fluid accumulation beneath the gas hydrate stability zone, for example) or due to a change in processes (less peridotite→serpentine for example, less microfracturing driving long-lived serpentinization, lesser seawater percolation to depth, less heat//too much heat). In either case the Svyatogor Ridge and environs provide a natural laboratory to study abiotic methane and crustal fluid processes through time and space.

A proposal for IODP drilling on the Svyatogor Ridge is in preparation. Given the potential for deep drilling to occur here, the origin of methane here can be determined to remove the speculative nature of abiotic methane hydrate occurrences. Aside from this, noble gas in pore water should indicate the origin of other fluids (deep fluid vs. seawater), remineralisation processes and changes of remineralisation processes in the sediment through time can indicate changes in temperature, fluid chemistry and spreading regime, and the age of sediment can be constrained. Ideally, IODP drilling at this site should also indicate the amount of serpentinization (and following the amount of $H_2$ produced for abiotic methane), and hopefully constrain how long serpentinization can occur and the amount of methane produced.

# References


Abrajano, T., Sturchio, N., Kennedy, B., Lyon, G., Muehlenbachs, K., and Bohlke, J., 1990, Geochemistry of reduced gas related to serpentinization of the Zambales ophiolite, Philippines: Applied Geochemistry, v. 5, no. 5-6, p. 625-630.

Allen, D. E., and Seyfried Jr, W., 2004, Serpentinization and heat generation: constraints from Lost City and Rainbow hydrothermal systems1: Geochimica et Cosmochimica Acta, v. 68, no. 6, p. 1347-1354.

Amundsen, I. M. H., Blinova, M., Hjelstuen, B. O., Mjelde, R., and Haflidason, H., 2011, The Cenozoic western Svalbard margin: sediment geometry and sedimentary processes in an area of ultraslow oceanic spreading: Marine Geophysical Research, v. 32, no. 4, p. 441-453.

Andreassen, K., Hubbard, A., Winsborrow, M., Patton, H., Vadakkepuliyambatta, S., Plaza-Faverola, A., Gudlaugsson, E., Serov, P., Deryabin, A., and Mattingsdal, R., 2017, Massive blow-out craters formed by hydrate-controlled methane expulsion from the Arctic seafloor: Science, v. 356, no. 6341, p. 948-953.

Anderson, E. M., 1905, The dynamics of faulting: Transactions of the Edinburgh Geological Society, v. 8, no. 3, p. 387-402.

Axen, G. J., 1992, Pore pressure, stress increase, and fault weakening in low-angle normal faulting: Journal of Geophysical Research: Solid Earth, v. 97, no. B6, p. 8979-8991.

Berndt, C., 2005, Focused fluid flow in passive continental margins: Philosophical Transactions of the Royal Society of London A: Mathematical, Physical and Engineering Sciences, v. 363, no. 1837, p. 2855-2871.

Beszczynska-Möller, A., Fahrbach, E., Schauer, U., and Hansen, E., 2012, Variability in Atlantic water temperature and transport at the entrance to the Arctic Ocean, 1997–2010: ICES Journal of Marine Science: Journal du Conseil, p. fss056.

Beutel, E. K., 2005, Stress-induced seamount formation at ridge-transform intersections: SPECIAL PAPERS-GEOLOGICAL SOCIETY OF AMERICA, v. 388, p. 581.

Biastoch, A., Treude, T., Rüpke, L. H., Riebesell, U., Roth, C., Burwicz, E. B., Park, W., Latif, M., Böning, C. W., and Madec, G., 2011, Rising Arctic Ocean temperatures cause gas hydrate destabilization and ocean acidification: Geophysical Research Letters, v. 38, no. 8.

Blackman, D. K., and Forsyth, D. W., 1989, Axial topographic relief associated with ridge-transform intersections: Earth and planetary science letters, v. 95, no. 1-2, p. 115-129.

Brown, A. R., 2004, Interpretation of Three-Dimensional Seismic Data, Tulsa, Oklahoma, USA, AAPG and the Society of Exploration Geophysicists, AAPG Memoir.

Buck, W. R., Lavier, L. L., and Poliakov, A. N., 2005, Modes of faulting at mid-ocean ridges: Nature, v. 434, no. 7034, p. 719.

Calvert, S., 1987, Oceanographic controls on the accumulation of organic matter in marine sediments: Geological Society, London, Special Publications, v. 26, no. 1, p. 137-151.

Canfield, D. E., 1993, Organic matter oxidation in marine sediments, Interactions of C, N, P and S biogeochemical Cycles and Global Change, Springer, p. 333-363.

Cann, J. R., Prichard, H. M., Malpas, J. G., and Xenophontos, C., 2001, Oceanic inside corner detachments of the Limassol Forest area, Troodos ophiolite, Cyprus: Journal of the Geological Society, v. 158, no. 5, p. 757-767.

Cannat, M., Sauter, D., Mendel, V., Ruellan, E., Okino, K., Escartin, J., Combier, V., and Baala, M., 2006, Modes of seafloor generation at a melt-poor ultraslow-spreading ridge: Geology, v. 34, no. 7, p. 605-608.

Cartwright, J., James, D., and Bolton, A., 2003, The genesis of polygonal fault systems: a review: Geological Society, London, Special Publications, v. 216, no. 1, p. 223-243.

Cartwright, J., and Santamarina, C., 2015, Seismic characteristics of fluid escape pipes in sedimentary basins: implications for pipe genesis: Marine and Petroleum Geology, v. 65, p. 126-140.

Cathles, L., Su, Z., and Chen, D., 2010, The physics of gas chimney and pockmark formation, with implications for assessment of seafloor hazards and gas sequestration: Marine and petroleum Geology, v. 27, no. 1, p. 82-91.

Cathles, L. M., 1990, Scales and effects of fluid flow in the upper crust: Science, v. 248, no. 4953, p. 323-329.

Célérier, B., 2010, Remarks on the relationship between the tectonic regime, the rake of the slip vectors, the dip of the nodal planes, and the plunges of the P, B, and T axes of earthquake focal mechanisms: Tectonophysics, v. 482, no. 1-4, p. 42-49.

Charlou, J. L., Fouquet, Y., Bougault, H., Donval, J. P., Etoubleau, J., Jean-Baptiste, P., Dapoigny, A., Appriou, P., and Rona, P. A., 1998, Intense CH4 plumes generated by serpentinization of ultramafic rocks at the intersection of the 15 20′ N fracture zone and the Mid-Atlantic Ridge: Geochimica et Cosmochimica Acta, v. 62, no. 13, p. 2323-2333.

Chopra, S., and Marfurt, K. J., 2007, Seismic attributes for prospect identification and reservoir characterization, Society of Exploration Geophysicists and European Association of ….

Claypool, G. E., and Kvenvolden, K. A., 1983, Methane and other hydrocarbon gases in marine sediment: Annual Review of Earth and Planetary Sciences, v. 11, no. 1, p. 299-327.

Collins, R. E., 1976, Flow of fluids through porous materials.

Crane, K., Doss, H., Vogt, P., Sundvor, E., Cherkashov, G., Poroshina, I., and Joseph, D., 2001, The role of the Spitsbergen shear zone in determining morphology, segmentation and evolution of the Knipovich Ridge: Marine geophysical researches, v. 22, no. 3, p. 153-205.

Davy, B., Pecher, I., Wood, R., Carter, L., and Gohl, K., 2010, Gas escape features off New Zealand: Evidence of massive release of methane from hydrates: Geophysical Research Letters, v. 37, no. 21.

Delaney, J. R., Johnson, H. P., and Karsten, J. L., 1981, The Juan de Fuca ridge—hot spot—propagating rift system: new tectonic, geochemical, and magnetic data: Journal of Geophysical Research: Solid Earth, v. 86, no. B12, p. 11747-11750.

Delvaux, D., and Sperner, B., 2003, Stress tensor inversion from fault kinematic indicators and focal mechanism data: the TENSOR program: New insights into structural interpretation and modelling, v. 212, p. 75-100.

Dick, H. J., Lin, J., and Schouten, H., 2003, An ultraslow-spreading class of ocean ridge: Nature, v. 426, no. 6965, p. 405-412.

Dickens, G. R., and Quinby-Hunt, M. S., 1997, Methane hydrate stability in pore water: a simple theoretical approach for geophysical applications: Journal of Geophysical Research: Solid Earth, v. 102, no. B1, p. 773-783.

Dott Jr, R., 1963, Dynamics of subaqueous gravity depositional processes: AAPG Bulletin, v. 47, no. 1, p. 104-128.

Eiken, O., and Hinz, K., 1993, Contourites in the Fram Strait: Sedimentary Geology, v. 82, no. 1, p. 15-32.

Engen, Ø., Faleide, J. I., and Dyreng, T. K., 2008, Opening of the Fram Strait gateway: A review of plate tectonic constraints: Tectonophysics, v. 450, no. 1-4, p. 51-69.

Escartin, J., Smith, D. K., Cann, J., Schouten, H., Langmuir, C. H., and Escrig, S., 2008, Central role of detachment faults in accretion of slow-spreading oceanic lithosphere: Nature, v. 455, no. 7214, p. 790-794.

Etiope, G., and Klusman, R. W., 2002, Geologic emissions of methane to the atmosphere: Chemosphere, v. 49, no. 8, p. 777-789.

Etiope, G., and Sherwood Lollar, B., 2013, Abiotic methane on Earth: Reviews of Geophysics, v. 51, no. 2, p. 276-299.

Etiope, G., Tsikouras, B., Kordella, S., Ifandi, E., Christodoulou, D., and Papatheodorou, G., 2013, Methane flux and origin in the Othrys ophiolite hyperalkaline springs, Greece: Chemical Geology, v. 347, p. 161-174.

Etiope, G., and Whiticar, M., 2019, Abiotic methane in continental ultramafic rock systems: Towards a genetic model: Applied Geochemistry.

Faugères, J.-C., Stow, D. A., Imbert, P., and Viana, A., 1999, Seismic features diagnostic of contourite drifts: Marine Geology, v. 162, no. 1, p. 1-38.

Fossen, H., and Rotevatn, A., 2016, Fault linkage and relay structures in extensional settings—A review: Earth-Science Reviews, v. 154, p. 14-28.

Foustoukos, D. I., and Seyfried, W. E., 2004, Hydrocarbons in hydrothermal vent fluids: the role of chromium-bearing catalysts: Science, v. 304, no. 5673, p. 1002-1005.

Früh-Green, G. L., Connolly, J. A., Plas, A., Kelley, D. S., and Grobéty, B., 2004, Serpentinization of oceanic peridotites: implications for geochemical cycles and biological activity: The subseafloor biosphere at mid-ocean ridges, v. 144, p. 119-136.

Fujita, K., and Sleep, N. H., 1978, Membrane stresses near mid-ocean ridge-transform intersections: Tectonophysics, v. 50, no. 2-3, p. 207-221.

Grindlay, N. R., Madsen, J. A., Rommevaux, C., Sclater, J., and Murphy, S., 1996, Southwest Indian Ridge 15 E–35 E: A geophysical investigation of an ultra-slow spreading mid-ocean ridge system: InterRidge News, v. 5, no. 2, p. 15-17.

Hansen, J., Cartwright, J., Huuse, M., and Clausen, O. R., 2005, 3D seismic expression of fluid migration and mud remobilization on the Gjallar Ridge, offshore mid-Norway: Basin Research, v. 17, no. 1, p. 123-139.

Hardy, S., and McClay, K., 1999, Kinematic modelling of extensional fault-propagation folding: Journal of Structural Geology, v. 21, no. 7, p. 695-702.

Hustoft, S., Bünz, S., Mienert, J., and Chand, S., 2009, Gas hydrate reservoir and active methane-venting province in sediments on <20 Ma young oceanic crust in the Fram Strait, offshore NW-Svalbard: Earth and Planetary Science Letters, v. 284, no. 1, p. 12-24.

Huuse, M., Jackson, C. A.-L., Van Rensbergen, P., Davies, R. J., Flemings, P. B., and Dixon, R. J., 2010a, Subsurface sediment remobilization and fluid flow in sedimentary basins: an overview: Basin Research, v. 22, no. 4, p. 342-360.

Huuse, M., Jackson, C. A. L., Van Rensbergen, P., Davies, R. J., Flemings, P. B., and Dixon, R. J., 2010b, Subsurface sediment remobilization and fluid flow in sedimentary basins: an overview: Basin Research, v. 22, no. 4, p. 342-360.

Johnson, J. E., Mienert, J., Plaza-Faverola, A., Vadakkepuliyambatta, S., Knies, J., Bünz, S., Andreassen, K., and Ferré, B., 2015, Abiotic methane from ultraslow-spreading ridges can charge Arctic gas hydrates: Geology, v. 43, no. 5, p. 371-374.

Judd, A., and Hovland, M., 2007, Seabed fluid flow: the impact on geology, biology and the marine environment, Cambridge University Press.

-, 2009, Seabed fluid flow: the impact on geology, biology and the marine environment, Cambridge University Press.

Kearey, P., Klepeis, K. A., and Vine, F. J., 2009, Global tectonics, John Wiley & Sons.

Kelley, D. S., Karson, J. A., Blackman, D. K., FruÈh-Green, G. L., Butterfield, D. A., Lilley, M. D., Olson, E. J., Schrenk, M. O., Roe, K. K., and Lebon, G. T., 2001, An off-axis hydrothermal vent field near the Mid-Atlantic Ridge at 30 N: Nature, v. 412, no. 6843, p. 145.

Kelley, D. S., Karson, J. A., Früh-Green, G. L., Yoerger, D. R., Shank, T. M., Butterfield, D. A., Hayes, J. M., Schrenk, M. O., Olson, E. J., Proskurowski, G., Jakuba, M., Bradley, A., Larson, B., Ludwig, K., Glickson, D., Buckman, K., Bradley, A. S., Brazelton, W. J., Roe, K., Elend, M. J., Delacour, A., Bernasconi, S. M., Lilley, M. D., Baross, J. A., Summons, R. E., and Sylva, S. P., 2005, A Serpentinite-Hosted Ecosystem: The Lost City Hydrothermal Field: Science, v. 307, no. 5714, p. 1428-1434.

Knies, J., and Mann, U., 2002, Depositional environment and source rock potential of Miocene strata from the central Fram Strait: introduction of a new computing tool for simulating organic facies variations: Marine and Petroleum Geology, v. 19, no. 7, p. 811-828.

Knies, J., Matthiessen, J., Vogt, C., Laberg, J. S., Hjelstuen, B. O., Smelror, M., Larsen, E., Andreassen, K., Eidvin, T., and Vorren, T. O., 2009, The Plio-Pleistocene glaciation of the Barents Sea–Svalbard region: a new model based on revised chronostratigraphy: Quaternary Science Reviews, v. 28, no. 9, p. 812-829.

Kvenvolden, K., 1998, A primer on the geological occurrence of gas hydrate: Geological Society, London, Special Publications, v. 137, no. 1, p. 9-30.

Kvenvolden, K., Ginsburg, G., and Soloviev, V., 1993, Worldwide distribution of subaquatic gas hydrates: Geo-Marine Letters, v. 13, no. 1, p. 32-40.

Lamarche, G., and Lebrun, J.-F., 2000, Transition from strike-slip faulting to oblique subduction: active tectonics at the Puysegur Margin, South New Zealand: Tectonophysics, v. 316, no. 1-2, p. 67-89.

Lebrun, J. F., Lamarche, G., Collot, J. Y., and Delteil, J., 2000, Abrupt strike-slip fault to subduction transition: The Alpine fault-Puysegur trench connection, New Zealand: Tectonics, v. 19, no. 4, p. 688-706.

Liu, X., and Flemings, P. B., 2006, Passing gas through the hydrate stability zone at southern Hydrate Ridge, offshore Oregon: Earth and Planetary Science Letters, v. 241, no. 1-2, p. 211-226.

-, 2007, Dynamic multiphase flow model of hydrate formation in marine sediments: Journal of Geophysical Research: Solid Earth, v. 112, no. B3.

Lonsdale, P., 1977, Clustering of suspension-feeding macrobenthos near abyssal hydrothermal vents at oceanic spreading centers: Deep-Sea Research, v. 24, no. 9, p. 857-863.

Lowrie, W., 2007, Fundamentals of geophysics, Cambridge university press.

Mattingsdal, R., Knies, J., Andreassen, K., Fabian, K., Husum, K., Grøsfjeld, K., and De Schepper, S., 2014, A new 6 Myr stratigraphic framework for the Atlantic–Arctic Gateway: Quaternary Science Reviews, v. 92, p. 170-178.

McCaig, A. M., 1988, Deep fluid circulation in fault zones: Geology, v. 16, no. 10, p. 867-870.

Mienert, J., Vanneste, M., Bünz, S., Andreassen, K., Haflidason, H., and Sejrup, H. P., 2005, Ocean warming and gas hydrate stability on the mid-Norwegian margin at the Storegga Slide: Marine and Petroleum Geology, v. 22, no. 1, p. 233-244.

Mitchum Jr, R., Vail, P., and Sangree, J., 1977, Seismic stratigraphy and global changes of sea level: Part 6. Stratigraphic interpretation of seismic reflection patterns in depositional sequences: Section 2. Application of seismic reflection configuration to stratigraphic interpretation.

Mohammadi, A. H., Afzal, W., and Richon, D., 2008, Gas hydrates of methane, ethane, propane, and carbon dioxide in the presence of single NaCl, KCl, and CaCl2 aqueous solutions: Experimental measurements and predictions of dissociation conditions: The Journal of Chemical Thermodynamics, v. 40, no. 12, p. 1693-1697.

Moss, J., and Cartwright, J., 2010, 3D seismic expression of km-scale fluid escape pipes from offshore Namibia: Basin Research, v. 22, no. 4, p. 481-501.

Okino, K., Curewitz, D., Asada, M., Tamaki, K., Vogt, P., and Crane, K., 2002, Preliminary analysis of the Knipovich Ridge segmentation: influence of focused magmatism and ridge obliquity on an ultraslow spreading system: Earth and Planetary Science Letters, v. 202, no. 2, p. 275-288.

Pecher, I. A., Henrys, S. A., Wood, W. T., Kukowski, N., Crutchley, G. J., Fohrmann, M., Kilner, J., Senger, K., Gorman, A. R., and Coffin, R. B., 2010, Focussed fluid flow on the Hikurangi Margin, New Zealand—Evidence from possible local upwarping of the base of gas hydrate stability: Marine Geology, v. 272, no. 1, p. 99-113.

Peive, A., and Chamov, N., 2008, Basic tectonic features of the Knipovich Ridge (North Atlantic) and its neotectonic evolution: Geotectonics, v. 42, no. 1, p. 31-47.

Petersen, C. J., Bünz, S., Hustoft, S., Mienert, J., and Klaeschen, D., 2010, High-resolution P-Cable 3D seismic imaging of gas chimney structures in gas hydrated sediments of an Arctic sediment drift: Marine and Petroleum Geology, v. 27, no. 9, p. 1981-1994.

Pettijohn, F. J., 1957, Sedimentary rocks, Harper & Brothers New York.

Planke, S., Rasmussen, T., Rey, S. S., and Myklebust, R., Seismic characteristics and distribution of volcanic intrusions and hydrothermal vent complexes in the Vøring and Møre basins, in Proceedings Geological Society, London, Petroleum Geology Conference series2005, Volume 6, Geological Society of London, p. 833-844.

Proskurowski, G., Lilley, M. D., Seewald, J. S., Früh-Green, G. L., Olson, E. J., Lupton, J. E., Sylva, S. P., and Kelley, D. S., 2008, Abiogenic hydrocarbon production at Lost City hydrothermal field: Science, v. 319, no. 5863, p. 604-607.

Purdy, G. M., Kong, L. S. L., Christeson, G. L., and Solomon, S. C., 1992, Relationship between spreading rate and the seismic structure of mid-ocean ridges: Nature, v. 355, no. 6363, p. 815-817.

Rebesco, M., and Stow, D., 2001, Seismic expression of contourites and related deposits: a preface: Marine Geophysical Researches, v. 22, no. 5-6, p. 303-308.

Rebesco, M., Wåhlin, A., Laberg, J. S., Schauer, U., Beszczynska-Möller, A., Lucchi, R. G., Noormets, R., Accettella, D., Zarayskaya, Y., and Diviacco, P., 2013, Quaternary contourite drifts of the Western Spitsbergen margin: Deep Sea Research Part I: Oceanographic Research Papers, v. 79, p. 156-168.

Reeve, M. T., Bell, R. E., Duffy, O. B., Jackson, C. A.-L., and Sansom, E., 2015, The growth of non-colinear normal fault systems; What can we learn from 3D seismic reflection data?: Journal of Structural Geology, v. 70, p. 141-155.

Riboulot, V., Thomas, Y., Berné, S., Jouet, G., and Cattaneo, A., 2014, Control of Quaternary sea-level changes on gas seeps: Geophysical Research Letters, v. 41, no. 14, p. 4970-4977.

Ritzmann, O., Jokat, W., Mjelde, R., and Shimamura, H., 2002, Crustal structure between the Knipovich Ridge and the Van Mijenfjorden (Svalbard): Marine Geophysical Researches, v. 23, no. 5-6, p. 379-401.

Romeyn, R., 2017, Processing and interpretation of the Svyatogor 2016 high-resolution P-Cable 3D seismic dataset. Investigating the dynamics of a sub-seabed gas hydrate system with a potential abiotic methane source: Unpublished Master Thesis, v. UiT- Norges Arktiske Universitet, no. Tromsø, p. Norway.

Ruppel, C., 1997, Anomalously cold temperatures observed at the base of the gas hydrate stability zone on the US Atlantic passive margin: Geology, v. 25, no. 8, p. 699-702.

Ruppel, C., Dickens, G. R., Castellini, D. G., Gilhooly, W., and Lizarralde, D., 2005, Heat and salt inhibition of gas hydrate formation in the northern Gulf of Mexico: Geophysical Research Letters, v. 32, no. 4.

Rüpke, L. H., and Hasenclever, J., 2017, Global rates of mantle serpentinization and H2 production at oceanic transform faults in 3-D geodynamic models: Geophysical Research Letters, v. 44, no. 13, p. 6726-6734.

Schoell, M., 1988, Multiple origins of methane in the Earth: Chemical geology, v. 71, no. 1-3, p. 1-10.
Scholz, C. H., 2002, The mechanics of earthquakes and faulting, Cambridge university press.
Schroeder, T., John, B., and Frost, B. R., 2002, Geologic implications of seawater circulation through peridotite exposed at slow-spreading mid-ocean ridges: Geology, v. 30, no. 4, p. 367-370.
Searle, R., 2013, Mid-ocean ridges, Cambridge University Press.
Serié, C., Huuse, M., and Schødt, N. H., 2012, Gas hydrate pingoes: Deep seafloor evidence of focused fluid flow on continental margins: Geology, v. 40, no. 3, p. 207-210.
Sherwood Lollar, B., Frape, S. K., Weise, S. M., Fritz, P., Macko, S. A., and Welhan, J. A., 1993, Abiogenic methanogenesis in crystalline rocks: Geochimica et Cosmochimica Acta, v. 57, no. 23, p. 5087-5097.
Sibson, R., Moore, J. M. M., and Rankin, A., 1975, Seismic pumping—a hydrothermal fluid transport mechanism: Journal of the Geological Society, v. 131, no. 6, p. 653-659.
Sibson, R. H., 1981, Fluid flow accompanying faulting: field evidence and models: Earthquake prediction: an international review, v. 4, p. 593-603.
-, 1990, Conditions for fault-valve behaviour: Geological Society, London, Special Publications, v. 54, no. 1, p. 15-28.
-, 1994, Crustal stress, faulting and fluid flow: Geological Society, London, Special Publications, v. 78, no. 1, p. 69-84.
-, 1996, Structural permeability of fluid-driven fault-fracture meshes: Journal of Structural Geology, v. 18, no. 8, p. 1031-1042.
-, 2000, Fluid involvement in normal faulting: Journal of Geodynamics, v. 29, no. 3-5, p. 469-499.
Sloan, E. D., 1998, Gas hydrates: review of physical/chemical properties: Energy & Fuels, v. 12, no. 2, p. 191-196.
Stolper, D., Lawson, M., Davis, C., Ferreira, A., Neto, E. S., Ellis, G., Lewan, M., Martini, A. M., Tang, Y., and Schoell, M., 2014, Formation temperatures of thermogenic and biogenic methane: Science, v. 344, no. 6191, p. 1500-1503.
Stow, D., and Lovell, J., 1979, Contourites: their recognition in modern and ancient sediments: Earth-Science Reviews, v. 14, no. 3, p. 251-291.
Stow, D. A., Faugères, J.-C., Howe, J. A., Pudsey, C. J., and Viana, A. R., 2002, Bottom currents, contourites and deep-sea sediment drifts: current state-of-the-art: Geological Society, London, Memoirs, v. 22, no. 1, p. 7-20.
Sutherland, A. J., 1967, Proposed mechanism for sediment entrainment by turbulent flows: Journal of Geophysical Research, v. 72, no. 24, p. 6183-6194.
Thiede, J., Myhre, A. M., and Firth, J. V., 1995, Cenozoic Northern Hemisphere polar and subpolar ocean paleoenvironments (Smmary of ODP Leg 151 Drilling Results).
Vadakkepuliyambatta, S., Hornbach, M. J., Bünz, S., and Phrampus, B. J., 2015, Controls on gas hydrate system evolution in a region of active fluid flow in the SW Barents Sea: Marine and Petroleum Geology, v. 66, p. 861-872.
van Gent, H. W., Back, S., Urai, J. L., Kukla, P. A., and Reicherter, K., 2009, Paleostresses of the Groningen area, the Netherlands—Results of a seismic based structural reconstruction: Tectonophysics, v. 470, no. 1-2, p. 147-161.
Visher, G. S., 1969, Grain size distributions and depositional processes: Journal of Sedimentary Research, v. 39, no. 3.
Waghorn, K. A., Vadakkepuliyambatta, S., Plaza-Faverola, A., Johnson, J. E., Bünz, S., and Waage, M., Submitted, Crustal processes sustain Arctic abiotic gas hydrate and fluid flow systems: Scientific Reports
Waghorn, K. A., Bünz, S., Plaza-Faverola, A., and Johnson, J. E., 2018a, 3-D Seismic Investigation of a Gas Hydrate and Fluid Flow System on an Active Mid-Ocean Ridge; Svyatogor Ridge, Fram Strait: [Washington, DC] :, p. 2325-2341.
Waghorn, K. A., Pecher, I., Strachan, L. J., Crutchley, G., Bialas, J., Coffin, R., Davy, B., Koch, S., Kroeger, K. F., and Papenberg, C., 2018b, Paleo-fluid expulsion and contouritic drift formation on the Chatham Rise, New Zealand: Basin Research, v. 30, no. 1, p. 5-19.
Xu, W., and Ruppel, C., 1999, Predicting the occurrence, distribution, and evolution of methane gas hydrate in porous marine sediments: Journal of Geophysical Research: Solid Earth, v. 104, no. B3, p. 5081-5095.
Yilmaz, Ö., 2001, Seismic data analysis: Processing, inversion, and interpretation of seismic data, Society of exploration geophysicists.

Zoback, M. D., and Zoback, M. L., 2002, Stress in the earth's lithosphere: Encyclopedia of physical science and technology, v. 16, p. 143-154.

Zoback, M. L., Zoback, M. D., Adams, J., Assumpção, M., Bell, S., Bergman, E. A., Blümling, P., Brereton, N. R., Denham, D., Ding, J., Fuchs, K., Gay, N., Gregersen, S., Gupta, H. K., Gvishiani, A., Jacob, K., Klein, R., Knoll, P., Magee, M., Mercier, J. L., Müller, B. C., Paquin, C., Rajendran, K., Stephansson, O., Suarez, G., Suter, M., Udias, A., Xu, Z. H., and Zhizhin, M., 1989, Global patterns of tectonic stress: Nature, v. 341, no. 6240, p. 291-298.

# Supplementary Material

## Other Publications

Johnson, J.E., **Waghorn, K.A.,** Mienert, J., Bünz, S. (2016), The potential for Abiotic Methane in Arctic Gas Hydrates. *Invited submission to Fire in the Ice Newsletter*

**Waghorn, K. A**., Pecher, I. , Strachan, L. J., Crutchley, G. , Bialas, J. , Coffin, R. , Davy, B. , Koch, S. , Kroeger, K. F., Papenberg, C. , Sarkar, S. (2018), Paleo-fluid expulsion and contouritic drift formation on the Chatham Rise, New Zealand. *Basin Research 30*: 5-19. DOI:10.1111/bre.12237

Malin Waage, Stefan Bünz, Martin Landrø, Andreia Plaza-Faverola, **Kate Alyse Waghorn**. (2018). Repeatability of high-resolution 3D seismic data. *Geophysics, 84(1):* 1-60. DOI: 10.1190/geo2018-0099.1

Malin Waage, Alexey Portnov, Pavel Serov, Stefan Bünz, **Kate A. Waghorn**, Sunil Vadakkepuliyambatta, Jürgen Mienert, Karin Andreassen. (2019) Geological controls on fluid flow and gas hydrate pingo development on the Barents Sea margin. *Geochemistry, Geophysics, Geosciences, 20(2):* 630-650. DOI:10.1029/2018GC007930

Malin Waage, Pavel Serov, Karin Andreassen, **Kate A. Waghorn**, Stefan Bünz. Controls on giant methane blow-out craters and mounds on the Arctic seafloor. (2019) *Manuscript.*

Giacomo Osti, **Kate A. Waghorn**, Malin Waage, Benedicte Ferre, Andreia Plaza-Faverola. (2019). Evolution of contourite drifts in regions of gas-hydrate related bottom simulating reflectors and slope failures at Eastern Fram Strait. *Submitted to Arktos – The journal of Arctic Geosciences*.

Article I

*3D Seismic investigation of a Gas Hydrate and fluid flow system on an active mid-ocean ridge; Svyatogor Ridge, Fram Strait*

**Kate A. Waghorn,** Stefan Bünz, Andreia Plaza-Faverola and Joel E. Johnson

Geochemistry, Geophysics, Geosystems 2018 vol. 19 pp. 2325-2341

AGU100 ADVANCING EARTH AND SPACE SCIENCE

Geochemistry, Geophysics, Geosystems

RESEARCH ARTICLE
10.1029/2018GC007482

**Key Points:**
- A gas hydrate system is imaged with 3-D seismic data south of Vestnesa Ridge and exists on young, warm crust near the plate boundary
- The system is seeping fluid at the seafloor episodically, likely controlled by seismic activity
- We identify fracture networks, which we suggest a proxy to identify the extent of gas hydrate within the sediment column

**Correspondence to:**
K. A. Waghorn,
kate.a.waghorn@uit.no

**Citation:**
Waghorn, K. A., Bünz, S., Plaza-Faverola, A., & Johnson, J. E. (2018). 3-D seismic investigation of a gas hydrate and fluid flow system on an active mid-ocean ridge; Svyatogor Ridge, Fram Strait. *Geochemistry, Geophysics, Geosystems*, *19*, 2325–2341. https://doi.org/10.1029/2018GC007482

Received 15 FEB 2018
Accepted 8 MAY 2018
Accepted article online 12 MAY 2018
Published online 8 AUG 2018



# 3-D Seismic Investigation of a Gas Hydrate and Fluid Flow System on an Active Mid-Ocean Ridge; Svyatogor Ridge, Fram Strait

**Kate A. Waghorn[1], Stefan Bünz[1], Andreia Plaza-Faverola[1], and Joel E. Johnson[2]**

[1]Department of Geosciences, Centre for Arctic Gas Hydrate, Environment and Climate, UiT—The Arctic University of Norway, Tromsø, Norway, [2]Department of Earth Sciences, University of New Hampshire, Durham, NH, USA

**Abstract** Tectonic settings play a large role in the development of fluid flow pathways for gas migrating through sedimentary strata. Gas hydrate systems worldwide are located on either the slopes of passive continental margins, often in large contourite deposits, or in accretionary wedges on subduction margins. The Svyatogor Ridge, however, located at the northwestern flank of the Knipovich Ridge and south of the Molloy Transform Fault (Fram Strait), is a gas hydrate system which is located on an actively spreading margin. Svyatogor Ridge has evidence of shallow gas accumulations; a strong BSR indicating a gas hydrate and underlying free gas system, and fluid flow pathways to the seafloor culminating in pockmarks. Using a high-resolution P-Cable 3-D seismic survey, we investigate how tectonic and sedimentary regimes have influenced the formation of this well-developed gas hydrate system. Large-scale basement faults identified in the seismic data are interpreted as detachment faults, which have exhumed relatively young ultramafic rocks. These detachment faults act as conduits for fluid flow, and are responsible for the formation of folds in the overlying sediments that are breached by faults. We propose a model for fluid flow within this system whereby as sedimentary faults breach upward through the sedimentary strata, fluid is able to migrate further upward. We find that the tectonic regime on Svyatogor Ridge is the dominant driver of fluid migration and episodic release at the seafloor.

## 1. Introduction

Gas hydrates are solid compounds of water and gas (i.e., dominantly methane), which are stable in marine sediments or permafrost regions at high pressures and low temperatures (i.e., Sloan, 1998). Determinants for gas hydrate formation are salinity (high salinity inhibits hydrate formation), porosity, and a sufficient gas input. The gas that sustains gas hydrate accumulations in shallow sediments has been found to be predominantly of microbial or thermogenic origin (Klauda & Sandler, 2005). In the case of microbial in situ methane production, an input of organic matter into the system is also necessary (Paull et al., 1994). Therefore, many of the subaqueous gas hydrate and related fluid flow system occurrences worldwide are observed on TOC-rich sedimented continental margins (i.e., Hikurangi Margin (Pecher et al., 2005), Cascadia Margin (Suess et al., 1999), Gulf of Mexico (Shipley et al., 1979)) or in large contourite deposits (i.e., Vestnesa Ridge (Bünz et al., 2012), Blake Ridge (Faugères et al., 1999)) as these settings generally meet all the conditions for both gas hydrate formation and stability. Distal settings (i.e., abyssal plains), on the other hand, are generally characterized by deposition of clays and silts, and lower organic matter fluxes to the seafloor (Klauda & Sandler, 2005; Müller & Suess, 1979) and the common assumption is that these are not ideal settings for gas hydrate formation, even though they may fall within the gas hydrate stability zone.

In the Fram Strait, the Western Svalbard Margin and Vestnesa Ridge are known for storing large quantities of methane within the sedimentary strata, where large amounts of this shallow gas is sequestrated as gas hydrate (Bünz et al., 2012; Hustoft et al., 2009; Vanneste et al., 2005). The Western Svalbard margin is a passive continental margin that evolved in connection with the onset of rifting in the North Atlantic (e.g., Engen et al., 2008; Lundin & Doré, 2002). Vestnesa Ridge formed as a large contourite deposit that extends off the continental margin crossing the continental-oceanic crust transition (Bünz et al., 2012; Eagles et al., 2015; Engen et al., 2008). Although the distribution of fluid flow related features developed through the gas hydrate zone on Vestnesa Ridge is correlated with the presence of faults (Plaza-Faverola et al., 2015), the

gas hydrate system here is assumed to have developed post-rift (Bünz et al., 2012; Eiken & Hinz, 1993; Engen et al., 2008). However, to the west of the Western Svalbard Margin and south of Vestnesa Ridge is the Knipovich Ridge, which is an ultraslow spreading ridge (Dick et al., 2003). In such ultraslow settings, magmatism is limited and low-angle detachment faults accommodate the majority plate motion and can remain active for 1–3 Myr (Escartin et al., 2008; Tucholke et al., 1998). The Arctic mid-ocean ridges are all ultraslow and in particular, low-angle detachment faults and exhumed serpentinized peridotites have been observed and/or sampled on the Gakkel Ridge, Lena Trough, and Molloy Ridge (Dick et al., 2003; Michael et al., 2003; Snow et al., 2001). Abiotic methane has been, in recent years, identified as another potential gas source available for gas hydrate formation in slow to ultraslow spreading environments (Johnson et al., 2015; Rajan et al., 2012), forming during serpentinization of ultramafic rocks (Etiope & Sherwood Lollar, 2013). Serpentinites sampled on the seafloor in slow and ultraslow spreading mid-ocean ridges are often found in close proximity to detachment faults (Cann et al., 1997; Kelley et al., 2005), which provide easy access for seawater to drive serpentinization reactions. Due to the limited life span of slip on a detachment fault and the temperature range for maximum serpentinization, the window to form serpentinized methane is limited to young crust close to the spreading axis (Johnson et al., 2015). Additionally, serpentinites are commonly observed at the junctures between spreading ridges and transform faults, where detachment faults are well developed (Tucholke et al., 1998).

Due to the proximity of the Arctic mid-ocean ridges to the Western Svalbard Margin, and their ultraslow spreading rates, the Arctic mid-ocean ridges are often sedimented, and magma-limited conditions create geothermal gradients lower than at intermediate to fast spreading ridges. The flanks of the Knipovich Ridge and Molloy Ridge are not only within the temperature and pressure regime required for gas hydrate stability, but also are characterized by having similar sedimentary depositional regimes (Eiken & Hinz, 1993) and potentially even their own methane source—serpentinized abiotic methane (Johnson et al., 2015; Rajan et al., 2012).

Svyatogor Ridge is a sedimented, elongated ridge located on the flank of the Knipovich Ridge at the inner junction with the Molloy Transform Fault. Previous work has documented the presence of a gas hydrate system on the Svyatogor Ridge (Johnson et al., 2015). Unlike the other Fram Strait gas hydrate reservoirs, the gas hydrate system on the Svyatogor Ridge is on the flank of an actively spreading mid-ocean ridge, implying that unlike the other Arctic gas hydrate systems, Svyatogor Ridge is in an actively rifting environment. Using high-resolution 3-D seismic data, we investigate the first gas hydrate system identified on the flank of an actively rifting ultraslow spreading margin. Based on detailed descriptions of tectonic and sedimentary structures characterizing the gas hydrate bearing ridge, we explore the implications that this tectonically active ultraslow spreading setting has on the development of a gas hydrate system and associated seafloor seepage system.

## 2. Geologic Setting and Tectonic History

### 2.1. Study Area

Svyatogor Ridge is a contourite driven sedimented ridge with a length of 46 km and a width of ~5 km (Figure 1) (Johnson et al., 2015). Our study focuses on the southernmost part of the ridge.

### 2.2. Tectonic Background

The ultraslow spreading Knipovich Ridge extends for ~550 km in N-S direction (Okino et al., 2002), with a half-spreading rate for the Knipovich Ridge of 6.2 mm/yr, on the western, faster moving, side of the Ridge (Ehlers & Jokat, 2009). The Knipovich Ridge connects the Gakkel Ridge in the Arctic Ocean to the Mohns Ridge through a number of transform faults and small spreading centers (Figure 1). The Gakkel and Mohns Ridges most likely began spreading during Chron 24 at 53 Ma (Ehlers & Jokat, 2009; Vogt et al., 1978), and the Knipovich Ridge began propagating northward at Chron 13, 33 Ma (Ehlers & Jokat, 2009; Talwani & Eldholm, 1977). At the northernmost segment of Knipovich Ridge, magnetic anomaly C6 (19.6 Ma) is clearly delineated, and C5 (9.8 Ma) is present as a weaker lineation (Engen et al., 2008) on the western side of the Ridge. Conjugate magnetic anomalies are not present on the Svalbard side of the Ridge, leading Engen et al. (2008) to suggest that the junction between the Molloy Transform Fault and Knipovich Ridge has migrated northward. Faults and rift escarpments further north suggest that the Knipovich ridge is continuing to propagate northward under the West Svalbard Margin (Crane et al., 2001). Due to the nature of the

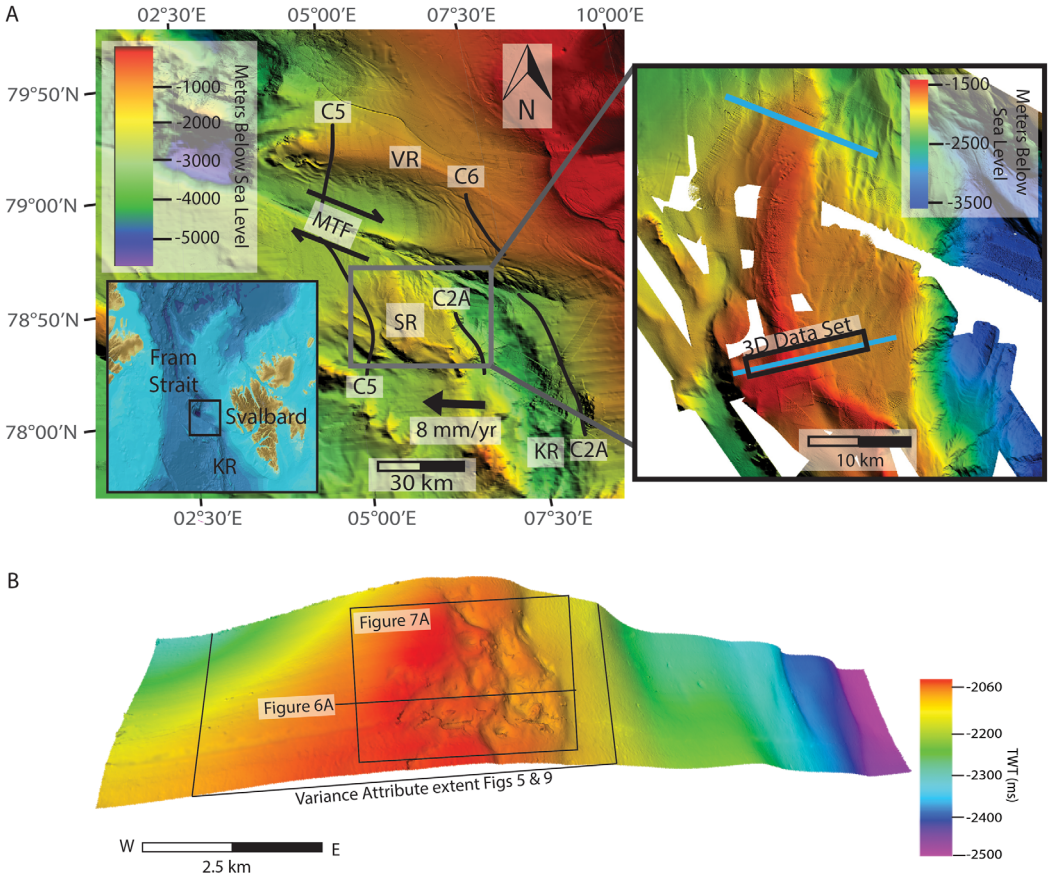


**Figure 1.** (a) The Svyatogor Ridge is a 46 km long, ~5 km wide feature at the intersection between the Molloy Transform Fault (MTF) and the Knipovich Ridge (KR). The Knipovich Ridge has a spreading rate of ~8 mm/yr (Ehlers & Jokat, 2009). Svyatogor Ridge is located between Chrons 5 and 2A (C2A, C5), correlating to 9.8 and 2.8 Ma, respectively (Engen et al., 2008). The location of the 3-D P-Cable Seismic survey is marked by the black box in the inset and seismic examples from Johnson et al. (2015) are marked by blue lines. Other tectonic and geologic features in the Fram Strait are the Vestnesa Ridge (VR), Molloy Ridge (MR), Yermak Plateau (YP), Lena Trough (LT), and Gakkel Ridge (GR). (b) Position of Figures 5–7 and 9 in relation to the 3-D seismic cube.

geologic and tectonic setting of the study area, close to the Knipovich Ridge, the crust is young and close to the seafloor (Amundsen et al., 2011).

### 2.3. Seismic Stratigraphy

Three main stratigraphic units provide chronological constraints on the West Svalbard Margin (Eiken & Hinz, 1993). YP-1 is the oldest unit, composed of syn-rift and post-rift sediments, which deposited directly on oceanic crust; YP-2 sequence comprises the onset of contourite facies with a basal age between 11 and 14.6 Ma; and YP-3 corresponds to the onset of glacially transported sediments, where contourites and glaciomarine turbidites and debris flows are the predominant facies. Correlation to cores drilled during Ocean Drilling Program Leg 151 (Geissler et al., 2011) provides the age control for these seismic stratigraphic units. The boundary between YP-2 and YP-3 is estimated to be 2.7 Ma (Eiken & Hinz, 1993; Mattingsdal et al., 2014), and has been identified in the region comprising the Yermak Plateau, the Vestnesa Ridge, and offshore Prins Karls Forland (Eiken & Hinz, 1993; Hustoft et al., 2009; Mattingsdal et al., 2014). Based on the supposition that the Svyatogor Ridge was offset to the west during growth of Vestnesa Ridge across the MTF during the last 2–3 Ma (Johnson et al., 2015), YP-2 and YP-3 seismic stratigraphic units should also be present on the Svyatogor Ridge. YP-1, however, is most likely too old compared to the estimated crustal age to be present on Svyatogor Ridge (Engen et al., 2008; Mattingsdal et al., 2014).

### 2.4. Oceanography

The Fram Strait channels warm, saline waters from the North Atlantic into the Arctic Ocean, and transports cold Arctic water southward (Beszczynska-Möller et al., 2012). The West Spitsbergen Current brings North Atlantic water northward, and is an important sediment supply system for the Western Svalbard Margin, having deposited the muddy-silty contourite deposits that dominate sedimentation (Howe et al., 2008; Rebesco et al., 2013). Although paleo-current indications suggest the West Spitsbergen Current has migrated up the West Svalbard Margin slope over time (Eiken & Hinz, 1993), this current may have been influencing the Svyatogor Ridge in the past (Johnson et al., 2015), thus, driving sedimentation that ultimately hosts the gas hydrate and free gas system observed there today. As the West Spitsbergen Current has migrated upslope through time, we expect the WSC influenced sedimentation to decrease through time on Svyatogor Ridge.

## 3. Data and Methods

A 2 × 10 km high-resolution P-Cable 3-D seismic data set was acquired in 2014 aboard R/V Helmer Hanssen. P-Cable seismic data were recorded using 14, 25 m long streamers spaced 12.5 m apart with eight channels per streamer (e.g., Planke et al., 2009). The source used was a mini-GI air gun with a capacity of 15/15 $in.^3$, fired every 5 s with the ship maintaining a speed of 4 km and sailing line spacing of ∼60 m. Data processing steps included: insertion of navigation data, CDP-Binning at 6.25 × 6.25 m (fold of approximately 7 traces per CDP bin), static corrections, bandpass filtering with a frequency of 10–20–400–500 Hz, attenuation and spherical divergence correction, NMO correction, stacking, interpolation in crossline direction and a 3-D Stolt (post-stack)|Migration. We used a constant velocity of 1,600 m/s for migration, constrained for the imaged sedimentary infill by Ritzmann et al. (2004), who used Ocean Bottom Seismometers for velocity analysis. Dominant frequency of this data is 120 Hz, so the vertical data resolution is <3.2 m ($\lambda$/4) at the seafloor assuming a water velocity of 1,490 m/s (measured by CTD at beginning of surveying). Data penetration is restricted to 3,200 ms TWT. Seismic interpretation used commercially available seismic interpretation software (Petrel). Variance maps were generated along major reflections for fault analysis and depositional reconstruction carried out for constraining the evolution of the study area. Seismic results are analyzed together with bathymetry data with a resolution of ∼10–20 m collected aboard the R/V Helmer Hanssen between 2014 and 2016. Repeated water column acoustic mapping (June 2014 and October 2015) during CAGE cruises 14-1, 14-2, and 15-6 reveled no active fluid expulsion above pockmarks on the crest of Svyatogor Ridge.

## 4. Results and Interpretations

### 4.1. Distinct Depositional Periods

Four main depositional periods (S1–S4) are identified in addition to the acoustic basement, based on: (1) the seismic character of the reflections; (2) faulting pattern; and time framework (i.e., syn-rift or post-rift deposition) (Figure 2).

Johnson et al. (2015) define the basement in this study area, which are indicated by the transition in seismic response between sediments and oceanic basement. Using the nearest published seafloor sampling results, seismic refraction data, and the tectonic setting, Johnson et al. (2015) suggest that the basement in the study area is likely composed of serpentinized ultramafic rocks. The basement has two prominent highs (East Peak, West Peak; Figure 3a), with a depression located in between. Associated with these two peaks, the acoustic basement tilts creating an additional two small basins at the western and eastern ends of the data set (Figure 3). Within the unit defined as basement, there are no seismic indications of stratified reflections from sediments. We interpret the basement as young crust formed as part of the Knipovich Ridge spreading regime.

Pockets of sediments infilling acoustic basement lows (Figures 2 and 3a) characterize the first period of deposition (Unit S4). In the central depression between the two basement peaks, this unit appears to onlap against the East Peak but abruptly truncates against the West Peak. Amplitude of reflections in this unit is very low. All reflectors in this unit dip at similar angles to the acoustic basement (Figure 3a). The reflector marking the top of Unit S4 appears to be erosional (truncating lower reflectors) on the western side of West

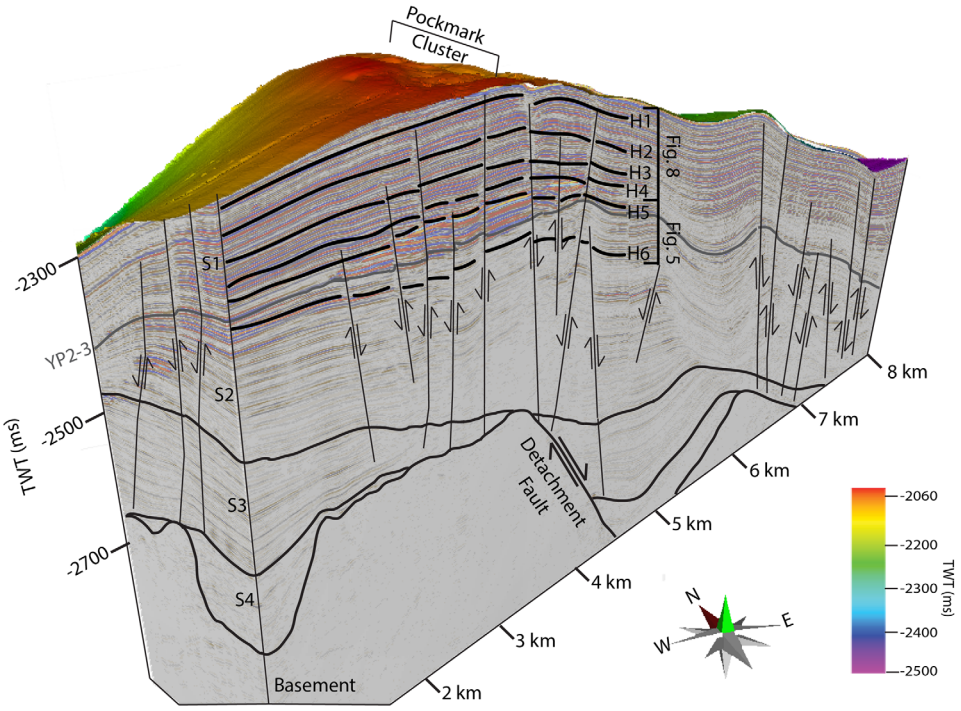


**Figure 2.** The data set is divided into four units representing depositional periods (S4–S1) and basement. These depositional periods are defined based on seismic properties that indicated a change in depositional regime and rock/sediment properties. Locations of structural maps in Figures 5 and 8 are annotated on this section. WP and EP are the west and east basement peaks, respectively.

Peak. Unit S4 is interpreted to be sedimentation infilling the basement highs and lows. It is difficult to interpret further owing to the extremely low amplitudes. The rotation of the few reflectors we could identify suggests this unit has tilted because of tectonic event(s).

Unit S3 also infills basement lows; however, it is not localized in the same manner as S4; the top reflections of this unit are nearly continuous throughout the entire data set, except in one area (west peak) where the acoustic basement protrudes above this unit (Figures 2 and 3a). While in the west of the data set, reflectors are subhorizontal to slightly rotated, the eastern half of this unit is rotated to conform to the dip trend of the acoustic basement (Figures 2 and 3a). Overall, the amplitudes and reflection frequency of this unit are low; however, moving upward through this unit reflectors appears to become increasingly less rotated (Figure 3a). We therefore interpret this unit to have continued to infill basement lows after the deposition of Unit S4.

Depositional period S2 consists of mostly subhorizontal deposition in the west and dipping reflectors in the east. In this unit, there is thickening of sedimentary packages toward the east (Figure 3). Disruption and vertical offset of reflections are prevalent within Unit S2. Based on the correlation with regional seismic lines (e.g., Hustoft et al., 2009), we interpret that the top reflection of our S2 depositional period coincides with the YP2/YP3 boundary. This indicates that the sediment deposited in this unit is older than 2.7 Ma. In addition, the unit thickens eastward so this unit is interpreted to deposit as the WSC was moving east, while simultaneously the Knipovich Ridge was propagating Svyatogor Ridge westward.

Depositional period S1 is composed of mostly subhorizontal reflectors in the west and dipping reflectors in the east (Figure 3). Unit S1 shows a clear thickening trend of sedimentary packages toward the east (Figure 3b). The amplitudes in this depositional period also cycle from high amplitude to low amplitude; however, the transition to low amplitude is abrupt and therefore there is a predominance of high amplitude (Figure 3a). Frequency of reflections in this unit is high. Like Unit S2, disruption and vertical offset of reflections are common. The uppermost reflector in this unit is the seafloor and the base has been correlated as YP2/3 (e.g., Hustoft et al., 2009); therefore, this unit must correlate to YP3 ($<$2.7 Ma) sediment. The eastward thickening of this unit is interpreted to result from the combined effects of the eastward migration of the WSC and the westward offset of the ridge along the MTF.

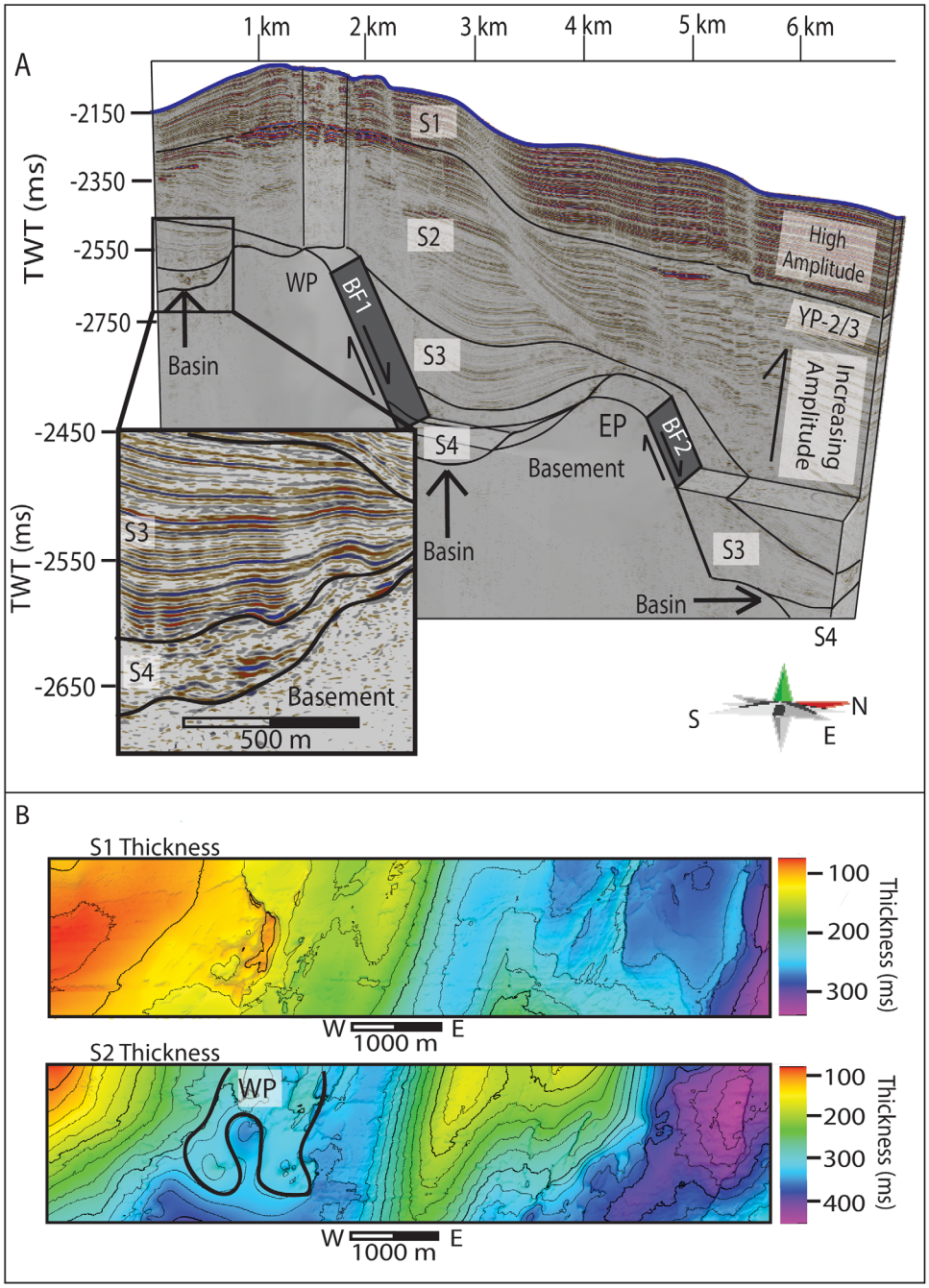


**Figure 3.** (a) The acoustic basement has two main peaks (WP, West Peak; EP, East Peak) that are defined by two normal faults, with basins surrounding the peaks. Units S4 and S3 infill these basement highs. Units S2 and S1 are composed of mainly subhorizontal reflectors in the west and dipping reflectors in the east. Inset: Units S4 and S3 are slightly rotated, and stretched, to conform to the tilt of the basement. This has led to the interpretation that these units have been deposited while these faults were active. (b) Isopach maps of Units S1 and S2 show that eastward thickening of strata is most pronounced in S2. Section marked "WP" is where the basement peak West Peak outcrops into S2.

### 4.2. Fault Analysis

#### 4.2.1. Major Tectonic Faults

Two normal faults (BF1, BF2) were identified at the lower limit of penetration of the data set (Figure 4). These faults occur in the acoustic basement and do not extend upward into the sedimentary sequences (Figure 4). The western-most basement fault (BF1) is the best imaged and closer to the surface. The eastern-

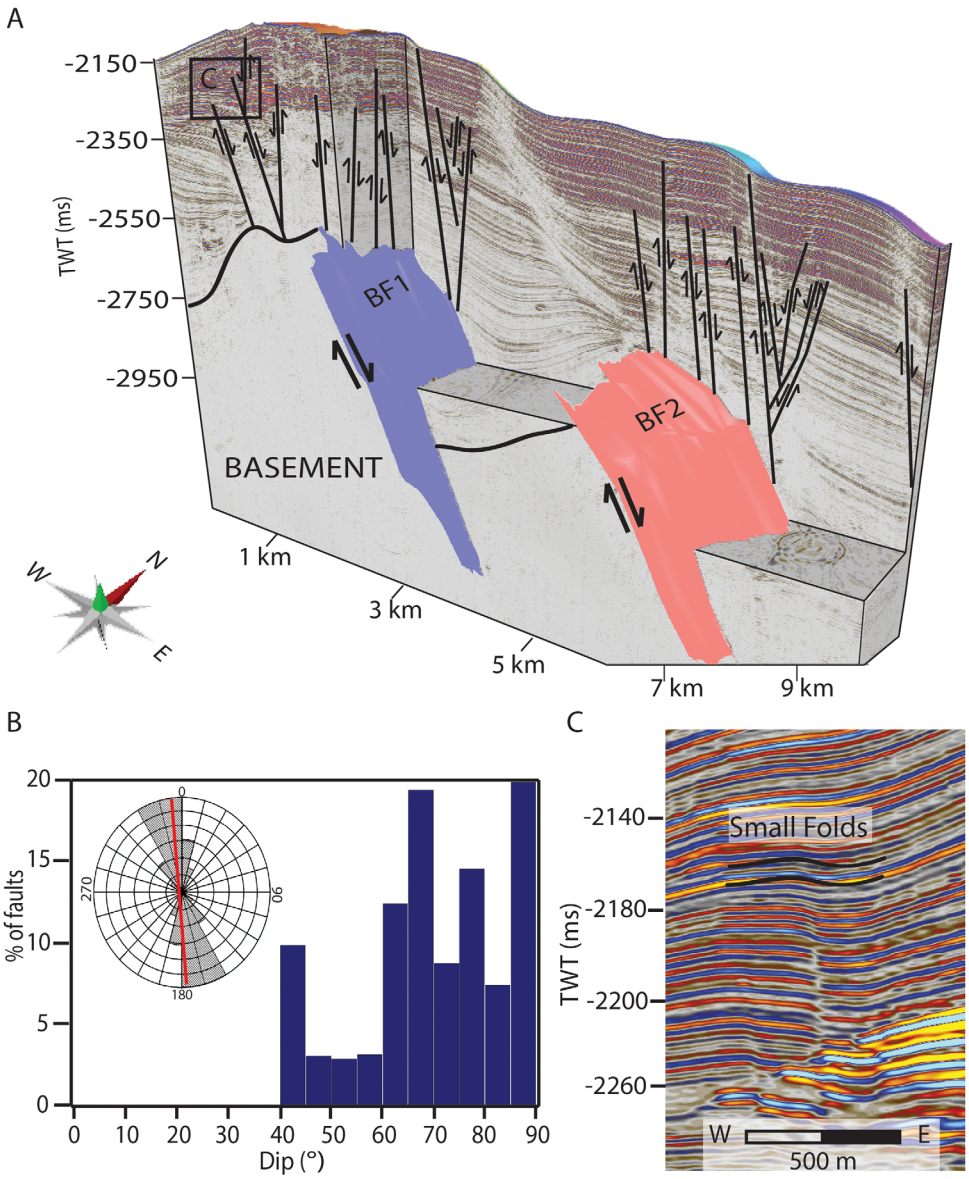


**Figure 4.** (a) BF1 and BF2 are two large normal detachment faults identified within the data set. These faults do not extend beyond the basement however, sedimentary fault arrays occur exclusively around the area where the basement faults occur. (b) The sedimentary faults mostly conform to the regional tectonic regime (strike of Knipovich Ridge marked in red on Stereonet, from Peive and Chamov (2008)). Dip of the sedimentary faults is between 40° and 90°. (c) Sedimentary faults from the eastern-most group shown in Figure 4a showing instances of small folds occurring above the fault termination, indicating that these are developing as growth faults.

most basement fault (BF2) is at the very edge of both lateral and vertical data extent; however, it is still possible to interpret a fault plane. The dip of BF1 and BF2 is calculated to be 30° and 20°, respectively (based on a velocity of 1,600 m/s adjacent to sedimentary sections), and dip azimuth of BF1 is ~80° while BF2 ~95°. Both faults conform to the regional tectonic setting. Offset of BF1 is at least 1,200 m and the offset of BF2 at least 1,000 m (Amundsen et al., 2011). These faults are interpreted to be detachment faults, which are related to spreading on the Knipovich Ridge (Amundsen et al., 2011; Johnson et al., 2015).

#### 4.2.2. Sedimentary Faults

In the sedimentary strata, there are numerous steeply dipping normal faults present throughout the data set. These faults are NNW-SSE oriented and have dips of between 40° and 90°, although most faults dip between 60° and 90° (Figure 4). Most of the faults upwardly terminate in Unit S2 although a few terminates within Unit S1 or reach the seafloor. These faults are all concentrated around the two major tectonic faults,

BF1 and BF2, in the acoustic basement (Figure 4). These faults mostly comply with the regional tectonic setting although some at the apex of the ridge do not (Figure 4) (Peive & Chamov, 2008). Sedimentary faults nearly exclusively terminate against the basement. At the upward termination of the faults, there is often a very small fold, which is indicative of a fault propagation folding (Hardy & McClay, 1999; Jackson et al., 2006). We interpret folding at the upper terminus of sedimentary faults to indicate upward and lateral propagation of normal faults through ductile sediment deposited over more rigid basement material (e.g., Corfield & Sharp, 2000).

#### 4.2.3. Radial Faults and Fracture Networks

Structural maps reveal smaller scale faults forming at random azimuths between larger scale NW-SE trending faults (Figure 5). We only identify this type of faulting in the area above West Peak. This type of faulting occurs in a linear, step-like fashion around a zone of acoustic blanking coincident above West Peak (Figure 5). This type of faulting is interpreted as radial faulting, and similarly to the radial-type faulting around sediment remobilization features (e.g., Hansen et al., 2005), is interpreted to be a function of the sediment doming around the peaks associated with the two major detachment faults BF1 and BF2 (Figure 4a). In this case, we interpret the structure causing sediment doming to be uplift of West Peak into the sedimentary sequence. Lastly, we also identify even smaller scale features in variance attribute that are also forming at random azimuths, and sometimes as circular features, and are often barely recognizable in the seismic section (Figure 5). These features are mostly associated with a very small depression at the upward termination, which may be interpreted as fluid flow features (Hartwig et al., 2012). As the depression structure is at the limit of seismic resolution, it is difficult to interpret whether it is a paleo-pockmark or associated with syn-tectonic infill; however, the circular features often form at intersections of the small scale, random azimuth features. Therefore, we interpret the random azimuth features as fracture networks.

### 4.3. Fluid Flow and Associated Gas Hydrate System

In Unit S1, located 150 ms TWT beneath the seafloor, at the apex of Svyatogor Ridge is a persistent crosscutting reflector with anomalously high amplitude, reverse polarity cf. the seafloor that simulates the seafloor

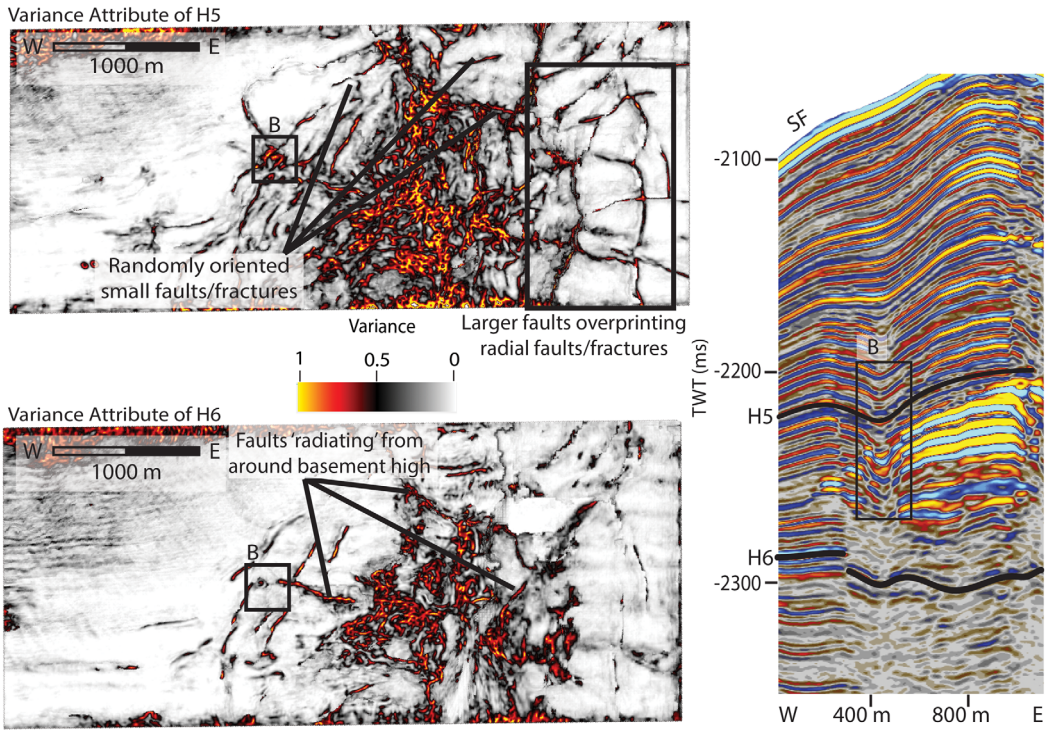


**Figure 5.** Structural maps (variance attribute) of horizons show radial faulting at depths greater than 2,150 ms TWT. These are interpreted to be caused by the uplift of the basement West Peak into its current position. We also identified fracture networks (b) which often present as small circular features in variance attribute, however, are often difficult to observe as faults in the seismic section. Location of horizons shown in Figure 2 and inset.

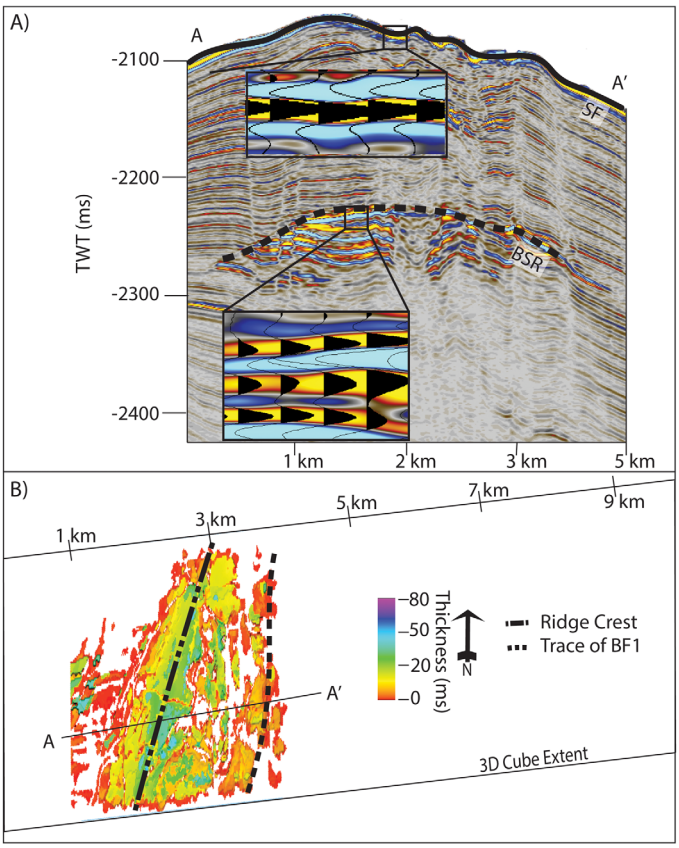


**Figure 6.** (a) The reflection identified as a BSR is characterized by being reverse polarity and mimicking the seafloor as well as being notably higher in amplitude than the surrounding strata. (b) The free gas zone beneath the BSR is relatively small in comparison to the extent of our 3-D cube, however important to note that it is limited to the area west of the BF1 footwall and is thickest at the ridge crest axis.

(Figure 6a). Such a distinct crosscutting reflection is known as the bottom-simulating reflector (BSR) which indicates the base of the GHSZ (Shipley et al., 1979). There is a zone (40–60 ms TWT thick) immediately below the BSR with enhanced amplitudes compared to the surrounding strata (Figure 7b).

This high amplitude zone is also a typical element of a gas hydrate system, where free gas is trapped underneath gas hydrate bearing sediments (e.g., Holbrook et al., 1996). The free gas zone in Svyatogor ridge is contained to the west of the BF1 footwall (Figure 6b), becoming thinner toward the flanks of the sedimentary ridge until disappearing ∼1 km away from the axis of the ridge (Figure 6b). Beneath the enhanced reflection zone is a diminished amplitude zone extending through Units 2, 3, and 4 (Figure 7b). This zone characterized by amplitude blanking is the result of energy attenuation and scattering when the waves travel through gas-bearing sediments (Anderson & Hampton, 1980; Cartwright & Santamarina, 2015; Løseth et al., 2009).

A number of circular-elliptical depression structures (90–350 m diameter) disturb the seafloor at the apex of Svyatogor Ridge (Figure 7a). We interpret these features as pockmarks related to fluid expulsion at the seafloor. There are two distinct fluid migration pathways leading to these seafloor pockmarks. First, underlying the apex of the ridge (Figure 7b) is a zone of hummocky, nonconformant reflections, which are notably lower in amplitude than the rest of Unit S1 (section 4.1.5). This zone is interpreted to be a zone of focused fluid migration, referred to as a chimney zone here. The second fluid migration pathway are faults that upwardly terminate at the base of pockmarks. Spatially, pockmarks with a chimney beneath occur at the crest of the ridge while pockmarks underlain by a fault occur <100 m east of the ridge crest (Figures 7a and 7b).

Within the chimney cluster, interleaved between sections of low amplitude, hummocky reflections are four horizons that have higher amplitude, are semicontinuous, and appear undulating in 2-D. In 3-D, these undulations are circular depressions, the flanks of which are truncating reflectors beneath (Figure 8). These depression structures are infilled with a low amplitude material which onlaps against the flanks of the depression (Figure 8). We interpret these features as buried pockmarks, with the disturbed, low amplitude zones beneath being individual chimneys. Buried pockmarks occur only in the chimney cluster. Although reflections are highly disturbed in the chimney cluster, we are unable to discern any faults leading to buried pockmarks. Buried pockmarks occur specifically on four stratigraphic intervals (Figure 9); however, they are not vertically stacked, nor are they of consistent size, either within the same stratigraphic interval or vertically throughout the data set; therefore, they are not velocity artifacts. Due to their locations on four specific stratigraphic intervals, these are interpreted to be recording episodic fluid expulsion at paleo-seafloors.

## 5. Discussion

### 5.1. Structural and Stratigraphic Evolution of Svyatogor Ridge

The Svyatogor Ridge has undergone much deformation as indicated by the numerous faults present in the data set. The configuration of reflections within the individual units provides information on the style and possible timing of faulting and deformation on the Svyatogor Ridge. The rotation angles and onlap/termination patterns of Units S4 and S3 indicate that these packages have undergone rotation during phases of movement on BF1 and BF2 (Figure 3). Units S2 and S1 are highly faulted, especially around the basement highs (Figures 2 and 5). This is indicative that there was still movement on the basement faults during or after deposition of these units. As the West Spitsbergen Current is the dominant sediment supply current to

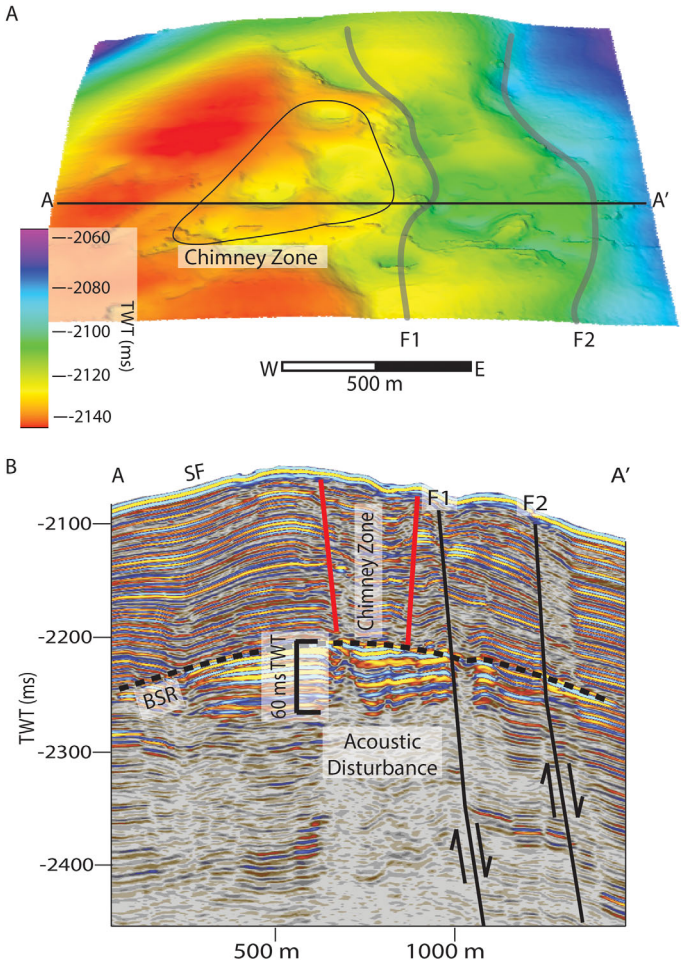


**Figure 7.** (a) Seafloor map (interpreted from the 3-D seismic) shows two groups of pockmarks are observed, those above the chimney zone, and those which are underlain by the western-most sedimentary fault (F1). (b) The chimney zone is immediately adjacent to F1. It is delineated by a change between regular subhorizontal deposition to hummocky irregular deposition. The free gas zone is 60 ms TWT thickest at the thickest point.

the West Svalbard Margin and Yermak Plateau (Eiken & Hinz, 1993), and that Svyatogor Ridge is isolated from downslope processes by the Knipovich Ridge axial valley, the West Spitsbergen Current has likely dominated sediment supply to Svyatogor Ridge in the past. Given that the West Spitsbergen Current has migrated upslope, away from the Svyatogor Ridge (Eiken & Hinz, 1993; Johnson et al., 2015), the Svyatogor Ridge has likely been sediment-limited since spreading began on the northern Knipovich Ridge (Johnson et al., 2015).

Two styles of faulting present in the data can be attributed to regional tectonism—the detachment faults, which are directly linked to spreading on the Knipovich Ridge (Amundsen et al., 2011; Johnson et al., 2015), and the sedimentary faults, which based on the strike of these faults, conform to the regional tectonic setting (Crane et al., 2001). There are two main possible mechanisms for the formation of such faults in this environment.

First, the creation of accommodation space as the Knipovich Ridge spreads can result in gravity driven extension (Bodego & Agirrezabala, 2013; Peel, 2014). Second, growth faulting, which occurs when a mechanically weaker material (sediment) overlies a mechanically stronger material (basement), and the stronger material faults (Hardy & McClay, 1999; Tvedt et al., 2013). As a fault in the basement moves, the sediment overlying the basement accommodates this by folding (Figure 10); however, as offset on the basement fault increases, the folds may become breached, forming the sedimentary faults (Ferrill et al., 2012; Hardy & McClay, 1999). The process of sedimentary fault propagation through this mechanism will occur at a rate determined by the movement of the basement fault (Allmendinger & Shaw, 2000; Ferrill et al., 2012). In this study area, the basement faults are accommodating the stress from the ultraslow extension at the plate boundary. Therefore, we would expect episodic movement on the basement faults implying that the sedimentary faults would have also grown over a much longer period than in a faster spreading environment. We suggest that this has also had consequences for fluid migration within this system.

### 5.2. Fluid Migration Evolution

The fluid migration system on Svyatogor Ridge is unique in that it occurs in a sedimented mid-ocean ridge system where the basement rock is identified only ~500 ms TWT beneath the seafloor. Additionally, all the fluid flow features, such as the BSR and pockmarks, occur exclusively above the basement faults. Although it is not clear whether the system is still actively leaking fluid today, buried pockmarks occurring along certain stratigraphic horizons would indicate episodic fluid release events. In such large water depths, temperature and pressure changes due to sea-level fluctuations during glacial cycles are unlikely to have had a significant effect on the dynamics of a gas hydrate and associated fluid flow system here. However, it remains uncertain whether glacial related isostatic adjustments as modeled on the West Svalbard shelf (Wallmann et al., 2018) may have influenced fault activity and fluid migration on Svyatogor Ridge.

Johnson et al. (2015) proposed that the basement faults imaged on Svyatogor Ridge are acting as fluid migration pathways for fluids from the mid-ocean ridge system to reach the shallow subsurface. In this scenario, periods of fluid activity (migration and release from the seafloor) are most likely tectonically controlled. As noted previously, faulting events on BF1 and BF2 have occurred as recently as the time Unit S2 was deposited.

On the seafloor, pockmarks occur above both the chimney zone and above faults 50–100 m east of the chimney zone. Buried pockmarks, however, occur only within the chimney zone and not associated with

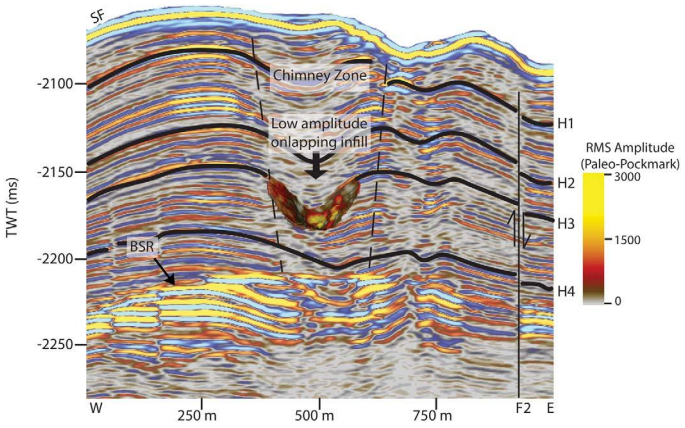


**Figure 8.** Paleo-pockmarks occur only within the Chimney zone, bordered by two sedimentary faults which are pervasive through the data, F1 and F2 (F2 annotated here). The paleo-pockmarks occur beneath the crest of the ridge, where the BSR is shallowest. One paleo-pockmark is highlighted in this figure, with the base of the paleo-pockmark displayed using RMS amplitude attribute to highlight that the paleo-pockmarks are circular-elliptical in shape and have a higher amplitude base than infill. Additionally, there is a higher amplitude at the base of the depression than the flanks, indicated by the RMS amplitude attribute. The infill is characterized by being onlapping against the base of the pockmark.

the faults to the east (Figures 8 and 9). This indicates that fluids bypassing the GHSZ have found an additional pathway over time; from releasing at paleo-seafloor(s) at the apex of the ridge indicated by paleo-pockmarks within the chimney zone to utilizing zones of weakness and fault planes, which culminates in pockmarks above faults. We interpret that this is a function of the time taken for sedimentary faults to develop. As shown in Figure 11, below the GHSZ fluid is able to utilize faults as migration pathways to the point of encountering the fold at the upper termination—the fold is acting as a structural seal. If the pore spaces of the sediment become overpressurized before another section of folded strata breaches into faults, fluid release to the seafloor will be characterized by "blow-out" type seal bypass systems (Cartwright et al., 2007) such as a chimney. As sedimentary faults propagate upward toward the seafloor they provide an additional seal bypass pathway (Figure 11). We have also identified small fracture networks, which are important in transporting fluid through the GHSZ. These fracture networks have randomly oriented strikes and therefore are not a consequence of the regional tectonic regime. We suggest that fracture networks are a consequence of hydraulic fracturing, occurring as fluids migrate through the subsurface. Small faults themselves have random strikes, but to the east of the free gas zone, these faults become integrated with sedimentary faults striking in compliance with the regional tectonic regime. Fracture networks appear to be restricted to a zone immediately above and within the free gas zone. We suggest that this is evidence for how fluid bypassed a seal created by hydrate clogging the pore space, a model consistent with Hornbach et al. (2004). We suggest that faults or planes of weakness were created in the past when the radial faulting formed that were then reactivated as the free gas zone became critically thick (Hornbach et al., 2004). In this scenario, planes of weakness across the seal need only be reactivated so that overpressure is released, and fluid can migrate upward without obstruction. We cannot determine from seismic data alone the type of brittle failure that is occurring to create these fractures (i.e., hydraulic extension fractures, extensional shear fractures, or meshes) (Sibson, 2003). However, we propose that in this case gas hydrate within the pore space of the sediment and the natural anticlinal structure of the ridge acts as an effective seal or cap rock. The fracture networks we identify here could be seismic evidence for the extent of the seal trapping free gas in this study location (Hornbach et al., 2004; Sibson, 2003).

Given that there are buried pockmarks found at ~30 ms TWT (~22 m) above the current BSR, and ~60 ms TWT (~45 m) above YP2–3 (Figures 9 and 11), gas migration into the free gas zone, gas hydrate formation, and migration to the (paleo-)seafloor has been ongoing during most of S1 deposition (Figures 2 and 11). Johnson et al. (2015) proposed that abiotic methane from serpentinization could be the origin of much of the gas here on Svyatogor Ridge. Our research suggests that the detachment faults here have indeed played a major role in driving fluid migration and expulsion in the subsurface and that methane may well have originated within these faults through serpentinization.

### 5.3. Consequence of Active Margin, Deep Ocean Setting on the Gas Hydrate and Fluid Flow System

The location of the Svyatogor Ridge on the flank of the Knipovich Ridge, atop detachment faults (which accommodate rifting), makes it a unique location for a gas hydrate and fluid flow system. In general the types of fluid flow systems normally identified on the flanks of spreading ridges are high temperature basalt hosted hydrothermal vent systems, generated by the increased heat flow provided by magmatic centers along axis (e.g., Guaymas Basin (Lizarralde et al., 2011)) or lower temperature peridotite hosted hydrothermal systems sustained by water-rock serpentinization reactions (e.g., Lost City Hydrothermal Field (Kelley et al., 2005)). In the case of the northern Knipovich Ridge, the ultraslow spreading regime, accommodated by observed detachment faults, implies it is a magma-limited environment, which would be inherently a lower temperature subseafloor regime, suitable for the development of the observed, stable gas hydrate system. There is documentation of magmatic instrusive bodies on the eastern flank of the Northern

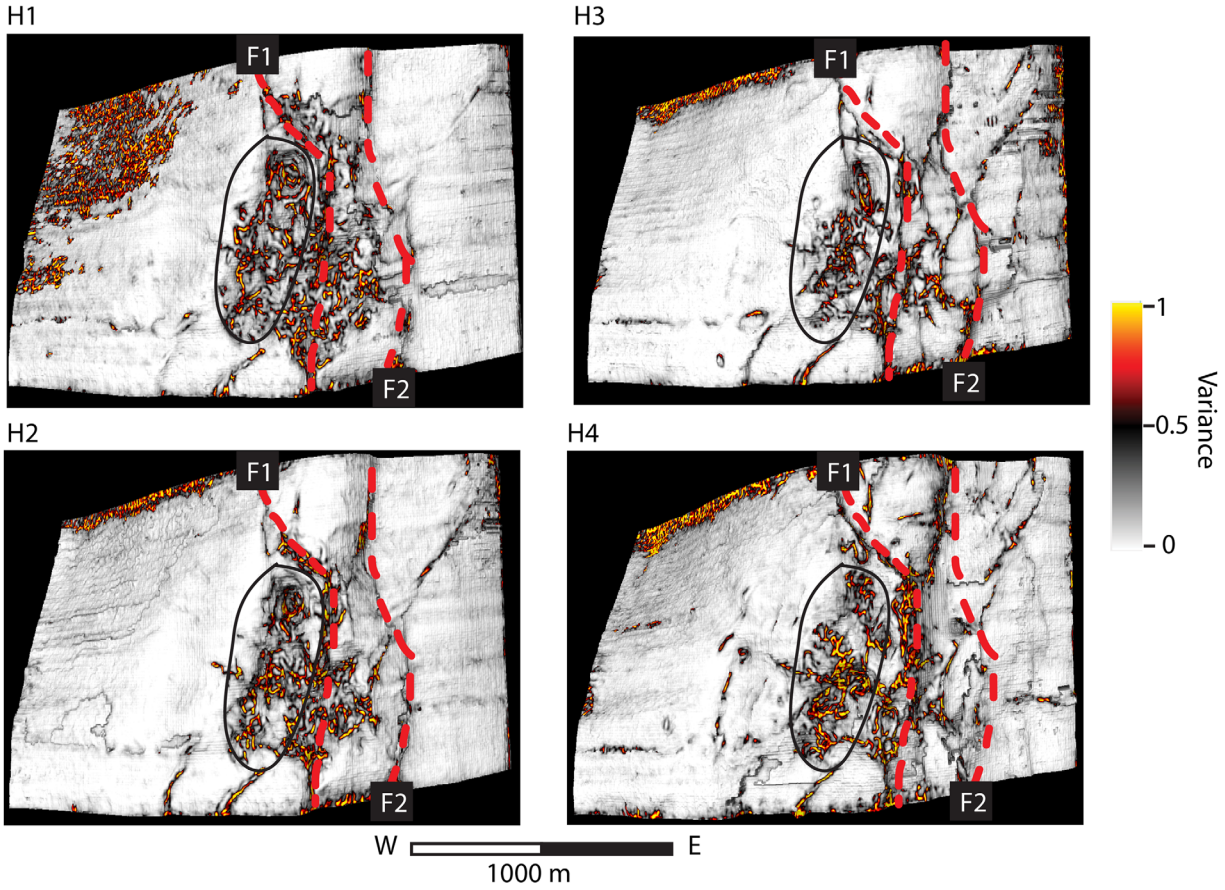


**Figure 9.** In variance attribute taken across horizons, the chimney zone (black oval) is characterized by being highly variant, but chaotic. The first two pervasive sedimentary faults (F1 and F2, red dotted lines) are clear in all four variance maps, and border the chimney zone to the east. Locations of horizons shown in Figures 2 and 8.

Knipovich Ridge (Ritzmann et al., 2004), which would have presumably formed in conjunction with rifting on either the Molloy Ridge or the Knipovich Ridge, in a mixed mode scenario of detachment fault and magmatic spreading in the past; however, other studies have not found evidence for magmatic instrusive bodies associated with the northern section of the Knipovich Ridge (i.e., Amundsen et al., 2011; Crane et al., 2001). Partial serpentinization of the crust at this location is supported by Ritzmann et al. (2004) who observe crustal velocities of ~7.6 km/s south of the Molloy Transform Fault. Hydrothermal system studies further south along the Knipovich Ridge also suggest that there is some methane flux from serpentinization along with other hydrothermally generated fluids (Cannat et al., 2010). That a fluid flow system exists on a spreading ridge is not unique in itself due to the abundance of hydrothermal systems present on mid-ocean ridges, but the lack of significant heat flow and therefore, potential for a stable gas hydrate stability zone, is an interesting case for Svyatogor Ridge, as gas hydrate systems are normally identified on passive continental margins, far from spreading ridges. Most of the world's oceans deeper than approximately 300 mbsl have potential for gas hydrate stability (Kvenvolden, 1993). However, a distal setting is commonly excluded from global gas hydrate concentration models due to a lack of organic matter deposition (Klauda & Sandler, 2005). A possible exception to this is of course in the case where the Continental-Oceanic crust boundary is proximal to a sediment source and has been active for a long period of time, for example, in the Gulf of Mexico or in the Fram Strait at Vestnesa Ridge. On the Svyatogor Ridge, however, asymmetric, ultraslow spreading of the Knipovich Ridge means that the Svyatogor Ridge has, since the underlying crust formed, been in proximity to the West Svalbard Margin and West Spitsbergen Current, allowing sedimentation at the northern extent of the Knipovich Ridge flanks (Eiken & Hinz, 1993; Johnson et al., 2015) and therefore providing suitable reservoir material for fluids generated by crustal processes.

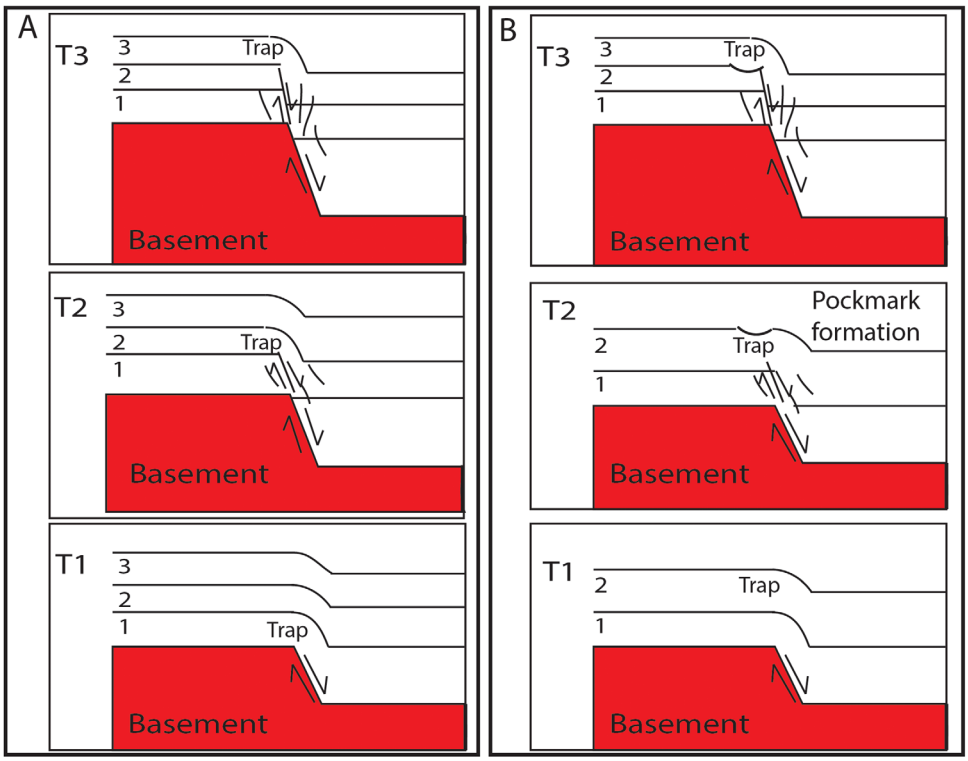


**Figure 10.** (a) Conceptual diagram of fault growth where a mechanically stronger basement, covered by a mechanically weaker strata, faults and causes folds to develop, and with continued movement on the basement fault these folds breach into faults. In this simple scenario, fluid () can utilize the faulted sections to migrate but may become trapped (labeled "trap") by the unfaulted strata (after Hardy & McClay, 1999). (b) When this process occurs close to the seafloor, fluid seepage across the seafloor results in pockmark formation. With continued syn-deformation sedimentation, pockmarks get buried and the process continues.

The occurrence of a gas hydrate system on the flank of an actively spreading margin presents an interesting case because active margin hydrate systems are better studied and more prolific on subduction margins, for example, the Hikurangi (Barnes et al., 2010; Crutchley et al., 2010; Faure et al., 2006; Pecher et al., 2005) and Cascadia margins (Bohrmann et al., 1998; Pohlman et al., 2009; Riedel & Collett, 2005; Suess et al., 1999). In a compressional tectonic system, we expect to identify particular structural fabrics related to the regional tectonic regime. However, these structural fabrics will differ in an extensional regime, and while we can compare a gas hydrate system in an extensional setting to, for example, a hydrothermal system in terms of fluid flow pathway development, the Svyatogor Ridge setting may be confounded by two additional factors: (1) the location proximal to a strike-slip tectonic setting could be influencing the tectonic setting and (2) it is difficult to determine what effect, if any, an ultraslow spreading regime has on the coupling between fluid migration pathway development, seepage and tectonic development. In this initial investigation of Svyatogor Ridge, we have not been able to determine with precision if the Molloy Transform Fault has an influence on the structural fabric and therefore fluid flow regime; however, we have posited that the ultraslow nature of the Knipovich Ridge might have played a role in the timing of fluid release on the Svyatogor Ridge. In contrast to the tectonic setting on Vestnesa Ridge, which is a contourite drift developed close to the mid-ocean ridge but on a passive margin slope, (Bünz et al., 2012; Plaza-Faverola et al., 2015; Vanneste et al., 2005), Svyatogor Ridge appears to be unique in that sedimentary sequences, the gas hydrate system, and the tectonic setting are developing in unison, particularly reliant on the tectonic setting to form as they have.

### 5.4. A Note on Gas Origin

Shallow penetrating gravity cores collected on Svyatogor Ridge during CAGE expeditions have yet to recover enough gas for isotopic analysis. As there are no other gas samples from the Svyatogor Ridge available to the authors, we note from the 3-D seismic survey that (1) faults appear to be controlling where and

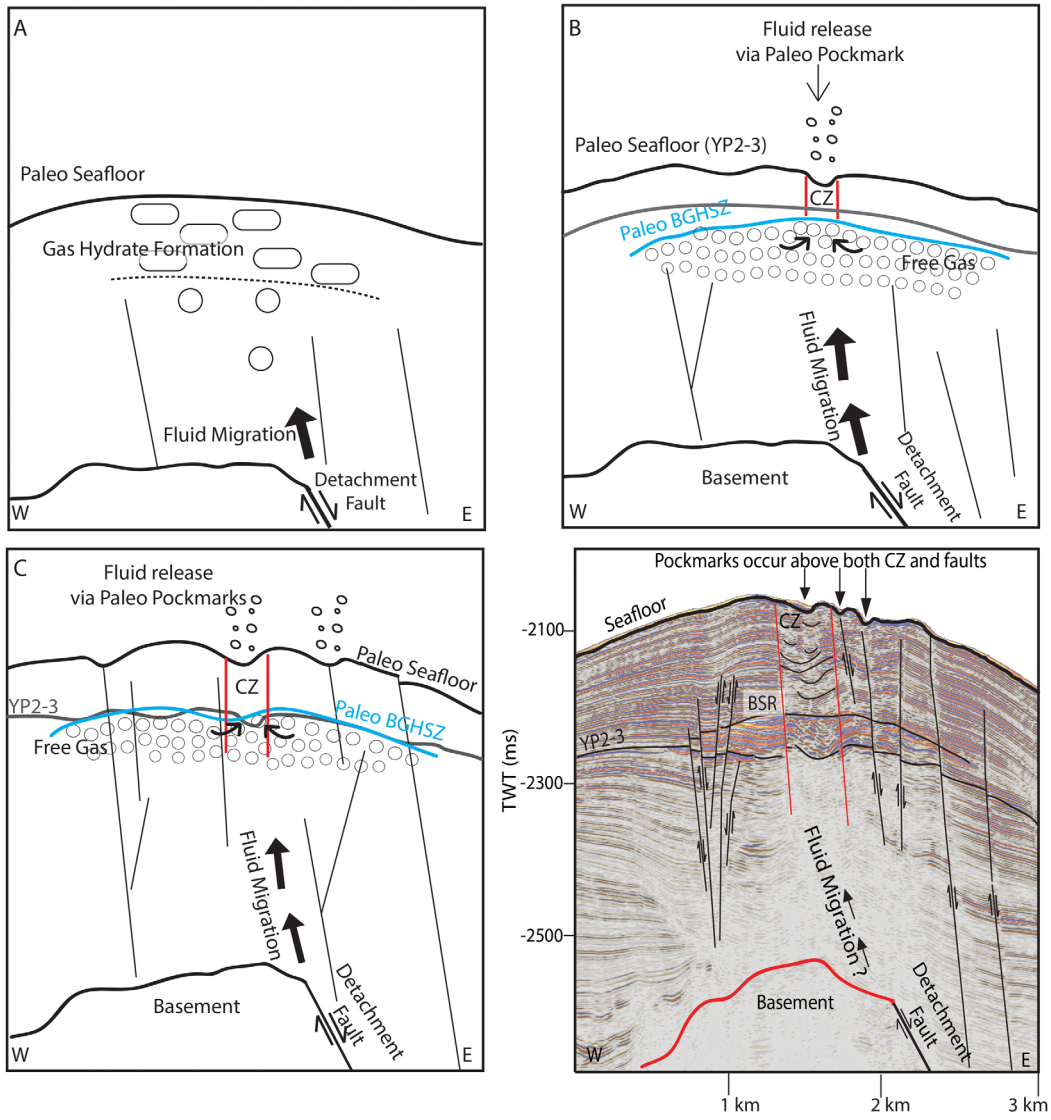


**Figure 11.** (a) During initial activation of the detachment fault, faults in the sedimentary strata had not propagated far through the sedimentary column so they were not fluid migration pathways to the seafloor. However, gas hydrate can develop as can a free gas zone. (b) With prolonged fluid migration into the system, fluids in the FGZ can become over-pressurized and force the chimney zone to form (c). As additional material deposited, the BGHSZ is able to migrate upward, and sedimentary faults propagated further due to further movement on detachment fault. This means that fluid migrating to the seafloor is able to use faults as fluid migration pathways to the seafloor. (d) Today, it is not clear whether the detachment faults are supplying fluid to Svyatogor Ridge; however, the evidence of past fluid migration and release is preserved.

how the gas hydrate system has formed and that (2) the detachment faults are the major linking factor to all the processes occurring on the Svyatogor Ridge (sedimentary fault development, fluid flow pathway development, and ridge topography). With regards to thermogenic gas production, we posit that there has been no thermogenic methane produced within the sediments on the Svyatogor Ridge itself as the criterion for generation (normally depths greater than 1,000 m below seafloor (Floodgate & Judd, 1992)) is not met. We cannot rule out that there is gas migrating from another source, for example, across the Molloy Transform Fault (Smith et al., 2014) or from Hovgård Ridge (Knies et al., 2018), which has also been shown to have some source rock present (Knies & Mann, 2002). We do note, however, that methane is generated in serpentinization reactions (Etiope & Sherwood Lollar, 2013) and that Cannat et al. (2010) and Proskurowski et al. (2008) show methane production from serpentinization is produced in slow to ultraslow spreading ridge settings. Additionally, Ritzmann et al. (2004) shows that there is potential for partially serpentinized

crust beneath Svyatogor Ridge. Given that the detachment faults are key for the dynamics of this gas hydrate system, we would not rule out some contribution from serpentinization produced methane. Active methane production via serpentinization beneath the study location today may be unlikely, however, as the detachment faults now are approaching the end, or are at the end, of their typical duration of activity (1–3 My), sedimentation above the oceanic crust restricts seawater peridotite interaction, and continued spreading and offset along the MTF has nearly removed Svyatogor Ridge sediments from the serpentinization driven abiotic methane window suggested by Johnson et al. (2015). Thus, any abiotic methane present within the gas hydrate system here today, must have formed while the detachment faults were active, Svyatogor Ridge was within the abiotic methane production window, and there was sufficient sedimentation to trap the gases. In this scenario, methane generated through serpentinization may be preserved in early developing gas hydrate systems, like Svyatogor Ridge, but with continued development, the influence of crustal sources of fluids and gases may be minimized. Given the history here, we associate the modern fluid flow system in this study area as a sediment hosted gas hydrate system that developed over the last ~3 million years.

## 6. Conclusion

The Svyatogor Ridge has developed on the North Western flank of the Knipovich Ridge in an active margin setting. The majority of sedimentation on the Svyatogor Ridge has been interpreted to deposit during the YP-2 and YP-3 sedimentation regimes, while the Svyatogor Ridge was still close to the spreading center and an active sediment supply. The tectonic environment here has greatly controlled all aspects of development in this setting, from sedimentary evolution to fluid flow system evolution. Sedimentary faults in the 3-D seismic data are directly linked to the movement on spreading related detachment faults and the seismic stratigraphy is largely based on changes of reflection patterns linked to phases of faulting on detachment faults. The gas hydrate system on the Svyatogor Ridge is located on the flank of the Knipovich ridge axis—in a natural trapping structure along the crest of the Svyatogor Ridge. Seepage from this system to the water column has been episodic in nature, occurring at four distinct intervals throughout the last ~2.7 Ma. Tectonism appears to be the major driver of fluid flow on Svyatogor Ridge, with movement on detachment faults shown to be impacting both the fluid flow into the gas hydrate and free gas zones, and release of at the (paleo-)seafloor.

Subaqueous gas hydrate reservoirs are generally found in settings with thick sedimentary sequences: on passive continental margins, contourite deposits, or active (subducting) continental margins. Svyatogor Ridge, however, is a sediment-limited, deep water drift located on an actively spreading plate boundary. Worldwide, this setting type is generally dominated by hydrothermal fluid systems sustained by seawater circulation in basalt or peridotite dominated crust. Due to the amagmatic nature of the northern Knipovich Ridge, there is no significant heat source for a magmatically heated hydrothermal system. Hydrothermal systems further south along the Knipovich Ridge have been shown to have methane as a fluid constituent, due to serpentinization reactions, and on the Svyatogor Ridge studies have shown that the acoustic velocity of basement material give a likelihood of serpentinitized mantle beneath the Svyatogor Ridge. Therefore, we conclude that the Svyatogor Ridge has developed a gas hydrate system in this ultraslow, amagmatic spreading setting largely due to the presence of detachment faults, which accommodate seafloor spreading and deformation of the overlying sediment column, enable seawater rock reactions to drive serpentinization, and serve as pathways for crustal fluid and gas migration to the overlying sediments.

**Acknowledgments**
This work was supported by the Research Council of Norway through its Centres of Excellence funding scheme, project 223259. We acknowledge the crew and scientific party aboard the R.V. Helmer Hanssen during CAGE expeditions 14-1, 14-2, and 15-6. We thank the reviewers for their insightful comments and suggestions for improvement. We also acknowledge Schlumberger for providing interpretational software. Seismic data can be accessed at UiT Open Research Data Repository.

## References

Allmendinger, R. W., & Shaw, J. H. (2000). Estimation of fault propagation distance from fold shape: Implications for earthquake hazard assessment. *Geology*, *28*(12), 1099–1102. https://doi.org/10.1130/0091-7613(2000)28<1099:EOFPDF>2.0.CO;2

Amundsen, I. M. H., Blinova, M., Hjelstuen, B. O., Mjelde, R., & Haflidason, H. (2011). The Cenozoic western Svalbard margin: Sediment geometry and sedimentary processes in an area of ultraslow oceanic spreading. *Marine Geophysical Research*, *32*(4), 441–453. https://doi.org/10.1007/s11001-011-9127-z

Anderson, A. L., & Hampton, L. D. (1980). Acoustics of gas-bearing sediments I. Background. *The Journal of the Acoustical Society of America*, *67*(6), 1865–1889. https://doi.org/10.1121/1.384453

Barnes, P. M., Lamarche, G., Bialas, J., Henrys, S., Pecher, I., Netzeband, G. L., et al. (2010). Tectonic and geological framework for gas hydrates and cold seeps on the Hikurangi subduction margin, New Zealand. *Marine Geology*, *272*(1–4), 26–48.

Beszczynska-Möller, A., Fahrbach, E., Schauer, U., & Hansen, E. (2012). Variability in Atlantic water temperature and transport at the entrance to the Arctic Ocean, 1997–2010. *ICES Journal of Marine Science: Journal Du Conseil*, *69*(5), 852–863. https://doi.org/10.1093/icesjms/fss056

Bodego, A., & Agirrezabala, L. M. (2013). Syn-depositional thin-and thick-skinned extensional tectonics in the mid-Cretaceous Lasarte sub-basin, western Pyrenees. *Basin Research*, *25*(5), 594–612. https://doi.org/10.1111/bre.12017
Bohrmann, G., Greinert, J., Suess, E., & Torres, M. (1998). Authigenic carbonates from the Cascadia subduction zone and their relation to gas hydrate stability. *Geology*, *26*(7), 647–650.
Bünz, S., Polyanov, S., Vadakkepuliyambatta, S., Consolaro, C., & Mienert, J. (2012). Active gas venting through hydrate-bearing sediments on the Vestnesa Ridge, offshore W-Svalbard. *Marine Geology*, *332–334*, 189–197. https://doi.org/10.1016/j.margeo.2012.09.012
Cann, J., Blackman, D., Smith, D., McAllister, E., Janssen, B., Mello, S., et al. (1997). Corrugated slip surfaces formed at ridge-transform intersections on the Mid-Atlantic Ridge. *Nature*, *385*(6614), 329. https://doi.org/10.1038/385329a0
Cannat, M., Fontaine, F., & Escartin, J. (2010). Serpentinization and associated hydrogen and methane fluxes at slow spreading ridges. In Rona, P. A., Devey, C. W., Dyment, J., & Murton, B. J. (Eds.), *Diversity of hydrothermal systems on slow spreading ocean ridges* (pp. 241–264). Washington, DC: American Geophysical Union.
Cartwright, J., Huuse, M., & Aplin, A. (2007). Seal bypass systems. *AAPG Bulletin*, *91*(8), 1141–1166. https://doi.org/10.1306/04090705181
Cartwright, J., & Santamarina, C. (2015). Seismic characteristics of fluid escape pipes in sedimentary basins: Implications for pipe genesis. *Marine and Petroleum Geology*, *65*, 126–140. https://doi.org/10.1016/j.marpetgeo.2015.03.023
Corfield, S., & Sharp, I. (2000). Structural style and stratigraphic architecture of fault propagation folding in extensional settings: A seismic example from the Smørbukk area, Halten Terrace, Mid-Norway. *Basin Research*, *12*(3–4), 329–341. https://doi.org/10.1111/j.1365-2117.2000.00133.x
Crane, K., Doss, H., Vogt, P., Sundvor, E., Cherkashov, G., Poroshina, I., et al. (2001). The role of the Spitsbergen shear zone in determining morphology, segmentation and evolution of the Knipovich Ridge. *Marine Geophysical Researches*, *22*(3), 153–205. https://doi.org/10.1029/91JB01231
Crutchley, G. J., Pecher, I. A., Gorman, A. R., Henrys, S. A., & Greinert, J. (2010). Seismic imaging of gas conduits beneath seafloor seep sites in a shallow marine gas hydrate province, Hikurangi Margin, New Zealand. *Marine Geology*, *272*(1–4), 114–126.
Dick, H. J., Lin, J., & Schouten, H. (2003). An ultraslow-spreading class of ocean ridge. *Nature*, *426*(6965), 405–412. https://doi.org/10.1038/nature02128
Eagles, G., Pérez-Díaz, L., & Scarselli, N. (2015). Getting over continent ocean boundaries. *Earth-Science Reviews*, *151*, 244–265.
Ehlers, B.-M., & Jokat, W. (2009). Subsidence and crustal roughness of ultra-slow spreading ridges in the northern North Atlantic and the Arctic Ocean. *Geophysical Journal International*, *177*(2), 451–462. https://doi.org/10.1111/j.1365-246X.2009.04078.x
Eiken, O., & Hinz, K. (1993). Contourites in the Fram Strait. *Sedimentary Geology*, *82*(1–4), 15–32. https://doi.org/10.1016/0037-0738(93)90110-Q
Engen, Ø., Faleide, J. I., & Dyreng, T. K. (2008). Opening of the Fram Strait gateway: A review of plate tectonic constraints. *Tectonophysics*, *450*(1–4), 51–69. https://doi.org/10.1016/j.tecto.2008.01.002
Escartin, J., Smith, D. K., Cann, J., Schouten, H., Langmuir, C. H., & Escrig, S. (2008). Central role of detachment faults in accretion of slow-spreading oceanic lithosphere. *Nature*, *455*(7214), 790–794. https://doi.org/10.1038/nature07333
Etiope, G., & Sherwood Lollar, B. (2013). Abiotic methane on Earth. *Reviews of Geophysics*, *51*, 276–299. https://doi.org/10.1002/rog.20011
Faure, K., Greinert, J., Pecher, I. A., Graham, I. J., Massoth, G. J., De Ronde, C. E., et al. (2006). Methane seepage and its relation to slumping and gas hydrate at the Hikurangi margin, New Zealand. *New Zealand Journal of Geology and Geophysics*, *49*(4), 503–516.
Faugeres, J.-C., Stow, D. A., Imbert, P. & Viana, A. (1999). Seismic features diagnostic of contourite drifts. *Marine Geology*, *162*, 1–38. https://doi.org/10.1016/S0025-3227(99)00068-7
Ferrill, D. A., Morris, A. P., & McGinnis, R. N. (2012). Extensional fault-propagation folding in mechanically layered rocks: The case against the frictional drag mechanism. *Tectonophysics*, *576–577*, 78–85. https://doi.org/10.1016/j.tecto.2012.05.023
Floodgate, G., & Judd, A. (1992). The origins of shallow gas. *Continental Shelf Research*, *12*(10), 1145–1156.
Geissler, W. H., Jokat, W., & Brekke, H. (2011). The Yermak Plateau in the Arctic Ocean in the light of reflection seismic data-implication for its tectonic and sedimentary evolution. *Geophysical Journal International*, *187*(3), 1334–1362. https://doi.org/10.1111/j.1365-246X.2011.05197.x
Hansen, J., Cartwright, J., Huuse, M., & Clausen, O. R. (2005). 3D seismic expression of fluid migration and mud remobilization on the Gjallar Ridge, offshore mid-Norway. *Basin Research*, *17*(1), 123–139. https://doi.org/10.1111/j.1365-2117.2005.00257.x
Hardy, S., & McClay, K. (1999). Kinematic modelling of extensional fault-propagation folding. *Journal of Structural Geology*, *21*(7), 695–702. https://doi.org/10.1016/S0191-8141(99)00072-3
Hartwig, A., Anka, Z., & di Primio, R. (2012). Evidence of a widespread paleo-pockmarked field in the Orange Basin: An indication of an early Eocene massive fluid escape event offshore South Africa. *Marine Geology*, *332–334*, 222–234.
Holbrook, W. S., Hoskins, H., Wood, W. T., Stephen, R. A., & Lizarralde, D. (1996). Methane hydrate and free gas on the Blake Ridge from vertical seismic profiling. *Science*, *273*(5283), 1840. https://doi.org/10.1126/science.273.5283.1840
Hornbach, M. J., Saffer, D. M., & Steven Holbrook, W. (2004). Critically pressured free-gas reservoirs below gas-hydrate provinces. *Nature*, *427*(6970), 142–144. https://doi.org/10.1038/nature02172
Howe, J. A., Shimmield, T. M., Harland, R., & Eyles, N. (2008). Late Quaternary contourites and glaciomarine sedimentation in the Fram Strait. *Sedimentology*, *55*, 179–200. https://doi.org/10.1111/j.1365-3091.2007.00897.x
Hustoft, S., Bünz, S., Mienert, J., & Chand, S. (2009). Gas hydrate reservoir and active methane-venting province in sediments on $<$20 Ma young oceanic crust in the Fram Strait, offshore NW-Svalbard. *Earth and Planetary Science Letters*, *284*(1–2), 12–24. https://doi.org/10.1016/j.epsl.2009.03.038
Jackson, C., Gawthorpe, R., & Sharp, I. (2006). Style and sequence of deformation during extensional fault-propagation folding: Examples from the Hammam Faraun and El-Qaa fault blocks, Suez Rift, Egypt. *Journal of Structural Geology*, *28*(3), 519–535. https://doi.org/10.1016/j.jsg.2005.11.009
Johnson, J. E., Mienert, J., Plaza-Faverola, A., Vadakkepuliyambatta, S., Knies, J., Bünz, S., et al. (2015). Abiotic methane from ultraslow-spreading ridges can charge Arctic gas hydrates. *Geology*, *43*(5), 371–374. https://doi.org/10.1130/G36440.1
Kelley, D. S., Karson, J. A., Früh-Green, G. L., Yoerger, D. R., Shank, T. M., Butterfield, D. A., et al. (2005). A serpentinite-hosted ecosystem: The Lost City hydrothermal field. *Science*, *307*(5714), 1428–1434.
Klauda, J. B., & Sandler, S. I. (2005). Global distribution of methane hydrate in ocean sediment. *Energy & Fuels*, *19*(2), 459–470.
Knies, J., Daszinnies, M., Plaza-Faverola, A., Chand, S., Sylta, Ø., Bünz, S., et al. (2018). Modelling persistent methane seepage offshore western Svalbard since early Pleistocene. *Marine and Petroleum Geology*, *91*, 800–811. https://doi.org/10.1016/j.marpetgeo.2018.01.020
Knies, J., & Mann, U. (2002). Depositional environment and source rock potential of Miocene strata from the central Fram Strait: Introduction of a new computing tool for simulating organic facies variations. *Marine and Petroleum Geology*, *19*(7), 811–828.
Kvenvolden, K. A. (1993). Gas hydrates-geological perspective and global change. *Review of Geophysics*, *31*(2), 173–187. https://doi.org/10.1029/93RG00268

Lizarralde, D., Soule, S. A., Seewald, J. S., & Proskurowski, G. (2011). Carbon release by off-axis magmatism in a young sedimented spreading centre. *Nature Geoscience*, *4*(1), 50–54.
Lundin, E., & Doré, A. (2002). Mid-Cenozoic post-breakup deformation in the 'passive' margins bordering the Norwegian-Greenland Sea. *Marine and Petroleum Geology*, *19*(1), 79–93. https://doi.org/10.1016/S0264-8172(01)00046-0
Løseth, H., Gading, M., & Wensaas, L. (2009). Hydrocarbon leakage interpreted on seismic data. *Marine and Petroleum Geology*, *26*(7), 1304–1319. https://doi.org/10.1016/j.marpetgeo.2008.09.008
Mattingsdal, R., Knies, J., Andreassen, K., Fabian, K., Husum, K., Grøsfjeld, K., et al. (2014). A new 6 Myr stratigraphic framework for the Atlantic-Arctic Gateway. *Quaternary Science Reviews*, *92*, 170–178. https://doi.org/10.1016/j.quascirev.2013.08.022
Michael, P., Langmuir, C., Dick, H., Snow, J., Goldstein, S., Graham, D., et al. (2003). Magmatic and amagmatic seafloor generation at the ultraslow-spreading Gakkel ridge, Arctic Ocean. *Nature*, *423*(6943), 956–961. https://doi.org/10.1038/nature01704
Müller, P. J., & Suess, E. (1979). Productivity, sedimentation rate, and sedimentary organic matter in the oceans—I. Organic carbon preservation. *Deep-Sea Research Part A*, *26*(12), 1347–1362.
Okino, K., Curewitz, D., Asada, M., Tamaki, K., Vogt, P., & Crane, K. (2002). Preliminary analysis of the Knipovich Ridge segmentation: Influence of focused magmatism and ridge obliquity on an ultraslow spreading system. *Earth and Planetary Science Letters*, *202*(2), 275–288. https://doi.org/10.1016/S0012-821X(02)00790-2
Paull, C. K., Ussle, W., & Borowski, W. S. (1994). Sources of biogenic methane to form marine gas hydrates in situ production or upward migration? *Annals of the New York Academy of Sciences*, *715*(1), 392–409.
Pecher, I., Henrys, S., Ellis, S., Chiswell, S., & Kukowski, N. (2005). Erosion of the seafloor at the top of the gas hydrate stability zone on the Hikurangi Margin, New Zealand. *Geophysical Research Letters*, *32*, L24603. https://doi.org/10.1029/2005GL024687
Peel, F. J. (2014). The engines of gravity-driven movement on passive margins: Quantifying the relative contribution of spreading vs. gravity sliding mechanisms. *Tectonophysics*, *633*, 126–142. https://doi.org/10.1016/j.tecto.2014.06.023
Peive, A., & Chamov, N. (2008). Basic tectonic features of the Knipovich Ridge (North Atlantic) and its neotectonic evolution. *Geotectonics*, *42*(1), 31–47. https://doi.org/10.1134/S0016852108010044
Planke, S., Erikson, F. N., Berndt, C., Mienert, J., & Masson, D. (2009). P-Cable high-resolution seismic. *Oceanography*, *22*(1), 85. https://doi.org/10.5670/oceanog.2009.09
Plaza-Faverola, A., Bünz, S., Johnson, J. E., Chand, S., Knies, J., Mienert, J., et al. (2015). Role of tectonic stress in seepage evolution along the gas hydrate-charged Vestnesa Ridge, Fram Strait. *Geophysical Research Letters*, *42*, 733–742. https://doi.org/10.1002/2014GL062474
Pohlman, J., Kaneko, M., Heuer, V., Coffin, R., & Whiticar, M. (2009). Methane sources and production in the northern Cascadia margin gas hydrate system. *Earth and Planetary Science Letters*, *287*(3–4), 504–512.
Proskurowski, G., Lilley, M. D., Seewald, J. S., Fru h-Green, G. L., Olson, E. J., Lupton, J. E., et al. (2008). Abiogenic hydrocarbon production at Lost City hydrothermal field. *Science*, *319*(5863), 604–607.
Rajan, A., Mienert, J., Bünz, S., & Chand, S. (2012). Potential serpentinization, degassing, and gas hydrate formation at a young (<20 Ma) sedimented ocean crust of the Arctic Ocean ridge system. *Journal of Geophysical Research*, *117*, B03102. https://doi.org/10.1029/2011JB008537
Rebesco, M., Wåhlin, A., Laberg, J. S., Schauer, U., Beszczynska-Möller, A., Lucchi, R. G., et al. (2013). Quaternary contourite drifts of the Western Spitsbergen margin. *Deep-Sea Research Part I*, *79*, 156–168. https://doi.org/10.1016/j.dsr.2013.05.013
Riedel, M., & Collett, T. (2005). *Cascadia margin gas hydrates* (IODP Preliminary Rep. 311). College Station, TX: Ocean Drilling Program.
Ritzmann, O., Jokat, W., Czuba, W., Guterch, A., Mjelde, R., & Nishimura, Y. (2004). A deep seismic transect from Hovgård Ridge to northwestern Svalbard across the continental-ocean transition: A sheared margin study. *Geophysical Journal International*, *157*(2), 683–702. https://doi.org/10.1111/j.1365-246X.2004.02204.x
Shipley, T. H., Houston, M. H., Buffler, R. T., Shaub, F. J., McMillen, K. J., Ladd, J. W., et al. (1979). Seismic evidence for widespread possible gas hydrate horizons on continental slopes and rises. *AAPG Bulletin*, *63*(12), 2204–2213. https://doi.org/10.1306/2f91890a-16ce-11d7-8645000102c1865d
Sibson, R. H. (2003). Brittle-failure controls on maximum sustainable overpressure in different tectonic regimes. *AAPG Bulletin*, *87*(6), 901–908. https://doi.org/10.1306/01290300181
Sloan, E. D. (1998). Gas hydrates: Review of physical/chemical properties. *Energy & Fuels*, *12*(2), 191–196. https://doi.org/10.1021/ef970164+
Smith, A. J., Mienert, J., Bünz, S., & Greinert, J. (2014). Thermogenic methane injection via bubble transport into the upper Arctic Ocean from the hydrate-charged Vestnesa Ridge, Svalbard. *Geochemistry, Geophysics, Geosystems*, *15*, 1945–1959. https://doi.org/10.1002/2013GC005179
Snow, J., Hellebrand, E., Jokat, W., & Mühe, R. (2001). Magmatic and hydrothermal activity in Lena Trough, Arctic Ocean. *EOS, Transactions American Geophysical Union*, *82*(17), 193–198. https://doi.org/10.1029/01EO00101
Suess, E., Torres, M., Bohrmann, G., Collier, R., Greinert, J., Linke, P., et al. (1999). Gas hydrate destabilization: Enhanced dewatering, benthic material turnover and large methane plumes at the Cascadia convergent margin. *Earth and Planetary Science Letters*, *170*(1–2), 1–15.
Talwani, M., & Eldholm, O. (1977). Evolution of the Norwegian-Greenland sea. *Geological Society of America Bulletin*, *88*(7), 969–999. https://doi.org/10.1130/0016-7606(1977)88<969:EOTNS>2.0.CO;2
Tucholke, B. E., Lin, J., & Kleinrock, M. C. (1998). Megamullions and mullion structure defining oceanic metamorphic core complexes on the Mid-Atlantic Ridge. *Journal of Geophysical Research*, *103*(B5), 9857–9866. https://doi.org/10.1029/98JB00167
Tvedt, A. B., Rotevatn, A., Jackson, C. A.-L., Fossen, H., & Gawthorpe, R. L. (2013). Growth of normal faults in multilayer sequences: A 3D seismic case study from the Egersund Basin, Norwegian North Sea. *Journal of Structural Geology*, *55*, 1–20. https://doi.org/10.1016/j.jsg.2013.08.002
Vanneste, M., Guidard, S., & Mienert, J. (2005). Bottom-simulating reflections and geothermal gradients across the western Svalbard margin. *Terra Nova*, *17*(6), 510–516.
Vogt, P., Feden, R., Eldholm, O., & Sundvor, E. (1978). The ocean crust west and north of the Svalbard Archipelago: Synthesis and review of new results. *Polarforschung*, *48*(1/2), 1–19. https://doi.org/10.2312/polarforschung.48.1-2.1
Wallmann, K., Riedel, M., Hong, W. L., Patton, H., Hubbard, A., Pape, T., et al. (2018). Gas hydrate dissociation off Svalbard induced by isostatic rebound rather than global warming. *Nature Communications*, *9*, 83. https://doi.org/10.1038/s41467-017-02550-9

Manuscript II

*Crustal processes sustain Arctic abiotic gas hydrate and fluid flow systems*

**Kate A. Waghorn,** Sunil Vadakkepuliyambatta, Andreia Plaza-Faverola, Joel E. Johnson, Stefan Bünz and Malin Waage

Under review in Scientific Reports

# Crustal processes sustain Arctic abiotic gas hydrate and fluid flow systems

K. A. Waghorn[1]*, S. Vadakkepuliyambatta[1], A. Plaza-Faverola[1], J. E. Johnson[2], S. Bünz[1] and M. Waage[1]

[1]CAGE – Centre for Arctic Gas Hydrate, Environment and Climate, Department of Geosciences, UiT – The Arctic University of Norway, Dramsveien 201, 9037 Tromsø, Norway
[2]Department of Earth Sciences, University of New Hampshire, 56 College Road, Durham, New Hampshire 03824, USA

* Corresponding Author: Kate Alyse Waghorn kate.a.waghorn@uit.no

## Abstract

Located on the western flank of the Northern Knipovich Ridge, the Svyatogor Ridge and surroundings are host to an enigmatic fluid flow system. The fluid flow system here manifests in the upper sedimentary sequence as a gas hydrate and free gas system, with BSR (bottom simulating reflection) occurrences. Using 2D seismic lines and bathymetric data, we map tectonic features such as faults, occurrences of basement outcropping, and indicators of the fluid flow system. Results indicate that there is a strong correlation between crustal faults, crustal highs and fluid accumulations, and a strong correlation with an increase in geothermal gradient over crustal faults. We conclude that a gas source is likely derived from the serpentinization of exhumed mantle rock, and that transform faulting may play a role in circulating fluids for and from serpentinization processes.

## Introduction

Intersections between Mid-Ocean Ridges (MOR) and Oceanic Transform Faults (OTF) are complex tectonic settings, where extensional and strike-slip tectonics meet. Inside corner highs form either at the Ridge-Transform Intersection (RTI) or at non-transform offsets along spreading ridges and are commonly topographically higher compared to the surrounding seafloor [1]. There is likely a relationship between relief and steepness of an inside corner high and spreading rate, and fossil inside corner highs

generally appear in less relief than active inside corner highs [1]. Generally, these features are coincident with crustal scale detachment faults, which exhume ultra-mafic mantle rocks and accommodate spreading at slow and ultraslow melt-poor spreading centers [2,3]. Proximity of an inside corner high to the spreading ridge, as well as comparative steepness [4] can indicate whether the underlying faults are actively exhuming mantle material, where areas of actively exhuming detachment faults are generally warmer, more buoyant and steeper than inactive or paleo-inside corner highs[1]. Fault splays and damage tips are also common at RTI's, as RTI's represent the juncture between two different faulting regimes. RTI's generally exhibit many different types of splay faulting, where the specific mode may vary depending on the kinematics of the moving blocks and relative angles between the main faults [5].

MOR's and OTF's are often associated with increased fluid flow, heat flow and increased tectonic activity compared to the surrounding older, colder basement or continental margins. Deep fluid flow and seawater cycling are often higher in spreading ridge settings, constituting biogeochemical exchange between oceans and the solid earth [6]. Hydrothermal vent systems are common on spreading ridges, either hosted on crustal scale detachment faults (peridotite hosted) or associated with magmatic centers. Hydrothermal systems in peridotite hosted environments commonly vent abiotic methane, a form of methane produced inorganically either through gas-water-rock interactions or magmatic processes[7]. Gas hydrates – crystalline compounds formed under high pressure and low temperature [8] - are inferred from geophysical data in marine sediments on the inside corner of a ridge transform intersection in the Fram Strait[9,10]. Johnson, et al. [9] and Waghorn, et al. [10] observe a close relationship between basement detachment faults and the overlying gas hydrate system and hypothesize that abiotic methane produced from serpentinization reactions may contribute methane to the overlying gas and gas hydrate system. In slow and ultraslow spreading MOR hydrothermal settings, large offset normal faults, or detachment faults, as well as secondary sedimentary faults, if present, are often invoked as fluid migration pathways [11,12] that allow for both downward seawater infiltration and upward fluid expulsion. Sedimentary faulting is also an important mechanism for gas migration in gas hydrate systems [13]. In addition, studies show that OTF's are also able to host increased

fluid flow and OTF's may meet the prerequisites for abiotic methane production via serpentinization, where the OTF acts as conduits for seawater circulating to peridotites at depth[6]. Thermogenic methane forms at a depth where organic matter/kerogen is appropriately heated (>150 °C) and pressured (usually between 2-4 km depth) to become methane[14], while microbial methane forms when microbes in the shallow subsurface generate methane through the decomposition of organic matter[15]. Generally, at the depth of most slow to ultraslow spreading mid-ocean spreading ridges, the pressure regime is appropriate for gas hydrate formation, however, some mid-ocean spreading ridges are sites of increased geothermal heat, which may inhibit hydrate formation. Additionally, in well-developed ocean basins the active plate boundary is often sediment starved, which also inhibits hydrate formation. Abiotic methane is found in vent fluids released from peridotite-hosted hydrothermal systems[16], however, it is still unclear whether abiotic methane is a contributing source to gas hydrate accumulations in settings where all the prerequisites for gas hydrate formation exist. Rajan, et al. [17] hypothesize the presence of abiotic methane on the eastern Knipovich Ridge flank, while Johnson, et al. [9] and Waghorn, et al. [10] and hypothesize abiotic methane may contribute to the gas hydrate system on the Svyatogor Ridge on the western Knipovich Ridge flank. Sedimentary faults on the Svyatogor Ridge have developed due to movement on already-sedimented detachment faults[10]. The ultra-slow spreading, melt-poor Knipovich Ridge has an azimuth of ~308° and a half spreading rate (eastwards) at ~6-8 mm/yr [18]. The strike-slip Molloy Transform Fault (MTF) is slightly oblique to the Knipovich Ridge[19]. Sedimentation on the western flank of the Knipovich ridge is dominated by contourites associated with the modern West Spitsbergen Current and its equivalent predecessor[9].

The aim of this study is to determine the role of the Knipovich Ridge and MTF in the development of deep marine Arctic gas hydrate systems throughout the region. The studied gas hydrate and fluid flow system extends from a sediment drift (the Svyatogor Ridge) atop a detachment fault on the inside corner of the Knipovich Ridge-MTF intersection[9,10], to the west along the MTF (Fig. 1). We find that there is a strong correlation between fluid accumulations, crustal faulting and localized geothermal gradient increases, indicating that active faulting on plate boundaries is responsible for gas hydrate

and free gas accumulations here. Observations in this study area support the hypothesis[9] that serpentinization reactions are producing abiotic methane, contributing to free gas accumulation and gas hydrate formation.

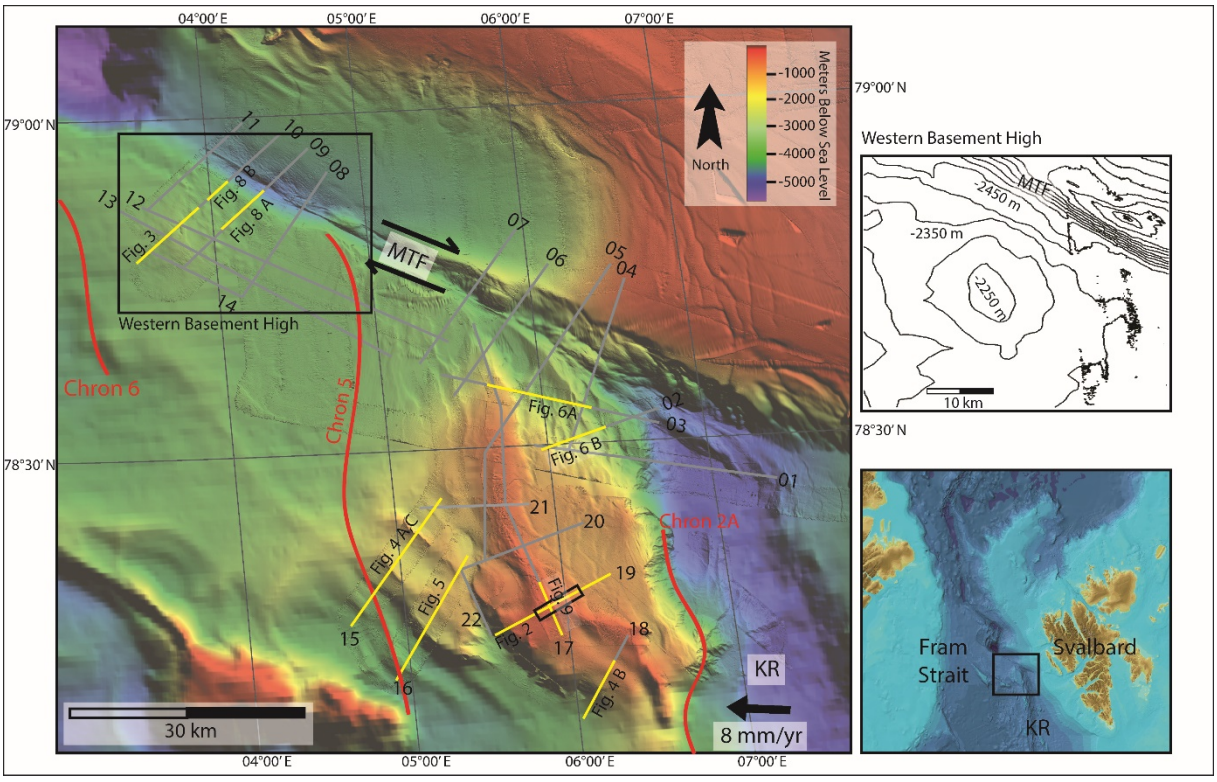


*Figure 1. The study area and 2D seismic lines used in this work. Red lines denote magnetic anomaly chrons – Chron 6- 19.6 Ma, Chron 5- 9.8 Ma, Chron 2A – 2 Ma[18]. The Knipovich Ridge (KR) separates the Eurasian plate from the north American plate, which is propagating westwards at about 8 mm/yr[20]. The Molloy Transform Fault (MTF) denotes the northern extent of the RTI, and the seismic lines cover most of the inside corner high between the KR and MTF. Figures following in the text are denoted with yellow lines and the figure reference. The 3D seismic survey used in Waghorn, et al. [10] is denoted with a black box, while line 19 is the seismic line also shown in Johnson, et al. [9].*

## Data and Methods

We use 22 high-resolution 2D seismic lines and bathymetry data across the Molloy Transform Fault and the Knipovich Ridge collected between 2014-2018 aboard RV Helmer Hanssen. The 2D streamer is 100 m long, consists of 32 receivers and the seismic signal was produced using two mini GI airguns with volumes of 15/15 $in^3$ and 30/30 $in^3$. Processing of these seismic lines has been consistent across the surveys and consisted of; 1) Geometry assignment, 2) simple bandpass filter (20 Hz-30 Hz-300 Hz-350 Hz), 3) true amplitude correction, 4) despiking, 5) CDP binning at 3.125 m spacing, 6) Stacking and 7) Kirchhoff Migration using a manual velocity model based on CTD water velocity, and prior published

velocity information in the area [21,22]. The base of gas hydrate stability (BGHSZ) for each seismic profile was modelled using the theoretical phase boundary curve for pure methane gas estimated using the CSMHYD program[8]. The program estimates multiphase equilibrium pressure values for a given temperature, with an error range of +/- 15%, assuming pure methane gas and a porewater salinity of 35 g $l^{-1}$. The pressure estimates are converted to water depth assuming hydrostatic pressure. The three-phase temperature-depth curve is then compared with the subsurface thermal profile at each location on the seismic profile estimated using the observed bottom water temperature and geothermal gradient[23,24]. Gas hydrates are considered stable at locations where the observed temperature is lower than the one predicted by the theoretical temperature-depth curve. All BGHSZ models are given as a range to account for the inherent mathematical error in pressure [8].

# Results

## Linking crustal scale tectonics with shallow sedimentary features

Imaging oceanic crustal structure in sediment covered mid-ocean ridge environments can be difficult. However, here we use high-frequency seismic data and can identify chaotic reflections, with undulating or rough upper boundaries. These features are usually located at the limit of seismic energy, with no coherent reflections appearing beneath (Fig. 2) and are interpreted as the top of oceanic crust. Consistent with the interpretation by Johnson, et al. [9] and Waghorn, et al. [10] the oceanic crust in our study area is clearly recognized at a depth of ~500 ms (Fig. 2). At the western end of the study area, bathymetric data shows a small ridge-like structure at the southern flank of the MTF (Fig. 1 inset). Seismic data there show chaotic, undulating reflections, and a quickly deteriorating seismic signal at ~200 ms below seafloor (Fig. 3). In correspondence to the eastern part of the study area, we interpret this also as an oceanic crustal high. One long, semi-coherent reflection pierces the interpreted crust at an angle of approximately 30°, located directly beneath the high. Following interpretations from Johnson et al. [9] and Waghorn et al. [10], This feature is tentatively interpreted as a crustal fault (Fig. 3).

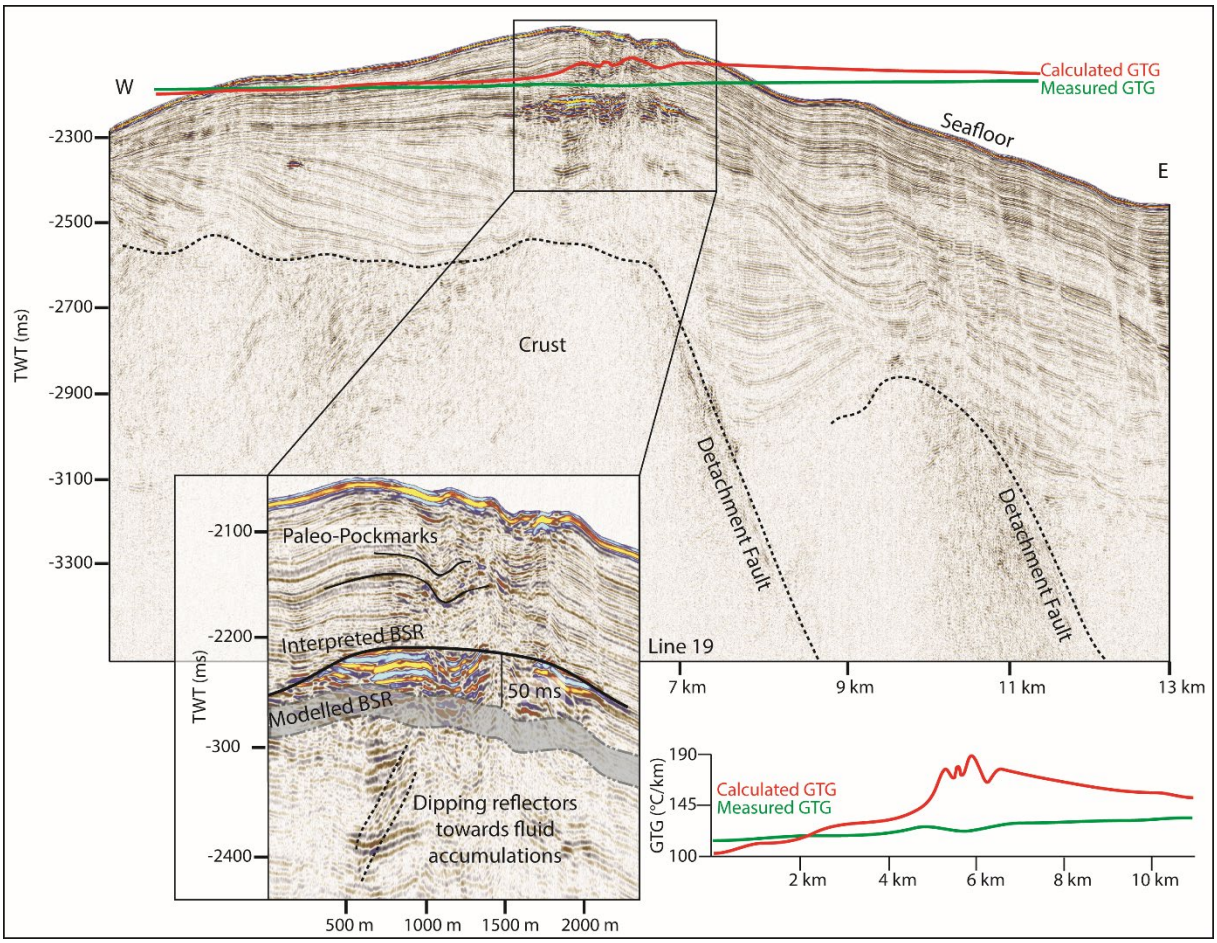


*Figure 2. On line 19, basement structure and detachment faults are interpreted based on the interpretations by Johnson, et al.* [9] *and Waghorn, et al.* [10]*. The upper reflection characterizing the basement is often undulating, while the internal reflections, where present, are chaotic. A reflection dipping approximately 30° pierces the basement structure in two places, interpreted by Johnson, et al.* [9] *and Waghorn, et al.* [10] *as detachment faults. Above the western detachment fault is a BSR reflector approximately 60 ms above the modelled BSR. Above the BSR reflector are horizons of paleo-pockmarks interpreted by Waghorn, et al.* [10]*, and seafloor pockmarks. We also identify reflections beneath the free gas zone dipping towards the fluid accumulation which crosscut the otherwise continuous strata. Measured geothermal gradient values (Measured GTG) (Green; Crane, et al.* [24]*) are plotted against the geothermal gradient calculated (Calculated GTG) based upon the depth of the BSR (Red).*

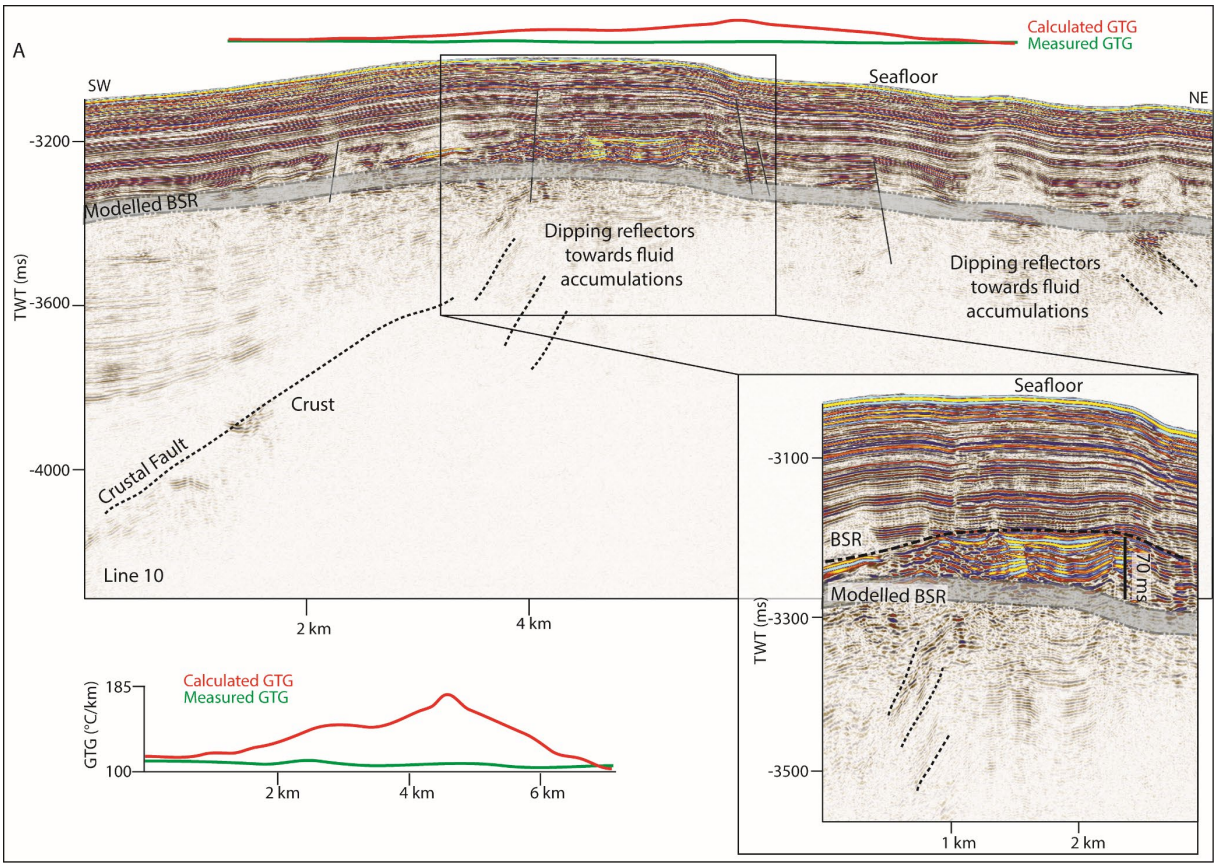


*Figure 3. The northwestern extent of the study area has a small bathymetric high where we observe a BSR (70 ms above the modelled BSR) with reflections dipping upwards towards the free gas zone. Reverse polarity reflections interpreted as fluid accumulations (RPFA) are observed off the bathymetric high also with reflections dipping upwards towards them. These are also interpreted as free gas trapped beneath hydrate. Measurde geothermal gradient values (Green; Crane, et al. [24]) are plotted against the geothermal gradient calculated based upon the depth of the BSR (Red).*

Southwest of the Svyatogor Ridge, correlating with a large scarp in bathymetry data we interpret a basement crust outcrop with steep, sediment covered flanks (Fig. 4A, B; 5). Due to the correlation of this scarp with other parallel scarps in bathymetric data (Fig. 1), we interpret these as additional basement crustal highs, likely faulted into their current position. The kinematics of these faults is unclear as the seismic lines are 2D; however, based on the extent of the scarps forming on the seafloor above, it appears they are normal faults dipping southwest at ~30° (Fig. 1; 5). In conjunction with this is a smaller scarp (Fig. 4C) which, although we do not image the crust beneath it, we interpret it to result from a crustal high and/or faulted crust. Based on the bathymetric map, these potential faults are not the same strike as the Knipovich spreading ridge fabric at Svyatogor Ridge, but instead more closely resemble the strike of the MTF (Fig. 1). In this region, Crane, et al. [25] interpret a paleo-transform fault with a similar strike.

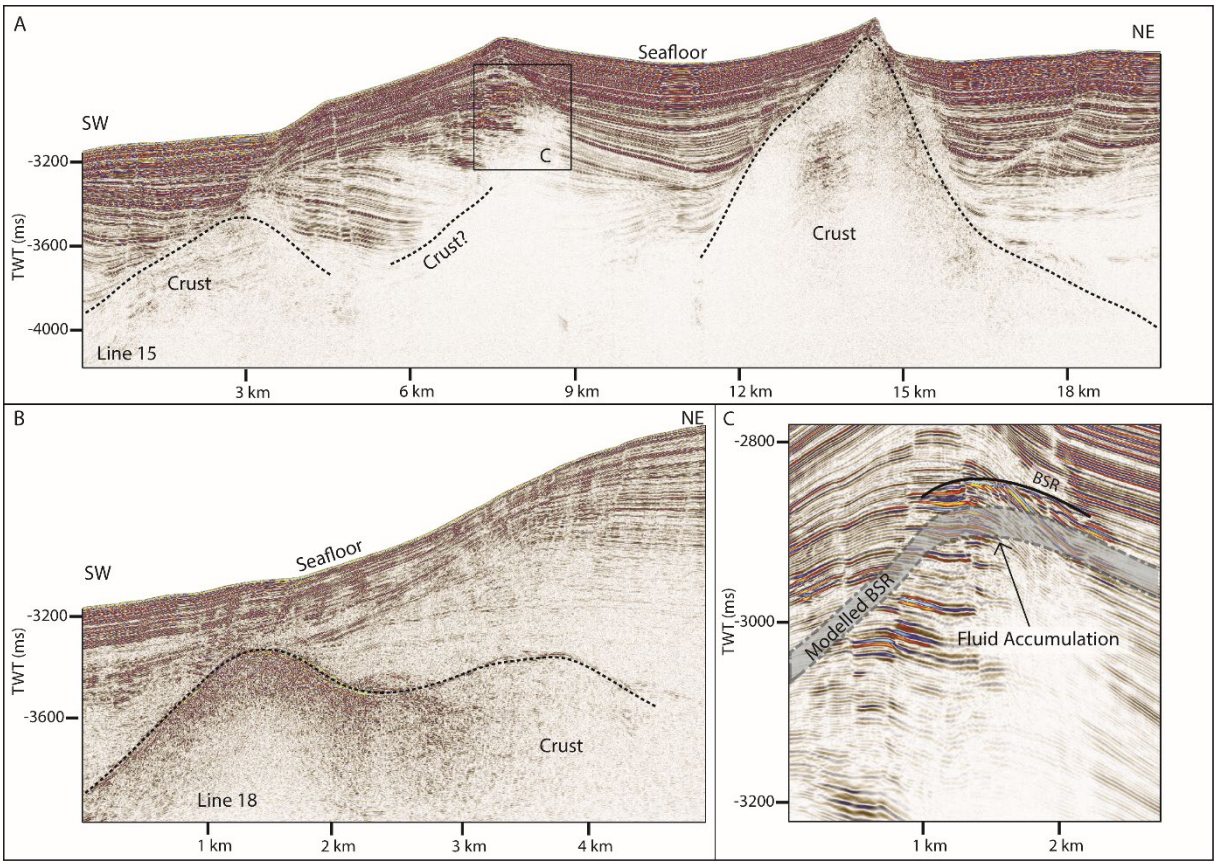


149

150 *Figure 4. Lines 15 and 18. Here basement is again interpreted, consisting of large peaks on line 15 (top) and a steep flank with*
151 *undulating top on line 18 (bottom left). Reflector configuration and seafloor topography suggests that on line 15 (top) there*
152 *is a third peak, however there is a fluid accumulation which correlates to the location of the modelled BSR which is likely*
153 *scattering seismic energy.*

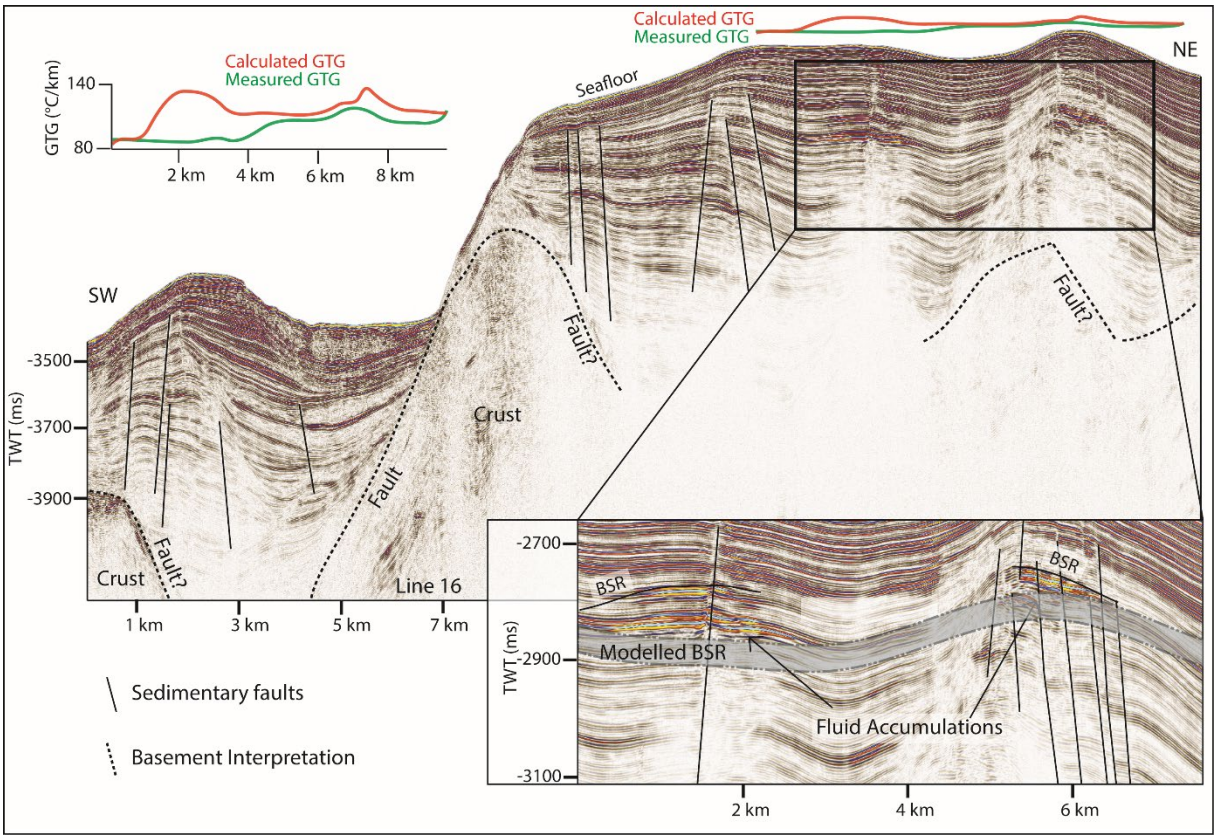


*Figure 5. Line 16. Here we interpret three, potentially four, areas of crust with steep flanks creating a marked change in seafloor topography. In addition to the interpreted crust faults, the areas of crust outcrop correspond to areas of increased sedimentary faulting. The inset figure shows high amplitude anomalies cutting across sedimentary strata. These anomalies are interpreted as fluid accumulations beneath a BSR. However, the BSR occurs significantly above the predicted base of gas hydrate stability. Measured geothermal gradient values (Green; Crane, et al. [24]) are plotted against the geothermal gradient calculated based upon the depth of the BSR (Red).*

In addition to major crustal scale tectonic features, we also interpret many sedimentary faults (Fig. 5; Fig. 6A; B). These are near vertical, very narrow zones of low amplitude, which offset reflections vertically. In general, almost all the faults imaged are normal faults, offsetting the sedimentary strata by up to 60 ms at depth and decreasing in offset towards the seafloor. The sedimentary faults on lines 02 and 03, however, are associated with a small anticlinal bend at the upper end of the fault plane, and although offset of reflections appears to be very small (~20-30 ms offset) amplitudes across the fault plane do not match taking into consideration their offset (Fig. 6A; B). These faults often exhibit steepening upwards, or a Y shaped pattern at the upper section of the fault (Fig. 6A). They also create a pronounced rolling topography on the seafloor. These characteristics indicate that these faults are forming under transpression (predominately strike-slip with a compressional component)[26,27]. All

sedimentary faults in this data are interpreted as forming in conjunction with deeper tectonic features related to either spreading on the Knipovich Ridge or offset on the MTF.

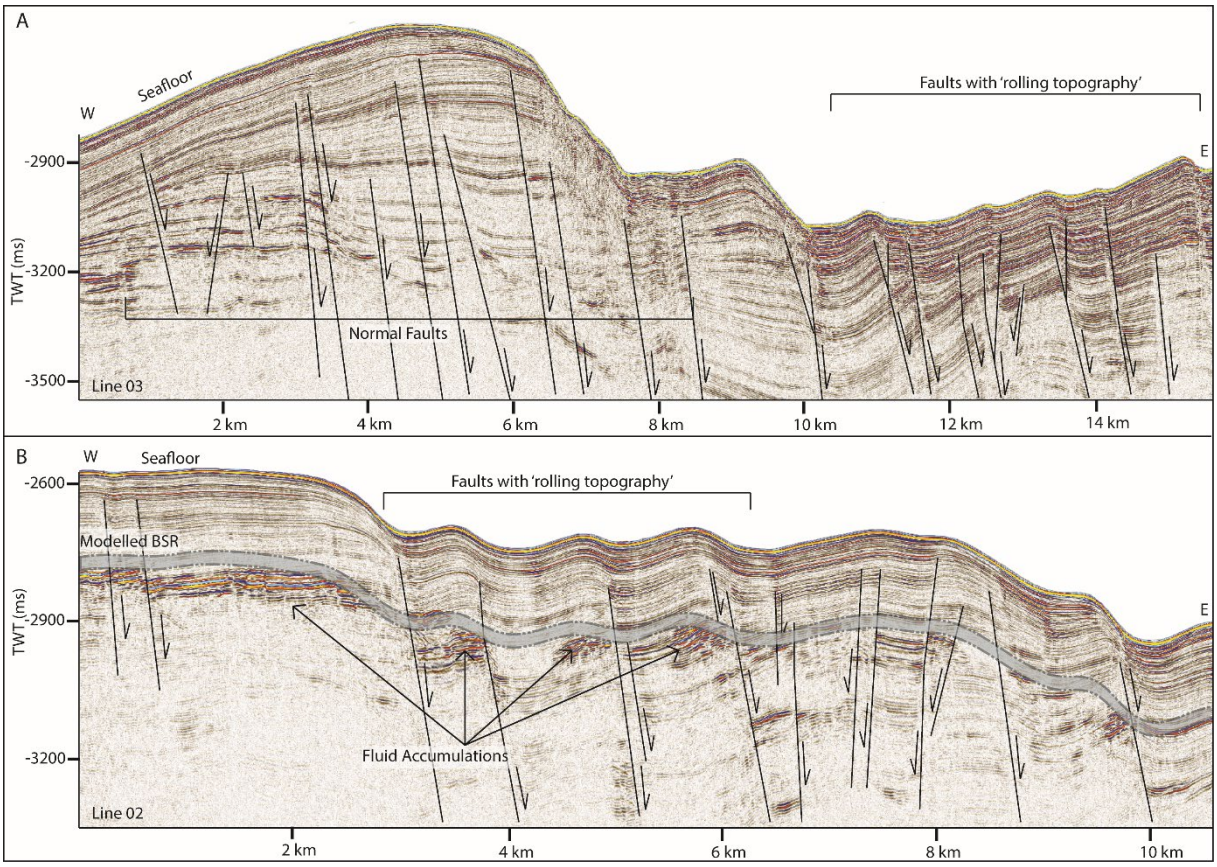


*Figure 6. On lines 02 (B) and 03 (A) we observe a change in sedimentary faulting style. Faults on the main ridge (left, both figures) are normal, while towards the Knipovich ridge, faults begin to 1) interact more with the seafloor, creating a 'rolling' topography, 2) have small folds at the upper termination – and on line 01 are associated with fluid accumulations which correspond to the location of the modelled BSR. In addition, faults that are associated with these small folds often appear to have very little reflection offset, a marked steepening towards the seafloor and sometimes a Y shape upper section of the fault.*

The proximity of fault tips to the seafloor indicates the faults with the most recent activity. Conveniently, the sediment cover over faults serves to illustrate the relative timing of fault activity, as sediment drape over inactive faults eventually smooths over fault scarps. In this sense, we observe that many faults with indications of recent activity are close to the Knipovich Ridge, towards the east of the study area (Fig. 7). We also note that the bathymetry towards the east and south of the study area is much more variable than towards the west of the study area, apart from the small bathymetric high (Fig. 1 Inset). This pattern in active faulting indicates that active deformation is focused near the Knipovich Ridge with decreasing tectonic activity with distance away from the ridge-as expected in this

active MOR tectonic setting. Based on the previous interpretation of faults confined in the sedimentary sequences that are interacting with the seafloor, with a strike-slip component along certain lines, we have also extended these interpretations across the study area using the bathymetry. We observe a small area at the northernmost end of the Knipovich Ridge that has sedimentary faults with a strike-slip component[26]. This area shows a small basin-like feature between the Svyatogor Ridge and an interpreted splay fault [25] related to the MTF. Therefore, we also interpret that the MTF kinematics are influencing at least the northern Svyatogor Ridge (Fig. 7).

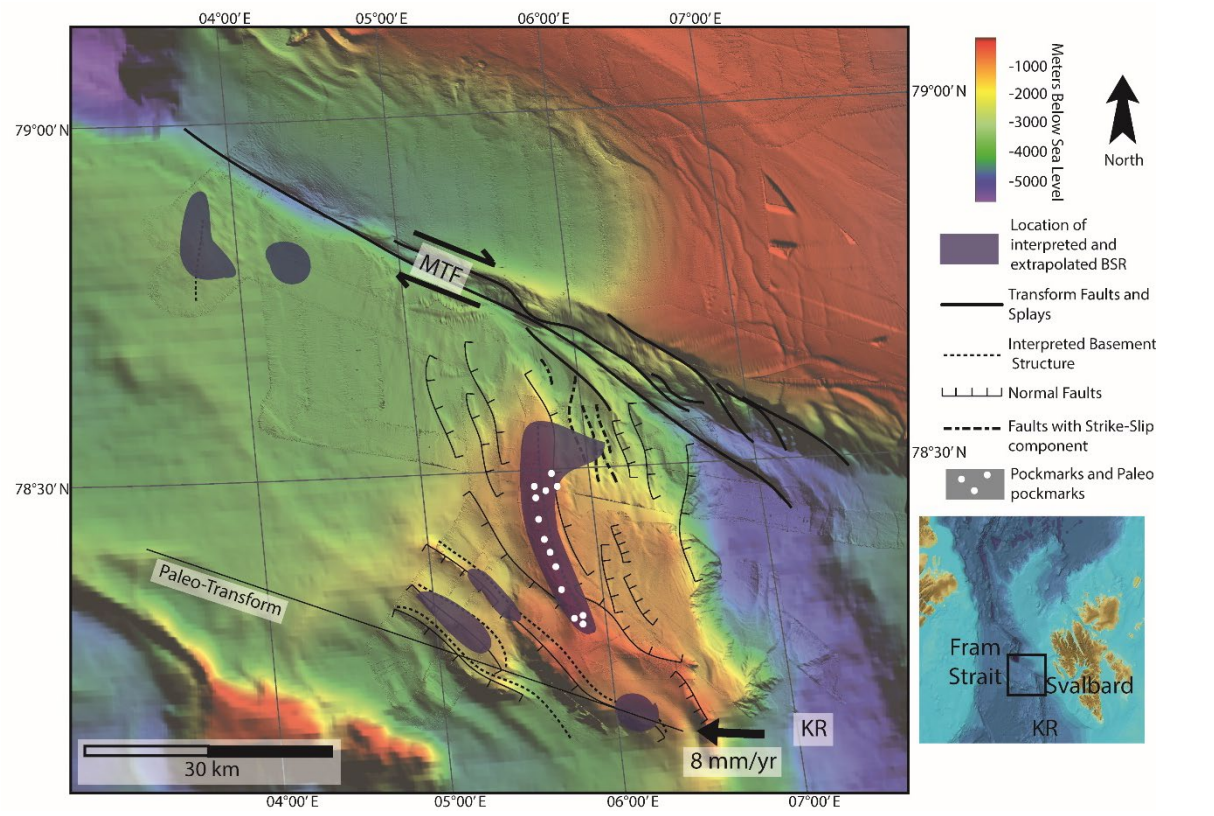


*Figure 7. Summary of major fault interpretations (dashed, dotted or solid lines), crustal structure (dashed line), BSR interpretations (blue blobs) and fluid flow indicators (white dots) based on bathymetry and 2D seismic data over the study area. Location of the paleo-transform from Crane, et al. [25].*

## Fluid Flow System

Reflections characterized by high amplitudes and reversed polarity, appearing to crosscut the stratigraphy while mimicking the seafloor are observed in numerous locations throughout the study area. These reflections correlate on line 19 to the bottom simulating reflection (BSR) – the base of the gas hydrate stability zone - interpreted by Johnson, et al. [9] and Waghorn, et al. [10]. All such reflections

205 in the 2D seismic lines are also interpreted here as BSR. The main ridge crest of Svyatogor Ridge
206 contains the thickest zone of high-amplitude anomalies indicating a thick free gas zone, while off the
207 main ridge crest, the thickness of this zone of high-amplitude anomalies is considerably decreased
208 (Figs. 2,3). There are two locations with anomalous BSRs. Firstly, we identify a BSR on the western
209 crustal high, which lies 70 ms above the interpreted crustal structure (Fig. 3). The BSR here is not
210 continuous, however appears to center on the interpreted crustal high, non-uniformly distributed off
211 the crustal high down dip towards the MTF (Fig. 1). Within the sediments between the crustal highs
212 and Knipovich Ridge axis, we also observe sporadic patches of high amplitude reflections denoting fluid
213 anomalies focused on the footwalls of sedimentary faults within small anticlinal structures (Fig. 6B).
214 Towards the MTF in the western section of the study area, there are also sporadic patches of a
215 reflection interpreted to be BSRs (Fig. 8A, B). However, here these reflections are mostly associated
216 with doming and lowered amplitudes either above or below the interpreted BSR (Fig. 8A; B). These
217 features are also interpreted as fluid anomaly indicators. In this location we interpret up to three
218 generations of domes (Fig. 8A; B), characterized by a seismically transparent 'core' and continuous
219 reflections separating the domes. Domes in this study area are associated with 1) a reverse polarity,
220 high amplitude reflection beneath (Fig. 8A; B) 2) small sedimentary faults with minimal offset around
221 the top of the mounds and 3) crosscutting reflections dipping upwards towards either the high
222 amplitude anomalies or the mound cores (Fig. 8A; B). Similar structures are observed in areas of
223 upwelling fluids[28], and serpentine diapirism[29,30] may also form such mound structures. We interpret
224 these structures as indicators of fluid migration from deep crustal processes.

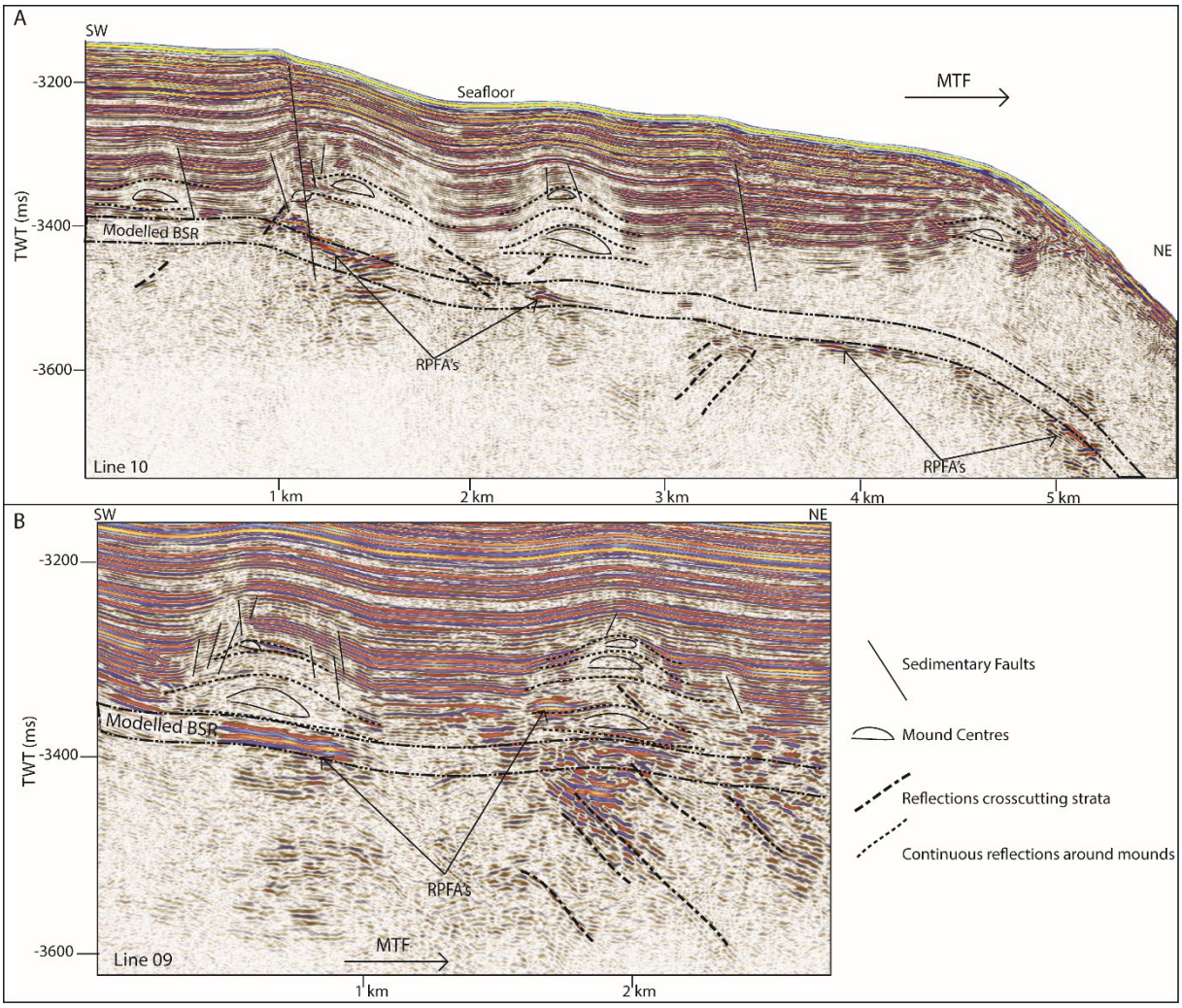


*Figure 8. On lines 09 (B) and 10 (A), mound-like features are interpreted from the western crust high (Fig. 1) to close to the MTF. These mounds have a center, with up domed reflections above. There does not appear to be any onlap or discordant stratigraphy around the mounds, other than the up doming. There are often multiple generations of mounds stacked atop each other, and they are often associated with reverse polarity fluid anomalies (RPFA's) which sometimes fall into the modelled BGHSZ range. They are also often associated with very small offset sedimentary faults around the top of the mound. Lastly, there are several reflections cross cutting the strata, dipping upwards towards the mounds and RPFA's.*

The distribution of BSRs across the entire study area is mainly limited to the Svyatogor Ridge crest and areas above crustal highs. Patchy BSRs are also interpreted towards the Knipovich Ridge and towards the MTF (Fig. 7) however there is an apparent strong correlation between the location of crustal highs, related crustal faults (interpreted and assumed) and BSRs in the study area. Modelling the depth of base of GHSZ yields a good fit between the observed BSR and the model output. However, in some instances we observe a systematic mismatch of between +80 ms and +20 ms between the observations and models. All other parameters fixed, the geothermal gradient would need to be 20°C/km-85°C/km higher to account for the mismatch. These anomalous BSRs occur over areas where we interpret

crustal highs and/or crustal faulting. We assert this is an indication that warmer crustal fluids are focused at these locations, because of the crustal structure.

Figure 9 shows examples of seafloor depression structures above the BSR, which have areas of decreased amplitude and are sometimes associated with faults, interpreted here as pockmarks following Waghorn, et al. [10]. U-shaped features with high amplitude bases and low amplitude infill that appear to truncate lower sedimentary horizons on lines 17 and 19 (Fig. 2, 9) are also interpreted as paleo-pockmarks[10]. We observe that all incidences of seepage indicators (paleo pockmarks and pockmarks) are limited to the Svyatogor Ridge and we do not observe such seepage structures anywhere else in the study area (Fig. 7).

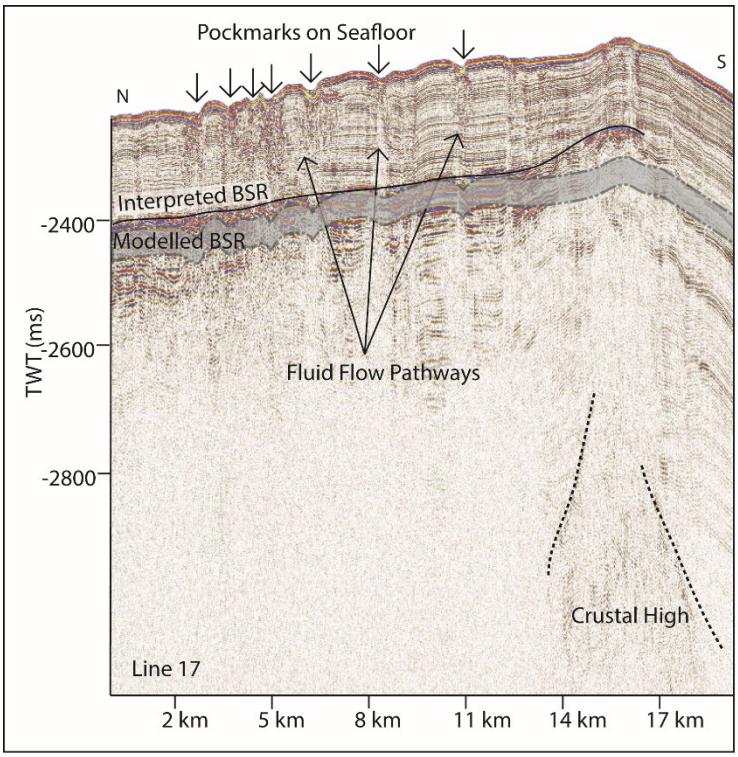


*Figure 9. We have interpreted a BSR which is slightly shallower than the modelled BSR in this area. At the southern end of the line, we note crustal structure at depth. At this end of line 17 there are many pockmarks on the seafloor, with vertical, columnar structures of lowered amplitude linking them to the BSR which we interpret as fluid flow pathways.*

## Discussion

### Tectonic Regimes

Our interpretations here indicate that the northeastern section of the study area is complex in terms of interactions between the MTF and Knipovich Ridge, where we identify dip-slip faults juxtaposed with oblique slip faulting and faults that appear to have a large strike-slip component (Fig. 6A, B). Splay faulting occurs off the MTF, transitioning into purely dip-slip or possibly oblique-slip faulting with distance southwards [10]. The crustal high interpreted in the west of the study area (Fig. 1), abutting the MTF may indicate the presence of an underlying paleo-detachment fault. It is relatively small compared to other inside corner highs worldwide (i.e. Troodos Ophiolite[31], the Kane Transform[32] or the Vema Transverse Ridge[33]) although this could be an effect of sediment cover smoothing over the crustal topography. The Svyatogor Ridge lies on crust estimated to be between 2.8-9.8 Ma[18], with the potential paleo-detachment in the western section of the study area near to Chron 6, giving an age of <19.6 Ma [18] (and 53 km between the two interpreted faults). Although using 2D seismic it is not possible to determine the true dip of the feature, its apparent dip is approximately 30°, consistent with the dips of other detachment faults in this region.

We also identified anomalous crustal structures southwest of the Svyatogor Ridge (Figs. 4, 5). Peive and Chamov [34] and Crane, et al. [25] have reported a paleo-transform fault in a similar location as this anomalous crustal structure (Fig. 7). Although the area where we identify shallow crustal structure is not precisely at the previously interpreted paleo-transform, we suggest that the structure here is representative of the uplifted crust along a strike-slip fault with a slight extensional component. Bathymetry data indicates that if this is indeed a paleo-transform fault, it is asymmetric with the northern flank being considerably elevated compared to the southern flank (Fig. 7). Seismic penetration through the basement structure here does not allow us to discern any faults or features that confirm whether this is representative of an upfaulted crustal block; however, the sedimentary sequences appear to have undergone uplift (Figs. 4, 5, 7). Alternatively, these structures, if related to

the hypothesized paleo-transform fault, could be representative of splay faults that have formed with continued propagation of the paleo-transform[5]. Splay structures often have large, or entirely, extensional components compared to the main transform fault segments[5], which could explain the apparent uplift of sediment along some tectonic lineaments (Fig. 4, 7). Given the uncertainty around the location of the hypothesized paleo-transform, estimating it strikes between 290° and 310° would imply that it is oblique to the spreading axis.

## Heat Flow Anomalies

BSRs overlying crustal faults are systematically shallower than modeled BSRs across the study area (Figs. 2, 3, 5). Modelled BSRs are were calculated assuming 100% methane, with no contribution from heavier hydrocarbons. A change in gas composition towards heavier hydrocarbons would deepen the BGHSZ, thus the BSR, and hence, this was ruled out as a factor in the mismatch. Due to the coincidence with crustal faults, we hypothesize that a likely factor for a slight BSR shoaling here would be localized, fault driven fluid flow that could circulate warmer fluids from depth towards the seafloor. Although the modelled BSR depth range accounts for inherent mathematical error in the pressure estimation [8], there are multiple assumptions such as salinity (assumed constant at 35 SU) bottom water temperature (assumed constant at -1°C based on World Ocean Database values) as well as errors in pre-existing geothermal gradient measurements. We also assume a linear change in geothermal gradient between measured points, which inherently provides error as well. The salinity of pore water over this study area is an unknown. We have no measured data to provide insight, and salinity of deep circulating fluids is highly dependent on numerous factors, such as temperature and pressure regimes at depth of formation as well as rock properties and water-rock reactions[35]. Hydrothermal vent sites around the world have greatly diverse fluid salinity values; however, mid-Atlantic hydrothermal vent sites have salinity values between ~23 SU at Menez Gwen[36] and ~42 SU at Rainbow[37]. The model used for BGHSZ modelling here only takes into consideration NaCl as a hydrate formation inhibitor[8]. However, using values between 3 SU and 42 SU as extremes indicates that given all other factors being equal, salinity of the pore fluid does not have a significant impact at the water depths at this study site.

Similar modelling exercises have been carried out on the Vestnesa Ridge[38] where the authors find that the largest contributor to error in BGHSZ prediction is related to the error in pressure estimates[8,38].

To determine the factors controlling 1) the location of observed BSR and 2) the reason for a discrepancy between observed BSR depth and modelled BGHSZ range, we consider that the geothermal gradient measurements provide a robust regional overview. In most areas of this study, BSR observations fall into the modelled range of BGHSZ based on the measurements recorded in Crane, et al. [23] and Crane, et al. [24], for example, line 03 (Fig. 2B), the mound areas on lines 09 and 10 (Fig. 8 A,B) as well as away from the detachment fault on line 17 (Fig. 9). The largest difference between observed and measured geothermal gradients is at the peak of the BSR over the western crustal high (Fig. 3), with a BSR-derived thermal gradient of ~204 °C/km vs ~120 °C/km interpolated between geothermal measurement stations from Crane, et al. [23] and Crane, et al. [24]. As this area is distal from the spreading axis, we expect that the crust is cooler than proximal to the spreading center. However, as this area is underlain by an interpreted crustal fault it is feasible that this mismatch is caused by advection of warm fluids from depth along the faults. Even if considered tectonically inactive, an oceanic crustal fault plane which may have undergone some serpentinization may still be important for fluid migration as recent work suggests the serpentinization process results in the creation of porosity and thus permeability through fluid-driven mineral fracturing[39], therefore crustal faults may remain long-lived pathways for crustal fluid circulation far from ridge axes. The results of this geothermal gradient comparison imply that there is still fluid circulation driving localized geothermal gradient increases, which may well be linked to ongoing crustal processes such as serpentinization[39].

## Fluid Flow Systems

We identify numerous locations with BSR, or anomalous amplitudes, which we interpret as fluid related anomalies (Figs. 3-5; Fig. 8; Fig 10) that coincide with oceanic crustal high structures (Fig. 2). The crustal high structures correspond with major tectonic features, such as detachment faults, the MTF, the Knipovich Ridge and an interpreted paleo-transform fault[25,34]. Given the available geothermal

329 gradient data[23,24] and water depth at this study location, as well as bottom water temperature
330 compared to hotter RTI's, the Knipovich-MTF RTI is in a regime where abiotic methane linked to
331 serpentinization could well be trapped as free gas and gas hydrate in the sedimentary sequences
332 overlying much of the crust.

333 Similar structures to the domes identified in this study (Fig. 8) are interpreted by Judd and Hovland [28]
334 to occur in response to an increase in pore pressure. Pingo-like features can also exhibit similar
335 amplitude effects and often appear as similar domed structures[40]; however, they are more common
336 on the seafloor above sediment covered crust. Underneath some domes, the presence of a high
337 amplitude, reverse polarity reflection (Fig. 3) may indicate their association to the gas hydrate system
338 here. Paleo-seafloor methane seepage forming carbonate material can also form mound structures[41],
339 as can sediment remobilization[42,43] and serpentine diapirism[29]. In the case of serpentine diapirism,
340 compressive forces are important in their formation. As serpentinization in our study may occur
341 preferentially along large normal or detachment faults, and serpentinized rocks are relatively low
342 strength, low density materials[29], given sufficient compressive or transpressive stress, serpentinite
343 bodies may undergo ductile deformation and form diapir structures. With the data available it is
344 difficult to interpret the specific mound forming process, however in any of these common mound-
345 forming processes, fluid flow is an important factor in the formation of the features. Therefore, we
346 assert that these dome structures are evidence of prior sustained fluid flow at a location, the top of
347 oceanic crust, deemed relatively unimportant to fluid flow processes in the past.

348 Waghorn, et al. [10], using 3D seismic data, showed that large-scale crustal faults do indeed underlie the
349 gas hydrate and fluid flow system in the area of the 3D seismic survey (Fig 1), however owing to the
350 lack of additional data, the origin of the methane remains untested. Here, we find that almost every
351 incidence of fluid accumulation, including BSRs, correlates strongly with the presence of crustal
352 basement highs. We have tentatively interpreted that many of these crustal highs are uplifted into
353 their current position due to crustal scale faulting, for example, the detachment faults underlying line

19 or the paleo-transform fault interpreted by Crane, et al. [25], in the area of lines 15, 16 and 18 (Fig. 1; Fig. 7). While abiotic methane is well documented in peridotite-hosted hydrothermal fluid flow systems, and on detachment faults[7,9], Rüpke and Hasenclever[6] also suggest where ultra-mafic mantle rocks come into close contact with OTF's, serpentinization is likely. It is striking that in the areas in this study that are above these major tectonic features we do observe fluid and gas/gas hydrate accumulations (Fig. 7). Thermogenic methane production in the area would require deep buried sediments containing sufficient organic matter to decompose to hydrocarbons, temperatures above 160 °C and pressures equivalent to burial at 2-4 km. The closest known locations where thermogenic methane production could occur are the Hovgård Ridge and the Vestnesa Ridge[44-46]. However, methane migrating from either of these localities would have to traverse significant tectonic lineaments to reach the study area, assuming the presence of the hypothesized paleo-transform[25] between the Hovgård Ridge and Svyatogor Ridge. Although it is documented that methane accumulations generated in the basin area north of the MTF reach a significant distance towards the transform[47], there is no evidence that methane is traversing the MTF. A very early gas charge of thermogenic methane might have occurred before the MTF formed, however, the implication of this is that it began ~19 Ma, before the western crustal high was offset – approximately when the Fram Strait began opening and sedimentation initiated [18], which is unlikely. Lastly, as we have noted the detachment faults imaged on line 19 (Fig. 2) and interpreted crustal structures elsewhere appear to be intrinsic in focusing fluid accumulations. This implies that if methane is not being generated through serpentinization reactions, these structures are in some way connected to a methane source and acting as pathways therefrom. Microbial methane production in the shallow sediment cannot be ruled out, however we would expect microbial methane production to occur over a widespread area and as noted by Waghorn, et al. [10] shallow penetrating gravity cores did not recover enough gas for isotopic analysis.

The fluid flow system presented in the study area is unique in that it is not centered on one large drift deposit (i.e. the Vestnesa Ridge [48], the Blake Ridge [49,50]) nor is it forming on a continental margin with

massive sedimentary sequences (i.e. Cascadia margin [51], Hikurangi margin[52], Vøring Basin[53]). The system in this study site also appears relatively stable compared to other systems (e.g. Vestnesa Ridge[48], Blake Ridge[54])– it is only on the Svyatogor Ridge crest that we find evidence of fluid release – in all other areas of interpreted BSR and free gas accumulations there are no pockmarks or seepage indicators. The dome structures while indicating the presence of a fluid system, do not necessarily imply leakage from a paleo-seafloor although more data would be required to determine their true nature and origin. Additionally, as the seafloor region cools and subsides with continued seafloor spreading, gas hydrate accumulations charged by abiotic methane will become more stable[9].

A gas hydrate system occurring on an ultra-slow mid-ocean ridge requires a unique methane source and thermal and sedimentary conditions that are generally rare. Elevated geothermal gradients at mid-ocean ridge flanks dominated by volcanic seafloor production typically exclude these settings in terms of temperature regime for gas hydrate formation. In addition, thermogenic methane production occurs generally at pressures equivalent to burial to >2 km depth[14] in the sedimentary column. Sediment columns reaching these depths are highly unlikely at the flank of actively spreading ridges. Therefore, the sedimented ultra-slow spreading ridges of the Arctic are ideal locations to explore and develop a framework for oceanic crust-linked gas hydrate systems. In addition, such Arctic sedimented mid-ocean ridge flanks provide an evolutionary context for prevalent fluid-rock interactions in such settings as fluids produced by deep crustal processes can become trapped in the sedimentary column and trapped abiotic methane may account for a carbon pool not previously accounted for in global inventories[9].

## Conclusion

The RTI between the MTF and Knipovich ridge is a unique setting for a gas hydrate system as normally such geologic settings consist of geothermal gradients too warm and minimal to no sedimentary cover for gas hydrate formation and accumulation. The Svyatogor Ridge has a documented gas and fluid flow system present and hosts an overlying gas hydrate system potentially fueled by abiotic methane. Here,

we show that in addition to the Svyatogor Ridge crest, hydrate systems occur across all bathymetric highs underlain by interpreted basement crustal structures. BSRs also overlay large basement crustal structures that may represent a paleo-transform fault immediately south of the Svyatogor Ridge. In addition, some evidence of past fluid flow, in the form of mound structures, are recorded near the western crustal high as well as evidence of sustained fluid flow on the Svyatogor Ridge in the form of paleo and present-day pockmarks. We speculate that the fault plane imaged underneath the western crustal high relates to spreading on the Knipovich Ridge after 19.6 Ma, as the Knipovich Ridge propagated northwards. We therefore propose that these large, crustal-scale, tectonic features are intrinsically involved in supplying methane into the system at this sedimented mid-ocean ridge flank, either through serpentinization of ultra-mafic rock forming methane or as fluid flow pathways dictating the locations of methane and fluid accumulations.

## Acknowledgements

This work was supported by the research council of Norway through its centres of excellence funding scheme, project number 223259.¨

## Additional Information

The authors declare **no** competing interests

## References

1 Cann, J. *et al.* Corrugated slip surfaces formed at ridge-transform intersections on the Mid-Atlantic Ridge. *Nature* **385**, 329 (1997).

2 Tucholke, B. E., Lin, J. & Kleinrock, M. C. Megamullions and mullion structure defining oceanic metamorphic core complexes on the Mid-Atlantic Ridge. *Journal of Geophysical Research: Solid Earth* **103**, 9857-9866 (1998).

3 Gràcia, E., Charlou, J. L., Radford-Knoery, J. & Parson, L. M. Non-transform offsets along the Mid-Atlantic Ridge south of the Azores (38 N–34 N): ultramafic exposures and hosting of hydrothermal vents. *Earth and Planetary Science Letters* **177**, 89-103 (2000).

4 Blackman, D. K. & Forsyth, D. W. Axial topographic relief associated with ridge-transform intersections. *Earth and planetary science letters* **95**, 115-129 (1989).

5 Fox, P. J. & Gallo, D. G. A tectonic model for ridge-transform-ridge plate boundaries: Implications for the structure of oceanic lithosphere. *Tectonophysics* **104**, 205-242 (1984).

6 Rüpke, L. H. & Hasenclever, J. Global rates of mantle serpentinization and H2 production at oceanic transform faults in 3-D geodynamic models. *Geophysical Research Letters* **44**, 6726-6734 (2017).

7 Etiope, G. & Sherwood Lollar, B. Abiotic methane on Earth. *Reviews of Geophysics* **51**, 276-299 (2013).

8 Sloan, E. D. & Koh, C. A. Clathrate Hydrates of Natural Gases Third Edition. *CHEMICAL INDUSTRIES-NEW YORK THEN BOCA RATON-MARCEL DEKKER THEN CRC PRESS*- **119** (2008).

9 Johnson, J. E. *et al.* Abiotic methane from ultraslow-spreading ridges can charge Arctic gas hydrates. *Geology* **43**, 371-374 (2015).

10 Waghorn, K. A., Bünz, S., Plaza-Faverola, A., & Johnson, J. E. 3-D seismic investigation of a gas hydrate and fluid flow system on an active mid-ocean ridge; Svyatogor Ridge, Fram Strait. *Geochemistry, Geophysics, Geosystems* **19**, 2325–2341 (2018).

11 Bartley, J. M. & Glazner, A. F. Hydrothermal systems and Tertiary low-angle normal faulting in the southwestern United States. *Geology* **13**, 562-564 (1985).

12 Sohn, R. A., Canales, J. P. & Humphris, S. E. Kinematics and geometry of active detachment faulting beneath the Trans-Atlantic Geotraverse (TAG) hydrothermal field on the Mid-Atlantic Ridge. *Geology* **35**, 711-714 (2007).

13 Plaza-Faverola, A. *et al.* Role of tectonic stress in seepage evolution along the gas hydrate-charged Vestnesa Ridge, Fram Strait. *Geophysical Research Letters* **42**, 733-742, doi:10.1002/2014GL062474 (2015).

14 Selley, R. C. & Sonnenberg, S. A. *Elements of petroleum geology*. (Academic Press, 2014).

15 Claypool, G. E. & Kvenvolden, K. A. Methane and other hydrocarbon gases in marine sediment. *Annual Review of Earth and Planetary Sciences* **11**, 299-327 (1983).

16 Proskurowski, G. *et al.* Abiogenic hydrocarbon production at Lost City hydrothermal field. *Science* **319**, 604-607 (2008).

17 Rajan, A., Mienert, J., Bünz, S. & Chand, S. Potential serpentinization, degassing, and gas hydrate formation at a young (< 20 Ma) sedimented ocean crust of the Arctic Ocean ridge system. *Journal of Geophysical Research: Solid Earth (1978–2012)* **117** (2012).

18 Engen, Ø., Faleide, J. I. & Dyreng, T. K. Opening of the Fram Strait gateway: A review of plate tectonic constraints. *Tectonophysics* **450**, 51-69, doi:10.1016/j.tecto.2008.01.002 (2008).

19 Plaza-Faverola, A. & Keiding, M. Correlation between tectonic stress regimes and methane seepage on the western Svalbard margin. *Solid Earth* **10**, 79-94, doi:10.5194/se-10-79-2019 (2019).

20 Ehlers, B.-M. & Jokat, W. Subsidence and crustal roughness of ultra-slow spreading ridges in the northern North Atlantic and the Arctic Ocean. *Geophysical Journal International* **177**, 451-462 (2009).

21 Petersen, C. J., Bünz, S., Hustoft, S., Mienert, J. & Klaeschen, D. High-resolution P-Cable 3D seismic imaging of gas chimney structures in gas hydrated sediments of an Arctic sediment drift. *Marine and Petroleum Geology* **27**, 1981-1994, doi:http://dx.doi.org/10.1016/j.marpetgeo.2010.06.006 (2010).

22 Ritzmann, O., Jokat, W., Mjelde, R. & Shimamura, H. Crustal structure between the Knipovich Ridge and the Van Mijenfjorden (Svalbard). *Marine Geophysical Researches* **23**, 379-401 (2002).

23 Crane, K. *et al.* Thermal evolution of the western Svalbard margin. *Marine Geophysical Researches* **9**, 165-194 (1988).

24 Crane, K., Sundvor, E., Buck, R. & Martinez, F. Rifting in the northern Norwegian-Greenland Sea: Thermal tests of asymmetric spreading. *Journal of Geophysical Research: Solid Earth* **96**, 14529-14550 (1991).

25 Crane, K. *et al.* The role of the Spitsbergen shear zone in determining morphology, segmentation and evolution of the Knipovich Ridge. *Marine geophysical researches* **22**, 153-205 (2001).

26 Reeve, M. T., Bell, R. E., Duffy, O. B., Jackson, C. A.-L. & Sansom, E. The growth of non-colinear normal fault systems; What can we learn from 3D seismic reflection data? *Journal of Structural Geology* **70**, 141-155 (2015).

27 SYLVESTER, A. G. Strike-slip faults. *GSA Bulletin* **100**, 1666-1703, doi:10.1130/0016-7606(1988)100<1666:Ssf>2.3.Co;2 (1988).

28 Judd, A. & Hovland, M. *Seabed fluid flow: the impact on geology, biology and the marine environment*. (Cambridge University Press, 2009).

29 Bonatti, E. Serpentinite protrusions in the oceanic crust. *Earth and Planetary Science Letters* **32**, 107-113, doi:https://doi.org/10.1016/0012-821X(76)90048-0 (1976).

30 Polonia, A. *et al.* Lower plate serpentinite diapirism in the Calabrian Arc subduction complex. *Nature Communications* **8**, 2172, doi:10.1038/s41467-017-02273-x (2017).

31 Granot, R., Abelson, M., Ron, H. & Agnon, A. The oceanic crust in 3D: Paleomagnetic reconstruction in the Troodos ophiolite gabbro. *Earth and Planetary Science Letters* **251**, 280-292 (2006).

32 Fujiwara, T. & Fujimoto, H. Seafloor geomagnetic vector anomaly of the intersection of the Mid-Atlantic Ridge and the Kane Transform Fault: Implications for magnetization of the oceanic crust. *Journal of Geophysical Research: Solid Earth* **103**, 30335-30349 (1998).

33 Kastens, K. *et al.* The Vema transverse ridge (central Atlantic). *Marine Geophysical Researches* **20**, 533-556 (1998).

34 Peive, A. & Chamov, N. Basic tectonic features of the Knipovich Ridge (North Atlantic) and its neotectonic evolution. *Geotectonics* **42**, 31-47 (2008).

35 Kharaka, Y. K. & Hanor, J. Deep fluids in the continents: I. Sedimentary basins. *Treatise on geochemistry* **5**, 605 (2003).

36 Charlou, J. *et al.* Compared geochemical signatures and the evolution of Menez Gwen (37 50' N) and Lucky Strike (37 17' N) hydrothermal fluids, south of the Azores Triple Junction on the Mid-Atlantic Ridge. *Chemical geology* **171**, 49-75 (2000).

37 Charlou, J., Donval, J., Fouquet, Y., Jean-Baptiste, P. & Holm, N. Geochemistry of high H2 and CH4 vent fluids issuing from ultramafic rocks at the Rainbow hydrothermal field (36 14' N, MAR). *Chemical geology* **191**, 345-359 (2002).

38 Plaza-Faverola, A. *et al.* Bottom-simulating reflector dynamics at Arctic thermogenic gas provinces: An example from Vestnesa Ridge, offshore west Svalbard. *Journal of Geophysical Research: Solid Earth* **122**, 4089-4105 (2017).

39 Tutolo, B. M., Seyfried, W. E., Jr., Saar, M. O., Mildner, D. F. R. & Gagnon, C. V. L. Nanoscale constraints on porosity generation and fluid flow during serpentinization. *Geology* **44**, 103-106, doi:10.1130/g37349.1 (2016).

40 Serié, C., Huuse, M. & Schødt, N. H. Gas hydrate pingoes: Deep seafloor evidence of focused fluid flow on continental margins. *Geology* **40**, 207-210 (2012).

41 Peckmann, J., Walliser, O. H., Riegel, W. & Reitner, J. Signatures of hydrocarbon venting in a Middle Devonian carbonate mound (Hollard Mound) at the Hamar Laghdad (Antiatlas, Morocco). *Facies* **40**, 281-296 (1999).

42 Waghorn, K. A. *et al.* Paleo-fluid expulsion and contouritic drift formation on the Chatham Rise, New Zealand. *Basin Research* **30**, 5-19 (2018).

43 Huuse, M. *et al.* Subsurface sediment remobilization and fluid flow in sedimentary basins: an overview. *Basin Research* **22**, 342-360 (2010).

44 Smith, A. J., Mienert, J., Bünz, S. & Greinert, J. Thermogenic methane injection via bubble transport into the upper Arctic Ocean from the hydrate-charged Vestnesa Ridge, Svalbard. *Geochemistry, Geophysics, Geosystems* **15**, 1945-1959 (2014).

45 Knies, J. & Mann, U. Depositional environment and source rock potential of Miocene strata from the central Fram Strait: introduction of a new computing tool for simulating organic facies variations. *Marine and Petroleum Geology* **19**, 811-828 (2002).

46 Knies, J. *et al.* Modelling persistent methane seepage offshore western Svalbard since early Pleistocene. *Marine and Petroleum Geology* **91**, 800-811 (2018).

47 Hustoft, S., Bünz, S., Mienert, J. & Chand, S. Gas hydrate reservoir and active methane-venting province in sediments on< 20 Ma young oceanic crust in the Fram Strait, offshore NW-Svalbard. *Earth and Planetary Science Letters* **284**, 12-24 (2009).
48 Bünz, S., Polyanov, S., Vadakkepuliyambatta, S., Consolaro, C. & Mienert, J. Active gas venting through hydrate-bearing sediments on the Vestnesa Ridge, offshore W-Svalbard. *Marine geology* **332**, 189-197 (2012).
49 Johnson, G. L. & Schneider, E. D. Depositional ridges in the North Atlantic. *Earth and Planetary Science Letters* **6**, 416-422 (1969).
50 Holbrook, W. *et al.* Escape of methane gas through sediment waves in a large methane hydrate province. *Geology* **30**, 467-470 (2002).
51 Suess, E. *et al.* Gas hydrate destabilization: enhanced dewatering, benthic material turnover and large methane plumes at the Cascadia convergent margin. *Earth and Planetary Science Letters* **170**, 1-15 (1999).
52 Crutchley, G. J., Pecher, I. A., Gorman, A. R., Henrys, S. A. & Greinert, J. Seismic imaging of gas conduits beneath seafloor seep sites in a shallow marine gas hydrate province, Hikurangi Margin, New Zealand. *Marine Geology* **272**, 114-126 (2010).
53 Chand, S. *et al.* Multiple episodes of fluid flow in the SW Barents Sea (Loppa High) evidenced by gas flares, pockmarks and gas hydrate accumulation. *Earth and Planetary Science Letters* **331**, 305-314 (2012).
54 Paull, C. K., Ussler III, W., Borowski, W. S. & Spiess, F. N. Methane-rich plumes on the Carolina continental rise: associations with gas hydrates. *Geology* **23**, 89-92 (1995).

Manuscript III

*Shallow gas redistribution coupled to arctic mid-ocean ridge tectonics*

**Kate A. Waghorn,** Rowan Romeyn, Andreia Plaza-Faverola and Stefan Bünz

Manuscript in preparation

# Shallow gas redistribution coupled to Arctic mid-ocean ridge tectonics

Kate A. Waghorn[1*], Rowan Romeyn[2], Andreia Plaza-Faverola[1], Stefan Bünz[1]

[1] CAGE – Centre for Arctic Gas Hydrate, Environment and Climate, Department of Geosciences, UiT – The Arctic University of Norway, N-9037 Tromsø, Norway

[2] Research Centre for Arctic Petroleum Exploration (ARCEx), UiT – The Arctic University of Norway, N-9037 Tromsø, Norway

[*]Corresponding Author: Kate Alyse Waghorn kate.a.waghorn@uit.no

## Abstract

Faults and fracture networks are important pathways for fluid migration and redistribution in the subsurface, and regional tectonic stresses as well as localized disruptions in the regional stress regime are important for determining the nature of fluid redistribution in the subsurface. Using high-resolution 3D seismic data sets, we are able to extract dip, dip direction and azimuth information from interpreted fault planes with enough confidence to analyse for stress and potentially paleo-stress. This type of analysis is useful for understanding how fluid migration systems change over time and space. We find that there appear to be two major phases of extension governing sedimentary fault development on the Svyatogor Ridge, and that small faults/fracture networks which do not conform to either of these extensional phases are more explicitly linked to fluid migration between a bottom simulating reflector and the seafloor in the southern-most data set. Fluid distribution appears greater in the northern dataset, although extensional faults are available for migration. In the present day, the stress regime imparted by the Molloy Transform Fault or hydrate sealing may be making these faults locked to fluid flow.

## Introduction

Faults and fracture networks are important mechanisms in invoking focused fluid flow in the subsurface and are fluid migration pathways in a number of systems, for example hydrothermal systems (Curewitz and Karson, 1997; Sibson, 1996), hydrocarbon reservoirs (Odling et al., 1999) and for gas migration through the shallow subsurface (Plaza-Faverola et al., 2015). Generally, brittle failures occur at an orientation that can be predicted based on the overall tectonic stress regime present (Zoback and Zoback, 2002). With the introduction of fluids into a system, fault and fracture network orientations become less predictable as brittle failure is sensitive to fluid pressure (Weinberger and Brown, 2006).

Gas hydrates are crystalline compounds composed of a gas molecule of low molecular weight – typically methane – encased within water molecules (Sloan, 1998; Weinberger and Brown, 2006). Gas hydrates are stable within a specific pressure and temperature regime and they are commonly

identified in organic rich sediments below 500 m water depth on continental margins world-wide (Kvenvolden and McMenamin, 1980) as well as in permafrost regions (Collett and Dallimore, 2000) and on the Knipovich Ridge flank (Johnson et al., 2015; Waghorn et al., 2018). The tectonic stress regime and structural controls at a gas hydrate bearing region plays an important role in determining the distribution and abundance of gas hydrate within sediment (Plaza-Faverola et al., 2015; Weinberger and Brown, 2006).

Low-displacement fault/fracture networks have been hypothesized to be, in some cases, more important than large-displacement single faults in fluid transport through the subsurface (Ligtenberg, 2005; Sibson, 1996). Extensive fracture network creation and fluid redistribution through the subsurface are well documented phenomena, however difficult to simulate due to their spatial relationships in 3D and temporal variability, especially in regard to active deformation settings (Caine and Forster, 1999). Fluid redistribution is often held accountable for earthquake swarms although in general fluid redistribution in the subsurface causes earthquakes on the micro-scale (Hill, 1977; Sibson, 2000). Fluid flow and redistribution in the subsurface can be halted due to the presence of a trap or seal, and in areas of gas hydrate accumulations, the gas hydrate itself may act as a seal to migrating fluids from depth (Kvenvolden, 1998). Hydrate formation and growth within sediment can act to consolidate the sediment, and in general change the physical properties of a sediment package such as mechanical strength, permeability and density (Waite et al., 2009). Faults can act as seal bypass mechanisms in gas hydrate systems, whereby free gas is able to migrate through the gas hydrate stability zone (GHSZ) by utilizing faults as focused fluid migration pathways (Berndt, 2005). Therefore, faults propagating through the GHSZ have the potential to be focused fluid flow pathways or, given appropriate conditions, gas hydrate may form within faults themselves, cementing the fault and sealing it to migrating fluids (Madrussani et al., 2010; Weinberger and Brown, 2006). Conversely, the formation of hydrate within pore space may change the physical properties of the sediment enough so that brittle failure criteria within the sediment changes (Waite et al., 2009).

Understanding fluid transport and redistribution processes through the subsurface is generally important for constraining global carbon budgets and understanding fluid flow systems. Using 3D seismic data for detailed analysis of fault systems allows for characterization of spatial and temporal interactions of faults and their involvement in subsurface fluid migration. High resolution 3D seismic data allows imaging of faults on smaller scales, such as the scale of fault networks important for fluid redistribution in the subsurface. In this study, we analyse faults, extract stress tensors and attempt to show how the tectonic stress environment is controlling fluid redistribution temporally and spatially on the flank of the Knipovich Spreading Ridge.

## Geologic Setting

The Svyatogor Ridge is a sedimented flank of the Knipovich Ridge. It is located at the Ridge-Transform Intersection (RTI) between the Knipovich Ridge and Molloy Transform Fault (Fig. 1). The sediment cover in the area is approximately 400-800 m thick (Waghorn et al., 2018). The crust underlying the Svyatogor Ridge lies between Chrons 5 and 2A (Engen et al., 2008) – corresponding to between 9.8 and 2.8 Ma (Fig. 1). Johnson et al. (2015) hypothesize that the Svyatogor Ridge was, in its early evolution, a younger extension of Vestnesa Ridge, which was isolated due to offsetting along the Molloy Transform Fault caused by spreading of the Knipovich Ridge. The Knipovich Ridge is an ultraslow, melt-poor spreading ridge, spreading obliquely at ~8 mm/yr (Ehlers and Jokat, 2009). In this segment of the Knipovich Ridge, spreading is accommodated by large, crustal scale detachment faults (Johnson et al., 2015; Waghorn et al., 2018) There has been no documentation of intrusive bodies underneath the Svyatogor Ridge, including in regional seismic studies (Amundsen et al., 2011). However, seismic velocity studies indicate that there may be intrusive features on the north-western flank of the Knipovich Ridge, around the Vestnesa Ridge (Ritzmann et al., 2002). Ritzmann et al. (2002) also notes that seismic velocities underneath the Svyatogor Ridge are consistent with an ultra-mafic, partially serpentinized mantle material.

RTI's are generally associated with topographic highs on the inside corner of the intersection, known as inside corner highs (Cann et al., 1997). The study area here forms the inside corner high at the Knipovich Ridge-Molloy Transform Fault intersection.

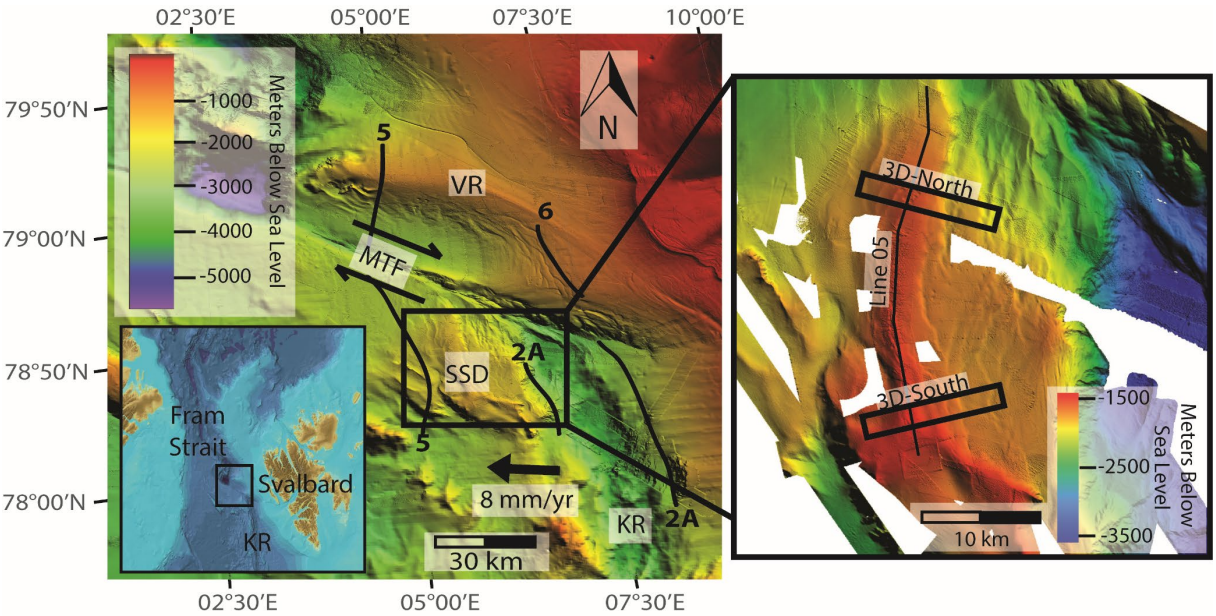


*Figure 1. The study area is location at the Knipovich Ridge (KR) and Molloy Transform Fault (MTF) intersection, on the inside corner high. The Svyatogor Ridge (SSD) is located between chrons 5 and 2A (9.8 and 2.8 Ma respectively). The Svyatogor Ridge is directly south across the MTF from the Vestnesa Ridge (VR), a well-studied gas hydrate hosting sediment drift. This study uses 2 3D seismic data cubes collected at the north and south of the Svyatogor Ridge, connected by a 2D seismic line.*

## Data and methods

The data used in this study are two 2 x 10 km 3D seismic cubes supplemented by bathymetry data and 2D seismic lines (Fig. 1). Seismic data was recorded using 14 25 m long streamers with 8 channels per streamer (Planke et al., 2009). Data processing included: Geometry assignment, CDP binning at 6.25 x 6.25 m, static corrections, simple band-pass filtering (10-20-400-500 Hz), amplitude corrections, NMO correction, stacking, crossline interpolation and 3D migration (using a velocity model based on prior published velocity information (Ritzmann et al., 2002). The vertical resolution of both data sets is <3.5 m ($\lambda$ = 120 Hz) at the seafloor, assuming water velocity ~1490 m/s. Seismic interpretation uses commercially available Petrel interpretation software. Analysis of faults was carried out using Win_Tensor software (Delvaux and Sperner, 2003). Faults were plotted in Schmidt Lower hemisphere stereonets to extract orientation of kinematic axes based on fault dip, fault dip direction and azimuth of fault trend. Each fault plane has a compressional axis (P) and a tensional axis (T) that can be used either as approximations of principal stress directions – to infer the Andersonian fault regime – or to indicate the rake of a slip vector and therefore group faults into movements (Angelier, 1979; Célérier, 2010). The direction of slip on a fault plane is determined by the orientation and relative magnitudes of the principal stresses. The T axis reflects the minimum compressive stress direction and the P axis reflects the maximum compressive stress direction, if we assume the kinematic axes are the best approximation of the principal stresses, although the principal stresses could plot anywhere within the P or T quadrants (Célérier, 2010).

To obtain dip, dip direction and trend of faults for analysis we interpreted fault planes in Petrel, obtained their dip and dip direction attributes, and then analysed them for trend, and changes in attributes both laterally and vertically. Bathymetric data was used to compare trends of faulting in the subsurface to the scarps and orientations we could identify on the seafloor. We used data from the open access World Stress Map (Heidbach et al., 2018) to obtain information on the regional stress regime and International Seismological Centre earthquake positions and magnitude data to compare results to recorded earthquake information (International Seismological Centre, 2016).

## Geophysical Data Interpretation

### Bathymetry

The bathymetry of the Svyatogor Ridge (Fig. 2) shows an elongate, curved ridge. The morphology of the ridge changes from steeper and narrower in the south to broader, west-curving and slightly deeper in the north (Fig. 2). Lineaments on the seafloor, interpreted as fault scarps (Fig. 2), become wider and more pronounced to the north, and they have a number of orientations in a general NNE trend (non-colinear). The westward curve of the ridge in the north is interpreted to be caused by offset of the

ridge along the Molloy Transform fault during ongoing sedimentation and ridge formation. Scarp lineaments are interpreted to be faults breaching the seafloor. Crane et al. (2001), using bathymetry and side-scan sonar data, have interpreted extensional faults and a paleo-transform fault in the area (Fig. 2) however our bathymetry data indicates that the paleo-transform fault is cross-cutting a fault scarp in such a way as to indicate that the hypothesized paleo-transform fault is either further south or striking at a different angle. (Waghorn et al., Submitted) interprets a number of faults north of the Svyatogor Ridge as splay faults related to the MTF (Fig. 2). Our 3D seismic data does not capture these faults however following interpretations in (Waghorn et al., Submitted), the presence of these faults in on the Svyatogor Ridge indicate that the MTF tectonic regime is likely influencing stress regimes at least as far south as these faults are identified.

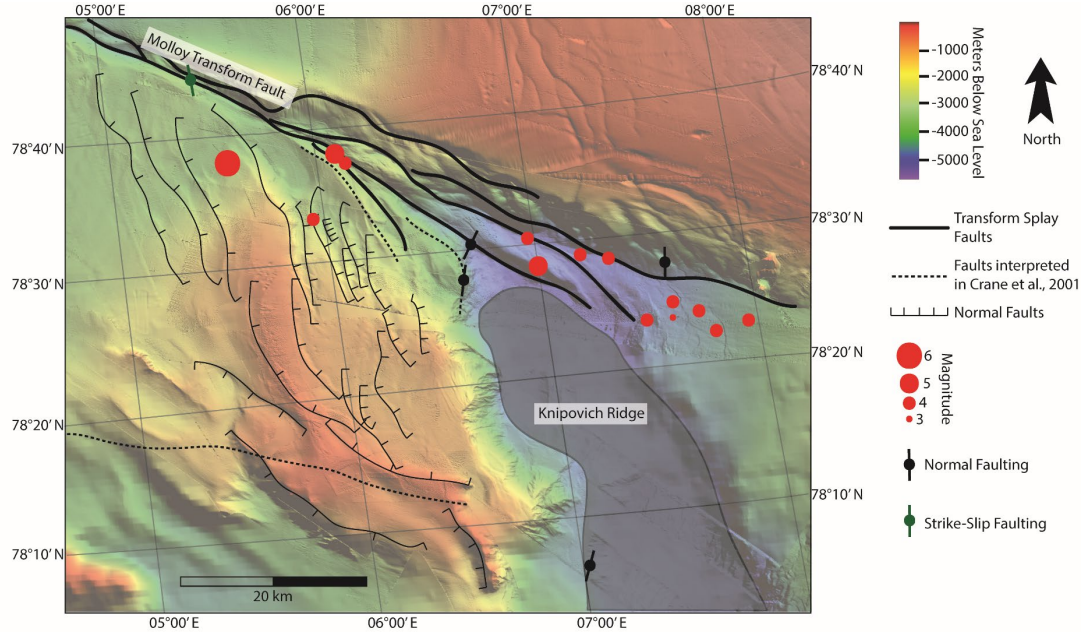


*Figure 2. A summary of major tectonic features in the study area, interpreted on bathymetry, following (Waghorn et al., Submitted). Earthquake data taken from the International Seismological Centre (International Seismological Centre, 2016) show that although tectonically active, earthquake magnitudes are not large and are focused around the Molloy Transform Fault (data is filtered for events above magnitude 3 with first motions for all available years, within the bounds of this figure). Data from the World Stress Map (Heidbach et al., 2018) gives an indication of whether normal (black dashed dot) or strike-slip faulting (green dashed dot) should be expected (dash indicates maximum horizontal stress). (Crane et al., 2001) interprets tectonic features over this study area using bathymetry and side-scan sonar. These features are labelled by dashed lines.*

## Southern 3D Dataset

In the southern dataset, a reflection which is anomalously high amplitude, reverse polarity, cross cutting and mimicking the seafloor is identified at the crest of the ridge. This reflection is interpreted by Johnson et al. (2015) and Waghorn et al. (2018) to be a BSR reflection, and is limited to the apex of the Svyatogor ridge crest in this data set. The zone of increased amplitude underneath the BSR, corresponding to free gas accumulation at the base of the GHZS, is ~60 ms thick (Fig. 3). Buried circular features constrained to the Svyatogor ridge crest (Fig. 4) are interpreted by Waghorn et al. (2018) to

be buried pockmarks, and the seafloor counterparts as present day pockmarks, indicating that there has been fluid migration through the hydrate stability zone and expulsion at the (paleo-) seafloor. Pockmarks on the seafloor follow the approximate strike of the Svyatogor Ridge crest (Waghorn et al., 2018).

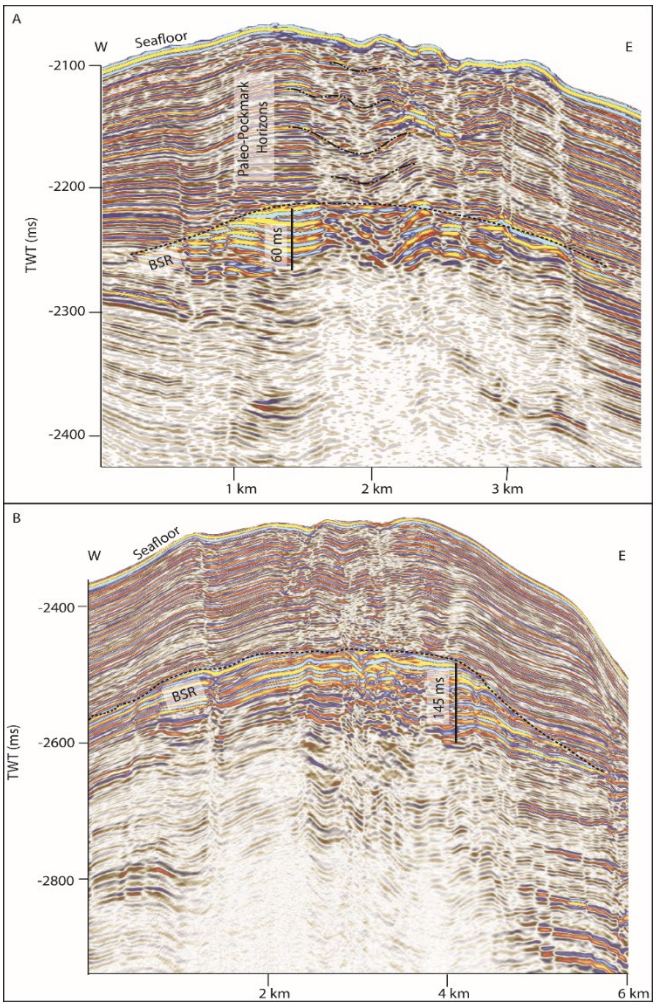


*Figure 3. Comparison seismic images of the Svyatogor Ridge crest BSR reflection and free gas zone in the northern (bottom) and southern (top) data sets.Paleo-pockmarks horizons interpreted by Waghorn et al., (2018) are shown here.*

Fault interpretations in the southern dataset follow Waghorn et al. (2018) where the authors interpret four major fault types; detachment faults, sedimentary growth faults, radial faults and fault/fracture networks. For this study, the sedimentary growth faults and fault/fracture networks are analysed. Growth faults are identified as clusters of normal faults around a larger fault contained in mechanically stronger material (in this case the detachment faults). Growth faults propagate upwards in the sedimentary strata and are often associated with a section of folded material at the upper terminus of the fault (Hardy and McClay, 1999), before the plane of weakness breaches into a fault. In the southern 3D dataset, these faults are striking approximately NNE, towards the Knipovich ridge. Dip values range from 40-80°, with most faults dipping 50-70° (Fig. 5). There are also a number of smaller faults, limited

to 100 ms (~2200-2300 ms), in the data set that are randomly striking and usually very close to 80° dips (Figure 5 in Waghorn et al., 2018). They are predominantly located at the boundary between the FGZ and GHSZ. These small faults are interpreted as networks of fractures/small faults associated with movement of fluids in the subsurface.

.

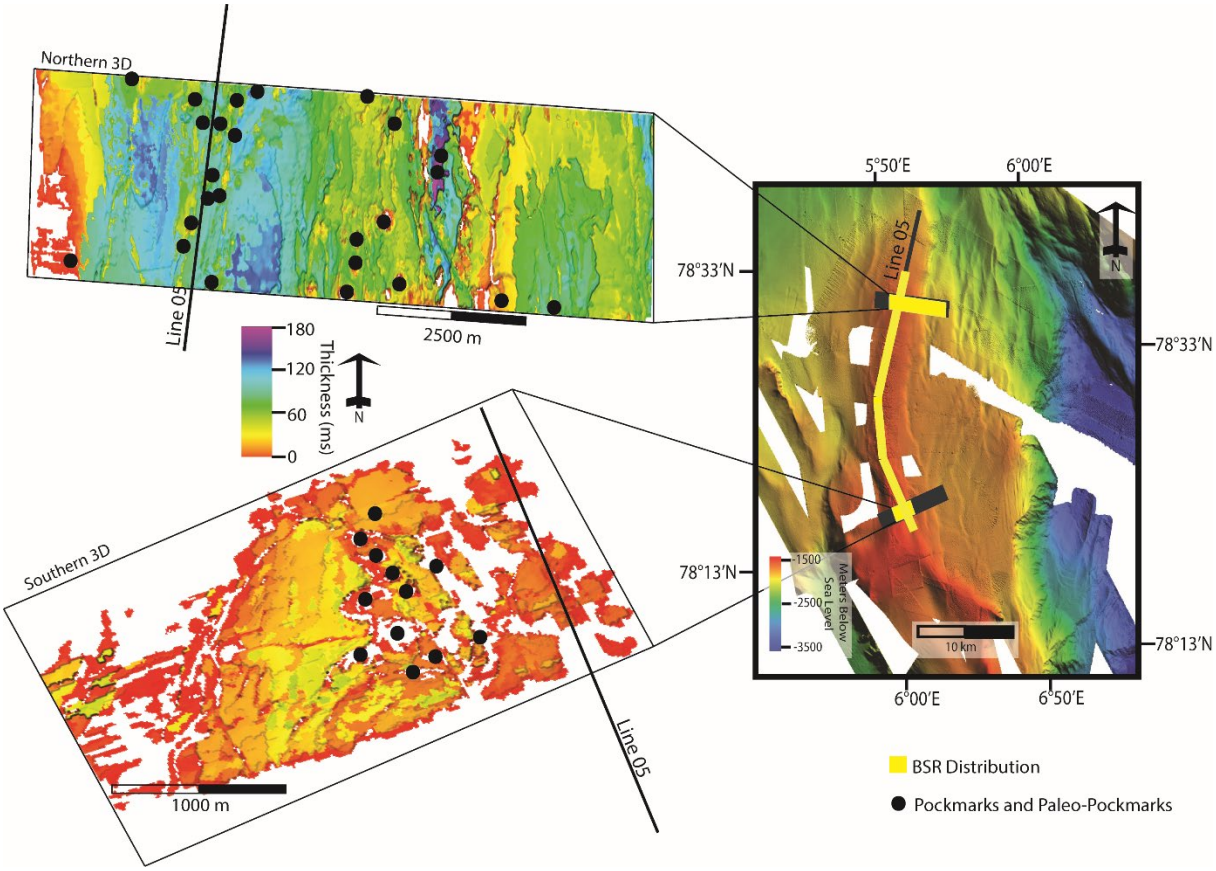


*Figure 4. Comparative BSR reflection extent in the two seismic data cubes. Thickness maps indicate the apparent thickness of the free gas zone in both. Note that the southern data cube BSR extent is limited to the crest of the ridge while in the northern data set it covers almost the entire seismic data cube. Pockmarks and paleo-pockmarks are denoted on the thickness maps by black dots.*

## Northern 3D Dataset

From the southern data set, the BSR reflector has been correlated to the northern data set using results from Waghorn et al. (Submitted). In the northern data set, the BSR and associated FGZ is much more extensive, both laterally across the dataset and in terms of seismic thickness of the zone. In the case of the northern dataset, many reflectors beneath the FGZ are attenuated and therefore it is difficult to determine whether we image the true vertical thickness of the FGZ. However, the section that is well imaged is between 127-145 ms thick. Here, the FGZ and presumably gas hydrate accumulations also extend off the Svyatogor ridge crest downslope towards the Knipovich Ridge (Fig. 4). As in the southern data set, buried and seafloor circular depression structures (Fig. 6) are identified which are characterized based on 1) a clear erosional base (i.e. representative of sediment erosion rather than

infilling deposition) and 2) a steepened profile. Occasionally the base of these structures correlates with a high amplitude seismic anomaly (Fig. 6). These circular depression structures are interpreted to be pockmarks associated with the expulsion of fluid. Due to their presence throughout the strata between the BSR and seafloor, we interpret them as evidence of an episodic, long lived fluid migration and expulsion system. Pockmarks are limited to the seafloor in the northern dataset; however, paleo-pockmarks are identified over a greater area than in the southern dataset.

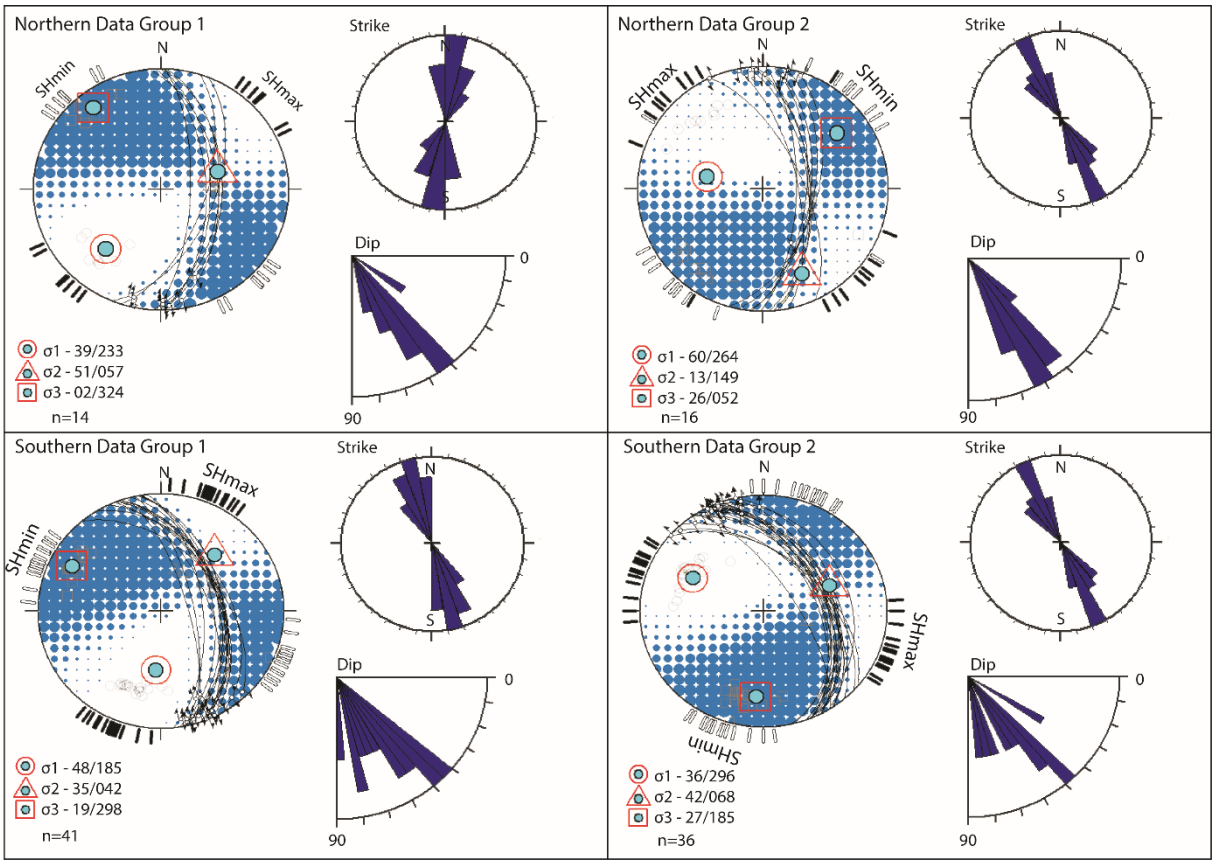


*Figure 5. Schmidt lower hemisphere stereonets showing the groups of faults with converging stress tensors (assuming that P,B and T tensors are approximate to σ1, σ2 and σ3). We find two consistent fault populations in the northern and two in the southern datasets. The orientation of $SH_{max}$ are indicated for each fault plane by a black mark on the stereonet while $SH_{min}$ is denoted by a while mark. Slip directions are noted by arrows on the fault planes. The average orientation of σ1, σ2 and σ3 for each fault group is marked by a blue circle with red shape (circle, triangle or square) around. Blue dots indicate the compressional first motion, larger blue dots indicate more certainty.*

Within this dataset, we observe that there are considerably fewer faults than in the southern dataset. Seismic energy penetration is not sufficient to determine if there are detachment faults present in the northern area as in the southern area. In a similar fashion to the southern dataset, faults in the northern data set strike NNE, dipping towards the Knipovich ridge. They are also dipping between 40-80° (Fig. 5). The faults in this dataset often exhibit offset strata upwards in the sedimentary column, transitioning to a small fold deflection at the upper termination of the fault. This type of transition from discrete offset to fold is often associated with growth faulting, however we do not image the mechanically stronger basal material in this dataset. We do not identify any randomly striking faults in

this data set that could be interpreted as radial faults or fracture networks following Waghorn et al. (2018) interpretations for the southern data set.

Both seafloor and paleo pockmarks are identified predominantly along the same strike as the faults, NNE, and appear to occur in conjunction with growth faults (Fig. 6).

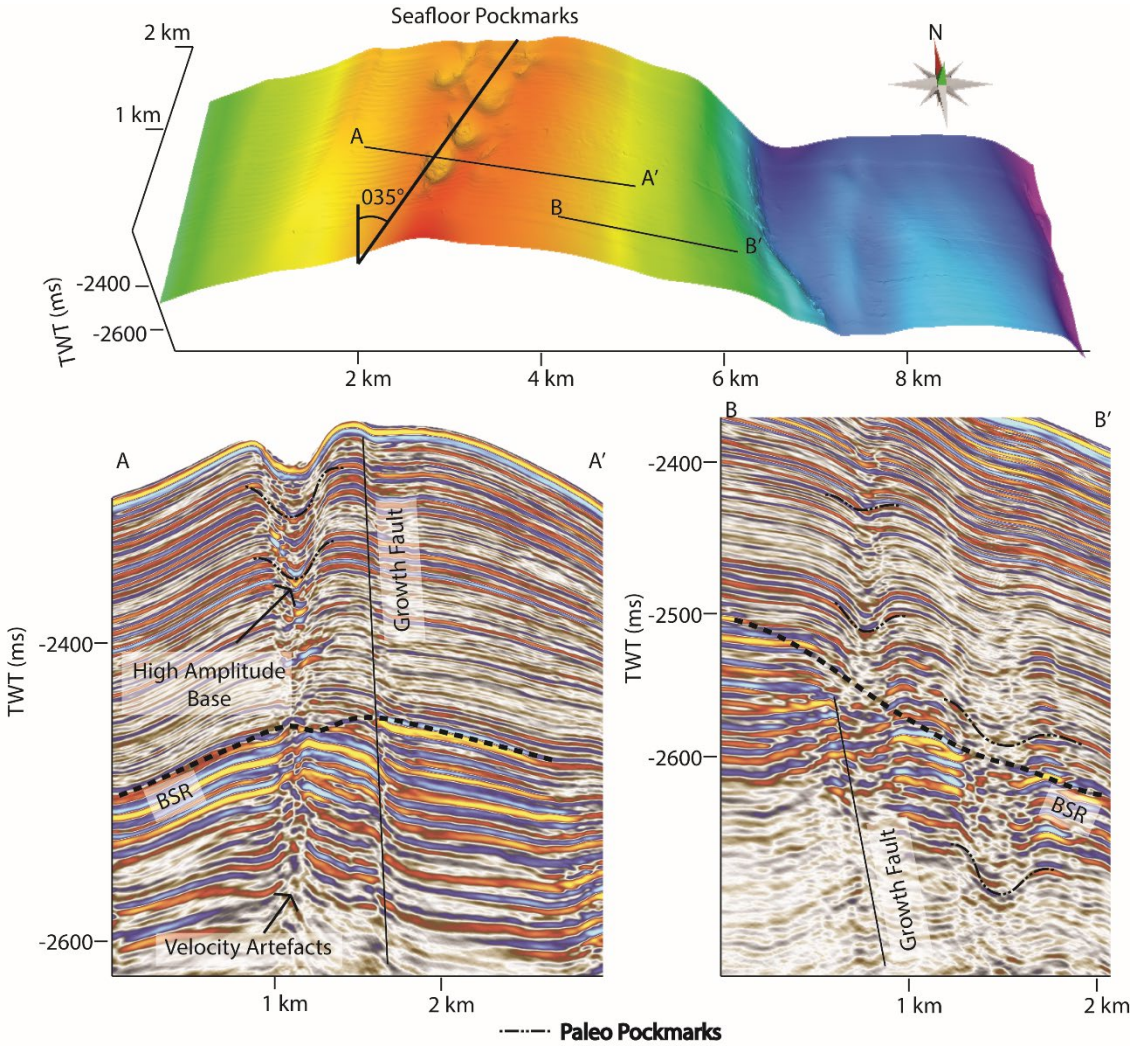


*Figure 6. Examples of the fluid flow system in the northern 3D data set. At the seafloor, there are only pockmarks on the crest of the Svyatogor Ridge, which are striking NNE-SSW – the approximate strike of fault group 2 (growth faults) in the north. Paleo-pockmarks are interpreted based on their circular U shape profile, circular in 3D, with generally an erosional, high amplitude base. Infil is generally low amplitude. Growth faults often exist is close proximity, or directly related to paleo-pockmarks. On the flank of the Svyatogor Ridge, paleo pockmarks below the level of the BSR are identified.*

## A spatially variable fluid flow system

Between the 3D datasets, representing north and south of the Svyatogor Ridge, we note a marked change in free gas extent and configuration, spatial extent of paleo-pockmarks, and style of faulting. In the northern dataset, we observe that paleo-pockmarks are common from the crest of the ridge extending eastwards towards the Knipovich ridge to the edge of the dataset, and are commonly associated with growth faults, while in the southern dataset, paleo pockmarks are only observed at

the crest of the ridge and are not associated with single fault planes. The BSR reflection and associated FGZ also extend considerably further towards the Knipovich ridge in the northern dataset cf. the southern data set (Fig. 4). Lastly, we identify a greater variety of fault types, faults with random strikes and faults with very small vertical extent and offset in the southern dataset while the northern dataset only contains growth faults striking NNE.

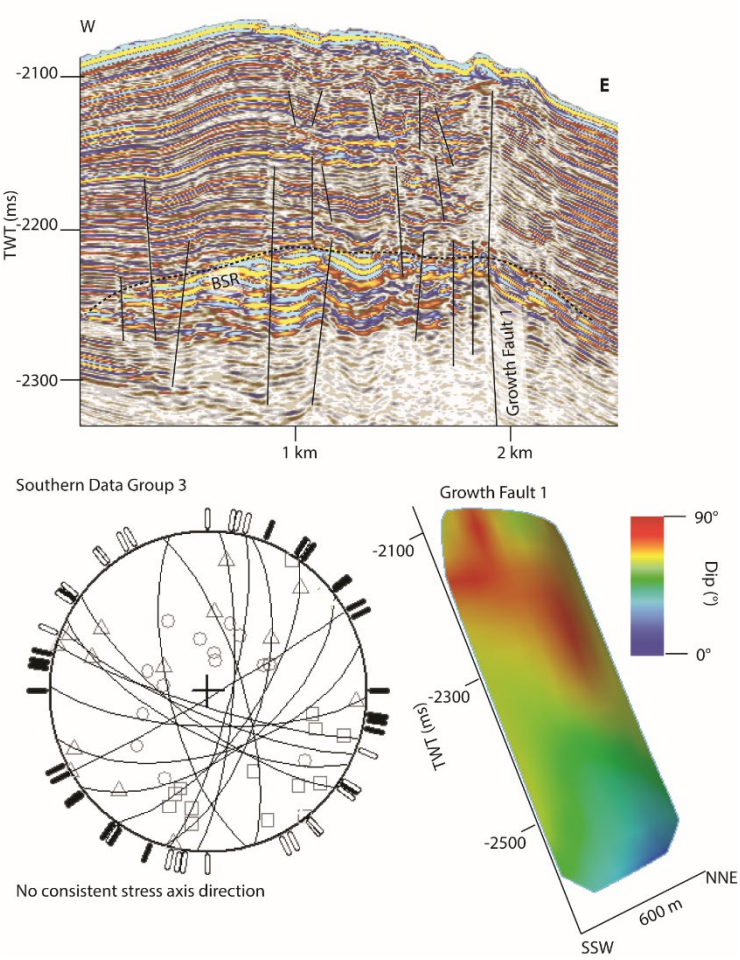


*Figure 7. Summary of faults inconsistent with groups 1 and 2 in the southern data set- group 3. These faults all occur in conjunction with the ridge-crest fluid flow system, often extending no more than ~150 ms. These faults are in general more steeply dipping and there are no consisten stress tensors nor first-motions (Schmidt lower hemisphere stereonet). Growth fault 1 is also inconsistent with formation under the same regimes as group 1 or 2, however we interpret this as due to it's deviation at the level of the BSR, where it's dip steepens and strike becomes more variable along the fault plane*

## Fault Analysis

### Fault Slip Analysis

In the southern dataset we were able to interpret 91 fault planes with enough confidence to use in this analysis. The northern dataset had considerably less faults, and we were able to identify 31 faults to analyse. We use an average dip and dip direction across the entire interpreted fault plane. Potential error in this type of analysis is mainly due to unconstrained velocity models, causing fault planes in the 3D seismic to not appear true to their steepness. To account for this, we have considered cases with a

higher interval velocity at depth. In this area, given the sedimentary column thickness and therefore compaction potential, velocities over 2400 m/s are unreasonable. Sonic logs for the ODP 910 well on the Yermak Plateau show that the average velocity at similar depths is 1827 m/s ($V_p$). We therefore consider the case where the velocity used to pick faults increases to 1800 m/s to estimate the error of this analysis.

### *Growth Faulting*

The fault planes plotted in Win_Tensor (Delvaux and Sperner, 2003) are divided into groups based on best-fit into specific P,T axial orientations (Fig. 5; Fig. 7). In both 3D data sets, faults can be divided into four groups (two in each data set) which have similar stress axes orientations. There are no instances of faults outlying in the northern dataset however there are a number of outliers in the southern dataset (Fig. 7). Assuming that P and T axes are comparable to the maximum and minimum horizontal stresses respectively, we find that the extensional stress axes in both the northern and southern datasets has changed, from ~320° (NW) to ~220° (SW) in the northern area and ~300° (NW) to ~195° (SSW) in the southern area (Fig. 8). On all these groups of faults, the deviation from vertical of the σ1 axis indicates that these faults are oblique dip-slip style faults, i.e. there is some lateral movement as well as vertical movement on the fault plane although the vertical movement is still dominant. In the southern dataset, faults forming two congruent groups are interpreted by Waghorn et al. (2018) as growth faults, forming as a consequence of continued uplift by a mechanically stronger fault block underlying the sedimentary strata (Hardy and McClay, 1999). Following this interpretation, sedimentary growth fault groups are likely composed of both reactivated and neo-formed faults. We interpret the two faults groups in the northern area as sedimentary growth faults, following the southern area interpretation (Waghorn et al., 2018). In the southern dataset, a notable exception to the dominant fault style identified here is the western-most interpreted growth fault (Fig. 7), which follows the same general trend as other growth faults until ~2300 ms TWT (20 ms beneath the BSR), where it steepens towards the seafloor. We interpret this to be related to the presence of the fluid flow system on the Svyatogor Ridge.

The minimum and maximum compressive stress orientations derived in this analysis indicate that group 1 faults in both areas are forming under a regime with similar stress orientations, as are group 2.

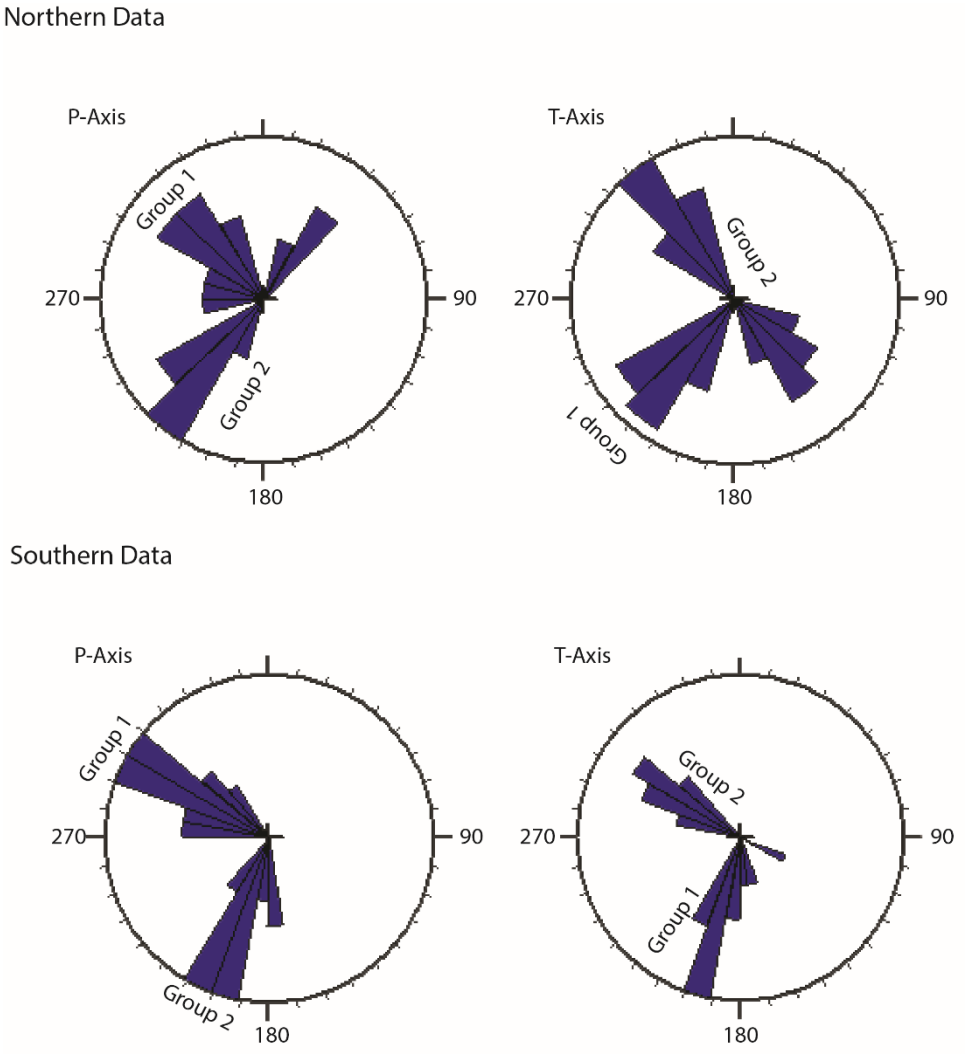


*Figure 8. From data presented in figure 5, the azimuths of all P and T axes for Groups 1 and 2 in both data sets, respectively. Group 1 and Group 2 P and T axes in both the north and the south have a relatively good correlation suggesting formation under the same extensional regime. Group 1 P axis azimuths are ~310° (Northern Dataset) and ~300° (Southern Dataset), group 2 P axis azimuths are ~220° (Northern Dataset) and ~200° (Southern Dataset). Lastly Group 1 T axis azimuths are approximately 195° in the southern dataset, 220° in the northern dataset and the group 2 T axis azimuths are ~300° and ~320° in the northern and southern datasets respectively.*

### *Error Estimation*

We find that when adjusting for an increasing velocity with depth, up to the maximum that we consider realistic of 1800 m/s, the average dip of the fault planes steepens by less than 3°, which translates to an error of 15 m given the average fault length of 300 m. A steepening of <3° is very difficult to discern on the stereonet plots, and 1800 m/s is not consistent with the velocity model presented for the sedimentary section of Svyatogor Ridge by Ritzmann et al. (2002) so for the purposes of this analysis we find using a velocity of 1600 m/s (Ritzmann et al., 2002) to be sufficient.

### Small offset faulting

In the southern dataset, we find a group of faults described by Waghorn et al. (2018) as fault and fracture networks, which are very small (<10 m offset) planes striking in random azimuths contained

within a limited area – around the FGZ and 60 ms into the GHSZ (Fig. 7). These faults were hypothesized to be important gas hydrate zone bypass mechanisms on the Svyatogor Ridge (Waghorn et al., 2018). Generally these faults are steeply dipping (Fig. 7) although in some cases the dip of the fault changes abruptly, and they are represented by fault group 3 – the non-compliant faults – in the fault plane analysis (Fig. 7). Due to their very limited occurrence in direct correlation with the area interpreted as hosting fluid flow in the southern Svyatogor ridge, we interpret these faults as playing an important role in fluid migration across the GHSZ here. We have not been able to interpret a similar set of faults in the Northern data set, however, note that in the northern dataset we find that there is a larger correlation between growth faulting and fluid flow features such as paleo-pockmarks (Fig. 6). This particular set of faults also have a higher coincidence of intersecting planes compared to growth fault sets.

## Faulting and fluid redistribution on the Svyatogor Ridge

The fluid flow system is more extensive in the north area of Svyatogor Ridge, with a larger areal extent of gas hydrate and free gas distribution, as evidenced by the larger spatial distribution of the BSR reflection (Fig. 4). The areal extent of paleo-pockmarks is also greater, with paleo-pockmarks identified on the crest of the ridge, the flank of the ridge and on a plateau east of the ridge crest (Fig. 4). The paleo-pockmarks in the northern dataset are more distributed in the sedimentary column compared to the southern dataset where Waghorn et al. (2018) interpret four horizons with paleo-pockmarks. There are also more paleo-pockmarks per horizon in the northern dataset.

Comparing faulting between the datasets, we interpret many more faults in the southern dataset, while the faults we interpret in the northern dataset are exclusively growth faults, however all the major sedimentary faults in both datasets appear to be forming under a similar, albeit rotated conditions. Interestingly, both groups of faults have an oblique component, which is not consistent with these faults forming in a purely extensional setting. All the paleo-pockmark fields in both data sets are striking NNE, i.e along the same strike as growth/oblique slip faults, however it is only in the northern dataset where growth faults feed these pockmarks. In the southern data set we have identified faults (group 3; Fig. 7) apparently feeding seafloor and paleo-pockmarks that do not strike at an orientation which suggests formation under similar stress conditions to the growth faults– and their P B and T axes in plotted stereonets suggest no overarching stress regime controlling their formation. These faults are also typically very small offset (<10 m) and limited to ~200 ms length. This is interpreted as a result of fluid movement in the subsurface forcing brittle failure where a pre-existing migration pathway did not previously exist (Sibson, 1996). The exception to this general pattern is a single fault (Fig. 7), interpreted by Waghorn et al. (2018) as a sedimentary growth fault whose stress orientations suggests that it initialized as a growth fault, however above the BSR is inconsistent with

continued formation as a growth fault. Comparatively, in the northern data set we do not identify any faults which are forming randomly to the identified stress orientations.

Fluid migration in the northern area appears to be controlled by growth faulting while in the south we interpret that fluid overpressure has been a significant forcing mechanism in development of fluid flow pathways.

# Discussion

## Spatial and Temporal Relationships between faults and fluid migration

In the southern dataset, the relationship between small-offset fault/fracture networks and, spatially, the BSR reflection, associated free gas system and presumed hydrate accumulations leads to the conclusion that these faults are forming as a consequence of fluid redistribution and migration in the subsurface. In addition, that these faults are forming with randomly oriented stress tensors in comparison to the sedimentary growth faults indicates that it is not the regional stress regime causing these brittle failures. However, the sedimentary growth faults and by extension the regional stress regime, are controlling seepage structure formation at the northern extent of the Svyatogor Ridge. This indicates that the fluid redistribution control mechanism between the north and south is different or has changed temporally. Notably, fluid pressure driven faults are not identified in the northern dataset indicating that there has been no necessity for their formation, either as the sedimentary growth faults were optimally positioned for fluid migration, or in the southern area there was another factor such as hydrate formation within faults or unfavourable orientation, position or timing of faulting acting to inhibit fluid migration through growth faults (Madrussani et al., 2010). Interestingly, an initial assumption in this study area was that the growth faults in the north would be less favourable for fluid migration and redistribution as Plaza-Faverola and Keiding (2019) note that much of this area is presently in a strike-slip tectonic regime while the southern area is in a extensional regime. However, as we image many paleo-pockmarks it is clear that time is an integral factor in the fluid migration system here, and given that the growth faults are extensional it is clear that for the development of growth faults, the northern data set was in an extensional environment. Following interpretations by Waghorn et al. (Submitted), areas off the Svyatogor Ridge crest, but still in close proximity to the northern dataset, exhibit transtensional faulting. Although the southern dataset is bathymetrically higher and up-dip from the northern dataset, there appears to be simply less free gas in the system which could be attributed to fluid migration limited by compressive stress environments (Fig. 4).

Mapping fault scarps on the seafloor indicated that the groups of faults here are non-colinear. Non-colinear fault arrays can have a number of formation mechanisms, for example; episodes of extension with changing extensional stress axes (Henza et al., 2011), pre-existing structural fabrics being

activated/reactivated (Morley et al., 2004), variations in displacement along strike leading to variable uplift and/or displacement (Stewart, 2001) or faults developing synchronously under a 3D strain field. In a model of multiple extensional phases, depending on the variation in extension direction, later phase brittle deformation may occur either as reactivations on pre-existing faults, or new faults may form. Clay models of such deformation phases have shown that initial phase faults, formed perpendicular to the extensional direction, are often reactivated with oblique slip however the dominance of first or second phase faulting depends on the magnitude of extension (Henza et al., 2011). We favour this model for producing extensional faults with oblique slip components, in non-colinear fashion in this study area. Given that many of the faults are obliquely slipping, it would seem that the first phase extension was dominant giving rise to a well-developed first phase fault population which has then strongly influenced the development of any second phase faults (Henza et al., 2011). However, in this study we find two distinct groups of predominantly oblique-slip faults, which indicates – under the aforementioned formation model – at least two phases of extension per fault group. If we assumed that fault group 1 in the south is forming synchronously with fault group 1 in the north we might assume that the average extensional stress orientation averaged across both datasets to represent the mid-point of stress rotation during formation (Fig. 9). In this case, for both faults groups 1 and 2, this would imply that there has been a significant change in the extensional stress orientation (up to 80°) between the two fault groups. Although this may be attributed to the propagation of the Knipovich Ridge northwards, we also consider that discrepancies between the extent of crustal uplift beneath the sediment is also likely controlling the growth fault orientations, i.e. the downthrown sediment block preferentially moves towards accommodation space when faulted.

As this study area is on an actively spreading mid-ocean ridge flank, with detachment faults as the dominant mode of spreading (Tucholke et al., 1998; Waghorn et al., 2018), we cannot rule out that the crustal structure imposing weaknesses in the sediment (Morley et al., 2004) has played a role in the development of the fault population here, especially as Waghorn et al. (2018) interpreted these faults as growth faults which implies an intrinsic link between the crust and overlying fault populations. However, this model does not necessarily explain the oblique nature of slip on what might otherwise be purely extensional faults. A 3D strain field should exhibit a more developed population of faults reflecting the additional dimension of the strain field (Reeve et al., 2015), which we do not see in this data. As all fault populations in the northern and southern 3D data sets are reactivated, it is difficult at this stage to determine the orientations of stress tensors for discrete phases of extension, and so following we cannot discuss whether the phases of extensional faulting in the north and south are products of the same extensional deformation phases or if we are observing multiple phases in multiple locations, however given the proximity of the two locations and the scale of the regional

tectonic features related to the study area it is likely that the phases of extensional faulting in both data sets are products of the same overarching extensional deformation phase. In addition, the West Svalbard Margin has an extensive history of glaciation-deglaciation cycles (Andersen et al., 1996; Faleide et al., 1996; Landvik et al., 1998), and stresses associated with isostacy are evoked mechanisms in controlling dilation of faults, reactivating pre-existing structural weaknesses and also controlling fluid dynamics in the subsurface (Plaza-Faverola and Keiding, 2019). Waghorn et al. (2018) attempt to correlate the 2.8 Ma horizon to the southern Svyatogor Ridge dataset, and show that many of the growth faults in the southern dataset terminate beneath this horizon, however faults interacting with the seafloor or any horizon above this boundary may have been influenced by stresses associated with loading and unloading of ice on the West Svalbard Margin. We find no evidence to conclude whether stress changes in response to glaciation and deglaciation cycles are influencing faulting, re-activation and the apparent change in stress orientations over this study site. We also find that trying to determine to what depth stresses associated with ice sheets in close proximity may have influenced the faulting regime is an important consideration for further studies.

With regard to fluid migration, if we assume that both study sites are undergoing deformation simultaneously (Fig. 9), the timing between deformation phases and fluid migration is likely key to determining the differences in the fluid flow system at either end of the Svyatogor Ridge. The paleo-pockmarks on the flank of the northern data set (Fig. 6) indicate that likely the ridge was less pronounced when these features were forming as it is unusual to encounter pockmarks on the flanks of ridges as opposed to the crest (i.e. Vestnesa Ridge (Bünz et al., 2012), Blake Ridge (Skarke et al., 2014)). The implication of these pockmarks for constraining timing between fluid migration and tectonic deformation is that either 1) crustal uplift along detachment faults had not/would not occur in this location or 2) a second phase of extensional deformation defined the ridge, and paleo-pockmarks on the Svyatogor Ridge flank occurred prior to this. In the southern data set, we propose that fluid migration occurred predominantly post-first phase deformation, and faults were sub-optimally positioned and/or oriented for dilation or seismic pumping of fluids (Sibson et al., 1975; Sibson, 1996, 2000).

In the present, Plaza-Faverola and Keiding (2019) have modelled that the southern area of this study is in a differing stress regime cf. the northern area. It is plausible that the differing stress regimes today are playing a role in the distribution of free gas and BSR reflections. Plaza-Faverola and Keiding (2019) model that the maximum compressive horizontal stress direction at the northern end of the study area is oblique to the overall fault strike direction, implying that these faults could be unfavourably oriented in the present day for fluid migration. In this case, fluid might remain trapped until 1) fluid

overpressures exceed lithostatic pressure or 2) stress orientations change and exert dilation on these faults.

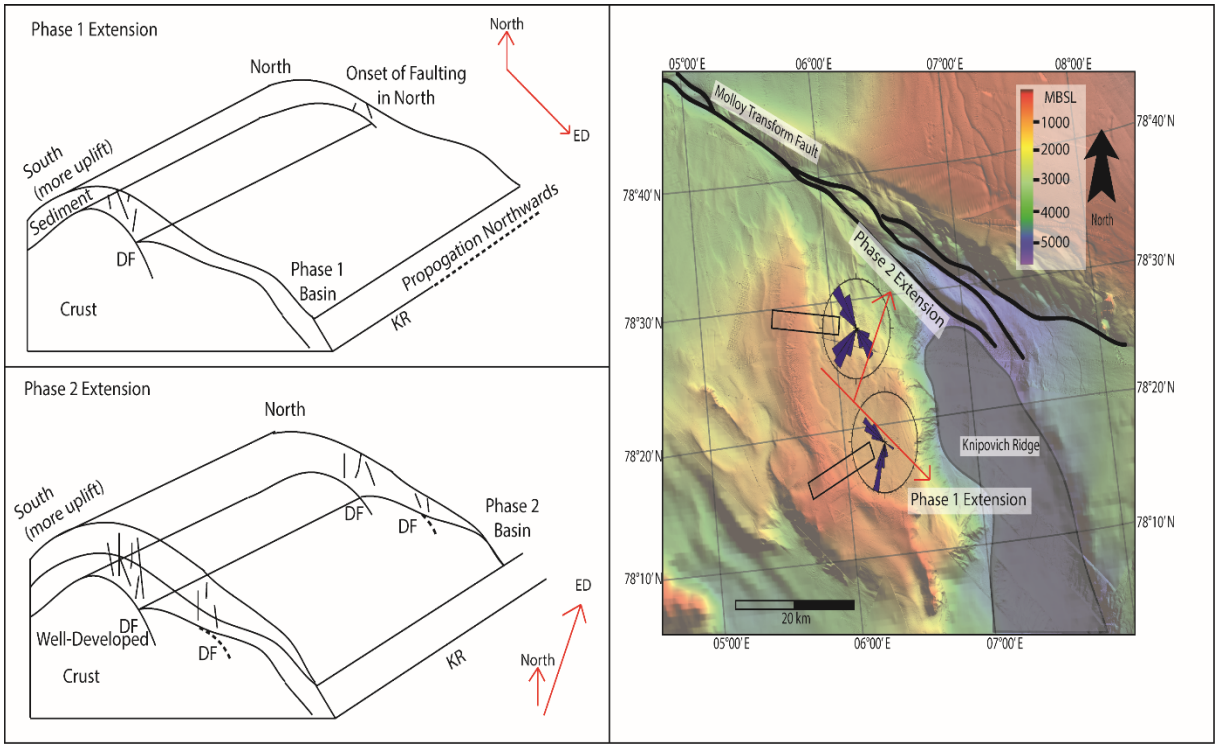


*Figure 9. Conceptual model of fault development on the Svyatogor Ridge through time with 2 main phases of extension. DF- Detachment Fault KR – Knipovich Ridge. In Phase 1, we conceptualize that northwards propagation of the Knipovich Ridge and more development of the detachment fault in the south led to a sediment accommodation space creation in the south, corresponding to the ~300-320° extensional azimuth from figure 6. Once the detachment fault began to develop in the north, and the Molloy Transform fault developed splays (thick black lines, bottom panels) the two study sites on the Svyatogor Ridge were predisposed to faulting towards sediment accommodation space created in the north corresponsing to the ~195-220° extensional azimuth from figure 6.*

Using high-resolution 3D seismic data for this type of stress analysis is relatively novel – prior studies (van Gent et al., 2009) have used conventional broadband seismic data for the same type of analysis and have encountered similar limitations and benefits as this study. The benefit of using 3D seismic studies is the ability to image a fault in 3D, however the confidence of processing and interpretational methods is important in determining the true nature and orientations of the fault. As our velocity model is based on OBS velocities, albeit somewhat coarse in resolution (Ritzmann et al., 2002) compared to the 3D seismic resolution, we are confident that any velocity induced variations in fault dip were not significant enough to influence the conclusions drawn. In this study, we determined that faults imaged in both 3D data sets are predominantly reactivated, i.e. multiple phases of extension reactivating the same fault planes (Henza et al., 2011; Reeve et al., 2015), therefore paleo-stress tensors cannot be resolved with certainty, however the overall pattern across both study sites suggest some approximate orientation of extensional phases. The Svyatogor Ridge, in particular the southern

dataset, has proven to be a very interesting site to test such methods due to the presence of a fluid flow and gas hydrate system, with a relatively limited free gas zone, has meant that faults and details through the free gas zone and underneath the free gas zone have been resolvable in finer detail than a system with significant amplitude blanking underneath the free gas zone (Waghorn et al., 2018). We assert that such quantitative stress and paleo-stress analysis in active fluid flow regions are important to integrate into any fluid, basin or fault modelling application.

## Conclusion

The tectonic regime is playing a large role in fluid redistribution in the subsurface, governing reactivation and orientation of potential fluid migration pathways, as well locking or exerting dilation upon certain faults for fluid migration. In the south of Svyatogor Ridge, fluid redistribution and migration in the subsurface appears dominated by fluid overpressure whereby large faults are not favourable for fluid migration and therefore small faults and fracture networks form in response while in the north of the Svyatogor Ridge sedimentary faults are acting as fluid migration pathways however may be presently unfavourably oriented for fluid migration. We find that fault analysis and subsequent stress tensor derivation indicates two main phases of extension, although note that reactivated faults may have undergone a number of phases of extension in order to appear obliquely slipping. The direction of second phase extension appears to correlate well with this faulting occurring after splay development on the Molloy Transform Fault. We find that high-resolution 3D seismic data is a good tool for analysing faults and stress in subsurface environments.

## References


Amundsen, I. M. H., Blinova, M., Hjelstuen, B. O., Mjelde, R., and Haflidason, H., 2011, The Cenozoic western Svalbard margin: sediment geometry and sedimentary processes in an area of ultraslow oceanic spreading: Marine Geophysical Research, v. 32, no. 4, p. 441-453.

Andersen, E. S., Dokken, T. M., Elverhøi, A., Solheim, A., and Fossen, I., 1996, Late Quaternary sedimentation and glacial history of the western Svalbard continental margin: Marine Geology, v. 133, no. 3-4, p. 123-156.

Angelier, J., 1979, Determination of the mean principal directions of stresses for a given fault population: Tectonophysics, v. 56, no. 3-4, p. T17-T26.

Berndt, C., 2005, Focused fluid flow in passive continental margins: Philosophical Transactions of the Royal Society of London A: Mathematical, Physical and Engineering Sciences, v. 363, no. 1837, p. 2855-2871.

Bünz, S., Polyanov, S., Vadakkepuliyambatta, S., Consolaro, C., and Mienert, J., 2012, Active gas venting through hydrate-bearing sediments on the Vestnesa Ridge, offshore W-Svalbard: Marine geology, v. 332, p. 189-197.

Caine, J. S., and Forster, C. B., 1999, Fault zone architecture and fluid flow: Insights from field data and numerical modeling: GEOPHYSICAL MONOGRAPH-AMERICAN GEOPHYSICAL UNION, v. 113, p. 101-128.

Cann, J., Blackman, D., Smith, D., McAllister, E., Janssen, B., Mello, S., Avgerinos, E., Pascoe, A., and Escartin, J., 1997, Corrugated slip surfaces formed at ridge-transform intersections on the Mid-Atlantic Ridge: Nature, v. 385, no. 6614, p. 329.

Célérier, B., 2010, Remarks on the relationship between the tectonic regime, the rake of the slip vectors, the dip of the nodal planes, and the plunges of the P, B, and T axes of earthquake focal mechanisms: Tectonophysics, v. 482, no. 1-4, p. 42-49.

Collett, T. S., and Dallimore, S. R., 2000, Permafrost-associated gas hydrate, Natural Gas Hydrate, Springer, p. 43-60.

Crane, K., Doss, H., Vogt, P., Sundvor, E., Cherkashov, G., Poroshina, I., and Joseph, D., 2001, The role of the Spitsbergen shear zone in determining morphology, segmentation and evolution of the Knipovich Ridge: Marine geophysical researches, v. 22, no. 3, p. 153-205.

Curewitz, D., and Karson, J. A., 1997, Structural settings of hydrothermal outflow: fracture permeability maintained by fault propagation and interaction: Journal of Volcanology and Geothermal Research, v. 79, no. 3-4, p. 149-168.

Delvaux, D., and Sperner, B., 2003, Stress tensor inversion from fault kinematic indicators and focal mechanism data: the TENSOR program: New insights into structural interpretation and modelling, v. 212, p. 75-100.

Ehlers, B.-M., and Jokat, W., 2009, Subsidence and crustal roughness of ultra-slow spreading ridges in the northern North Atlantic and the Arctic Ocean: Geophysical Journal International, v. 177, no. 2, p. 451-462.

Engen, Ø., Faleide, J. I., and Dyreng, T. K., 2008, Opening of the Fram Strait gateway: A review of plate tectonic constraints: Tectonophysics, v. 450, no. 1-4, p. 51-69.

Faleide, J. I., Solheim, A., Fiedler, A., Hjelstuen, B. O., Andersen, E. S., and Vanneste, K., 1996, Late Cenozoic evolution of the western Barents Sea-Svalbard continental margin: Global and Planetary Change, v. 12, no. 1-4, p. 53-74.

Hardy, S., and McClay, K., 1999, Kinematic modelling of extensional fault-propagation folding: Journal of Structural Geology, v. 21, no. 7, p. 695-702.

Heidbach, O., Rajabi, M., Cui, X., Fuchs, K., Müller, B., Reinecker, J., Reiter, K., Tingay, M., Wenzel, F., Xie, F., Ziegler, M. O., Zoback, M.-L., and Zoback, M., 2018, The World Stress Map database release 2016: Crustal stress pattern across scales: Tectonophysics, v. 744, p. 484-498.

Henza, A. A., Withjack, M. O., and Schlische, R. W., 2011, How do the properties of a pre-existing normal-fault population influence fault development during a subsequent phase of extension?: Journal of Structural Geology, v. 33, no. 9, p. 1312-1324.

Hill, D. P., 1977, A model for earthquake swarms: Journal of Geophysical Research, v. 82, no. 8, p. 1347-1352.

International, Seismological, and Centre, 2016, On-Line Bulletin, Internatl. Seismol. Cent., Volume http://www.isc.ac.uk: Thatcham, United Kingdom.

Johnson, J. E., Mienert, J., Plaza-Faverola, A., Vadakkepuliyambatta, S., Knies, J., Bünz, S., Andreassen, K., and Ferré, B., 2015, Abiotic methane from ultraslow-spreading ridges can charge Arctic gas hydrates: Geology, v. 43, no. 5, p. 371-374.

Kvenvolden, K., 1998, A primer on the geological occurrence of gas hydrate: Geological Society, London, Special Publications, v. 137, no. 1, p. 9-30.

Kvenvolden, K. A., and McMenamin, M. A., 1980, Hydrates of natural gas: a review of their geologic occurrence.

Landvik, J. Y., Bondevik, S., Elverhøi, A., Fjeldskaar, W., Mangerud, J., Salvigsen, O., Siegert, M. J., Svendsen, J.-I., and Vorren, T. O., 1998, The last glacial maximum of Svalbard and the Barents Sea area: ice sheet extent and configuration: Quaternary Science Reviews, v. 17, no. 1-3, p. 43-75.

Ligtenberg, J., 2005, Detection of fluid migration pathways in seismic data: implications for fault seal analysis: Basin Research, v. 17, no. 1, p. 141-153.
Madrussani, G., Rossi, G., and Camerlenghi, A., 2010, Gas hydrates, free gas distribution and fault pattern on the west Svalbard continental margin: Geophysical Journal International, v. 180, no. 2, p. 666-684.
Morley, C., Haranya, C., Phoosongsee, W., Pongwapee, S., Kornsawan, A., and Wonganan, N., 2004, Activation of rift oblique and rift parallel pre-existing fabrics during extension and their effect on deformation style: examples from the rifts of Thailand: Journal of Structural Geology, v. 26, no. 10, p. 1803-1829.
Odling, N., Gillespie, P., Bourgine, B., Castaing, C., Chiles, J., Christensen, N., Fillion, E., Genter, A., Olsen, C., and Thrane, L., 1999, Variations in fracture system geometry and their implications for fluid flow in fractures hydrocarbon reservoirs: Petroleum Geoscience, v. 5, no. 4, p. 373-384.
Planke, S., Eriksen, F. N., Berndt, C., Mienert, J., and Masson, D., 2009, P-Cable high-resolution seismic: Oceanography, v. 22, no. 1, p. 85.
Plaza-Faverola, A., Bünz, S., Johnson, J. E., Chand, S., Knies, J., Mienert, J., and Franek, P., 2015, Role of tectonic stress in seepage evolution along the gas hydrate-charged Vestnesa Ridge, Fram Strait: Geophysical Research Letters, v. 42, no. 3, p. 733-742.
Plaza-Faverola, A., and Keiding, M., 2019, Correlation between tectonic stress regimes and methane seepage on the western Svalbard margin: Solid Earth, v. 10, no. 1, p. 79-94.
Reeve, M. T., Bell, R. E., Duffy, O. B., Jackson, C. A.-L., and Sansom, E., 2015, The growth of non-colinear normal fault systems; What can we learn from 3D seismic reflection data?: Journal of Structural Geology, v. 70, p. 141-155.
Ritzmann, O., Jokat, W., Mjelde, R., and Shimamura, H., 2002, Crustal structure between the Knipovich Ridge and the Van Mijenfjorden (Svalbard): Marine Geophysical Researches, v. 23, no. 5-6, p. 379-401.
Sibson, R., Moore, J. M. M., and Rankin, A., 1975, Seismic pumping—a hydrothermal fluid transport mechanism: Journal of the Geological Society, v. 131, no. 6, p. 653-659.
Sibson, R. H., 1996, Structural permeability of fluid-driven fault-fracture meshes: Journal of Structural Geology, v. 18, no. 8, p. 1031-1042.
-, 2000, Fluid involvement in normal faulting: Journal of Geodynamics, v. 29, no. 3-5, p. 469-499.
Skarke, A., Ruppel, C., Kodis, M., Brothers, D., and Lobecker, E., 2014, Widespread methane leakage from the sea floor on the northern US Atlantic margin: Nature Geoscience, v. 7, no. 9, p. 657.
Sloan, E. D., 1998, Gas hydrates: Review of physical/chemical properties: Energy & Fuels, v. 12, no. 2, p. 191-196.
Stewart, S., 2001, Displacement distributions on extensional faults: Implications for fault stretch, linkage, and seal: AAPG bulletin, v. 85, no. 4, p. 587-599.
Tucholke, B. E., Lin, J., and Kleinrock, M. C., 1998, Megamullions and mullion structure defining oceanic metamorphic core complexes on the Mid-Atlantic Ridge: Journal of Geophysical Research: Solid Earth, v. 103, no. B5, p. 9857-9866.
van Gent, H. W., Back, S., Urai, J. L., Kukla, P. A., and Reicherter, K., 2009, Paleostresses of the Groningen area, the Netherlands—Results of a seismic based structural reconstruction: Tectonophysics, v. 470, no. 1-2, p. 147-161.
Waghorn, K. A., Bünz, S., Plaza-Faverola, A., and Johnson, J. E., 2018, 3-D Seismic Investigation of a Gas Hydrate and Fluid Flow System on an Active Mid-Ocean Ridge; Svyatogor Ridge, Fram Strait: [Washington, DC] :, p. 2325-2341.
Waghorn, K. A., Vadakkepuliyambatta, S., Plaza-Faverola, A., Johnson, J. E., Bünz, S., and Waage, M., Submitted, Crustal processes sustain Arctic abiotic gas hydrate and fluid flow systems: Scientific Reports
Waite, W. F., Santamarina, J. C., Cortes, D. D., Dugan, B., Espinoza, D., Germaine, J., Jang, J., Jung, J., Kneafsey, T. J., and Shin, H., 2009, Physical properties of hydrate-bearing sediments: Reviews of geophysics, v. 47, no. 4.

577 Weinberger, J. L., and Brown, K. M., 2006, Fracture networks and hydrate distribution at Hydrate
578 Ridge, Oregon: Earth and Planetary Science Letters, v. 245, no. 1-2, p. 123-136.
579 Zoback, M. D., and Zoback, M. L., 2002, Stress in the earth's lithosphere: Encyclopedia of physical
580 science and technology, v. 16, p. 143-154.

581